

Title	Study on Creep Damage in Thick Welded Joint of Mod.9Cr- 1 Mo Steel Plates
Author(s)	LI, Yongkui
Citation	高知工科大学, 博士論文.
Date of issue	2009-03
URL	http://hdl.handle.net/10173/513
Rights	
Text version	author



Kochi, JAPAN

<http://kutarr.lib.kochi-tech.ac.jp/dspace/>



**Study on Creep Damage in Thick Welded Joint
of Mod.9Cr-1Mo Steel Plates**

改良 9Cr-1Mo 鋼の厚板溶接継手のクリープ損傷に関する研究

PhD Dissertation

March 20, 2009

**Kochi University of Technology
Graduate School of Engineering Course**

LI Yongkui (李永奎)

Student ID: 1106405

SUMMARY

Most of the modern power generation plants depend on fossil fuels. Now we know that excessive burning of fossil fuels seriously endanger earth environment because the emission of carbon dioxide (CO_2). We need to reduce the greenhouse gases (GHG) discharged by the consumption of fossil fuels. In order to reduce GHG the thermal condition of steam must be raised. Extensive R&D for the advanced thermal power plants is ongoing worldwide. In Japan the ultra super critical power generation plants are being constructed and tested towards better thermal efficiency. The higher the steam temperature and pressure we get the better efficiency. Typically the steam temperature is more than 600°C . To meet these requirements a family of new heat-resisting steels with 9-12% chromium (high Cr steel) have been developed and applied to some supercritical power plants.

One of earliest high Cr steel put into practical use was the 9Cr-1Mo-V-Nb (Modified 9Cr-1Mo, P91/T91 in ASME/ASTM standards). At 600°C the 100,00h creep-rupture strength of this steel is more than 80MPa and is stronger than the austenitic stainless steel such as 304H and 316H. Typical use of the high Cr steel is the main steam tube which sends the steam from the boiler to the turbine. The tube must be welded to the boiler. However, there has been some severe fracture accidents using the weldment of Mod.9Cr-1Mo steel. In the welded joints of Mod.9Cr-1Mo the heat-affected-zone (HAZ) between the base metal (BM) and the WM (WM) of steel is consist of coarse and fine grain regions because of the ferritic phase transformation during the thermal cycling in the welding process. A common observation of the failure was the evolution of the creep voids that lead to micro-cracking in the fined grained reasion. This failure has been known as the Type IV creep cracking of the welded joint.

We have conducted the creep tests at 550, 600 and 650°C using conventional round bar specimens for the base metal and thin rectangular specimens cut from the joint. Thick (21mm) welded joint specimens were subjected to the interrupted creep tests at 600°C in order to measure the number of voids per area and the areal fraction. On the basis of the creep tests, the void measurement and extensive computer simulation (FEM), this thesis aims to clarify the Type IV cracking behavior in both macroscopic and microscopic fracture under creep exposure. One of powerful approaches in the research of Type IV cracking has been the continuum damage mechanics (CDM) originally proposed by Kachanov-Rabotonov and further developed by Hayhurst. From the creep tests we conducted we postulate the constitutive equation of inelastic creep deformation and combined with the creep damage mechanics equation. Furthermore, we discuss the fundamental process of the void nucleation and growth which leads to the Type IV cracking.

Contents

Chapter 1 Introduction

1.1 Background	1-1
1.2 Reviews on the Previous Work	1-7
1.2.1 Development of High Chromium Ferritic Steel	1-7
1.2.2 Investigation on Mechanical Properties with Finite Element Analysis	1-14
1.2.3 Review on Creep Damage Evaluation	1-17
1.2.3.1 Macroscopic Continuum Damage Mechanics	1-17
1.2.3.2 Microscopic Continuum Damage Mechanics	1-22
1.2.3.3 Prediction of Creep Life	1-24
1.3 Objective	1-25
References of Chapter 1	1-26

Chapter 2 Experimental Procedures

2.1 Material and Welding Processing	2-1
2.2 Creep Testing of Welded Joint, Base Metal and Welded Joint	2-5
2.3 Hardness Profile in the Welded Joint	2-8
2.4 Specimens of Simulated HAZ	2-9
2.5 Measurement of the Voids in Thick Welded Joint	2-14
2.5.1 Observation of Voids in HAZ of Welded Joint	2-15
2.5.2 Void Counting Using Image-Pro Plus Software	2-20
2.6 Summary of Chapter 2	2-25
References of Chapter 2	2-26
Appendix A Macroscopic Profiles of Interrupted Creep Specimens	2-27

Chapter 3 Evaluation of Creep Damages in HAZ of Thick Welded Joint for Mod.9Cr-1Mo Steel

3.1 Introduction	3-1
3.2 Experimental Procedure	3-2
3.2.1 Creep Tests	3-2
3.2.2 Measurement of Creep Voids	3-5
3.2.3 FEM Analysis	3-5
3.2.3.1 Constructing the Thick FEM Model	3-5
3.2.3.2 Constructing the Thin FEM Model	3-12
3.3. Experimental and Numerical Results	3-13
3.3.1 Creep Properties of Welded joint, Base Metal and Simulated HAZ	3-13
3.3.2 Evolution and Distribution of Creep Voids in HAZ	3-14
3.3.3 Results of Numerical Analysis	3-18

3.3.3.1 Stress-Strain Distribution and Evolution in Path A	3-18
3.3.3.2 Stress-Strain Distribution and Evolution in Path B.....	3-22
3.4 Roles of Mechanical Parameters during Creep	3-25
3.4.1 Equivalent Creep Strain and Stress Triaxial Factor	3-25
3.4.2 Effects of Von Mises Stress on the Creep-Rupture Time	3-28
3.5 Summary of Chapter 3	3-30
References of Chapter 3	3-31
Appendix B ·Typical Output Images of FEM	3-33

Chapter 4 Evaluation of Creep with Continuum Damage Mechanics

4.1 Introduction	4-1
4.2 Constitutive Damage Equations	4-2
4.2.1 Uniaxial Stress State	4-5
4.2.2 Multi-Material Conditions	4-5
4.3 Experiments and Discussions	4-6
4.3.1 Reviews of the Experiment	4-6
4.3.2 Logarithms of m and $1/\lambda$ Dependent on the Applied tresses.....	4-6
4.3.3 Global Evaluation for Strain and Damage of BM, Simulated HAZ and Weldment	4-9
4.3.4 Evaluation of Damage Distribution in the Weak HAZ	4-16
4.3.5 Creep Life Predictions	4-20
4.4 Effects of the Substitutions by the Stress on Creep-Rupture Life	4-22
4.5 Summary of Chapter 4	4-24
References of Chapter 4	4-25

Chapter 5 Creep Mechanism of a Welded Joint of Mod.9Cr-1Mo Steel

5.1 Introduction	5-1
5.2 Creep Damage Locations in the Welded Joint	5-1
5.2.1 HAZ in the Welded Joint	5-2
5.2.2 Weak Zone in the Welded Joint	5-3
5.2.2.1 Rupture Results	5-4
5.2.2.2 Weak Zone in HAZ Selecting	5-7
5.2.2.3 Microhardness and Voids Distribution	5-9
5.3 Void (Vacancy) Nucleation	5-14
5.3.1 Grain Boundary Sliding	5-15
5.3.2 Diffusion during Creep	5-20
5.4 Growth of Voids and Cracks in Type IV zone	5-23
5.5 Possible Countermeasures to Prevent Type IV Cracking	5-26
5.6 Summary of Chapter 5.....	5-28
References of Chapter 5	5-29

Chapter 6 Conclusions

Acknowledgement

Chapter 1

Introduction

1.1 Background

About ten years ago a failure occurred in a power plant of the Central Electricity Generating Board (CEGB) in UK, a large boiler was broken due to the failure of its header endplate [1-1]. The high temperature components was broken after service of 36,526 hours under the stress of 17.86 MPa at 568°C. It was less than the half service time of the prediction in this condition. It is a disaster since the instant damage leading to strong burst without any portent no defects detected by the observation of NDT methods before.

The material used for the header endplate of the boiler in the power plant was an F91 (forged modified 9Cr) ferritic steel, which was the substitution material for the previous 2.25Cr-1Mo and 0.5Cr-0.5Mo-0.25V steels. Because of the better creep strength the new steel allowed for thinner sections and hence lower through-wall temperature gradients during thermal cycling. The steel was introduced in the UK in the late 1980s [1-2]. Another reason for the steel was the demand for the plant with better thermal efficiency. The research and development of boilers and turbines with the USC (ultra-supercritical) steam conditions have been the national projects in USA, EU and Japan. The steam temperature of USC plant is about or more than 600°C. The exiting materials for the high temperature components in the USC power plants were the austenitic stainless steels such as 304H (18Cr-10Ni), 316H (18Cr-12Ni-Mo) and 321H (18Cr-10Ni-Ti). The austenitic stainless steels had an advantage against oxidation at high temperatures. The use of the austenitic stainless steels, however, was inevitable to give large thermal stress produced due to the crystal lattice of face centered cubic (FCC) during operation temperatures changes. Thus about 20 years ago, the Mod.9Cr-1Mo

steel was introduced to take place of the austenitic stainless steel in the USC power plant because of its good creep properties and economical considerations. The Mod.9Cr-1Mo ferritic heat resistant steel could also solve the problem of thermal stress during high temperature service because of its body centered cubic (BCC) crystal structure. The F91 (forged Mod.9Cr steel) was used in the main steam tube and the header in power plant as shown in Fig 1-1. One of the difficulties to apply the material is the structure integrity of the weldment components.

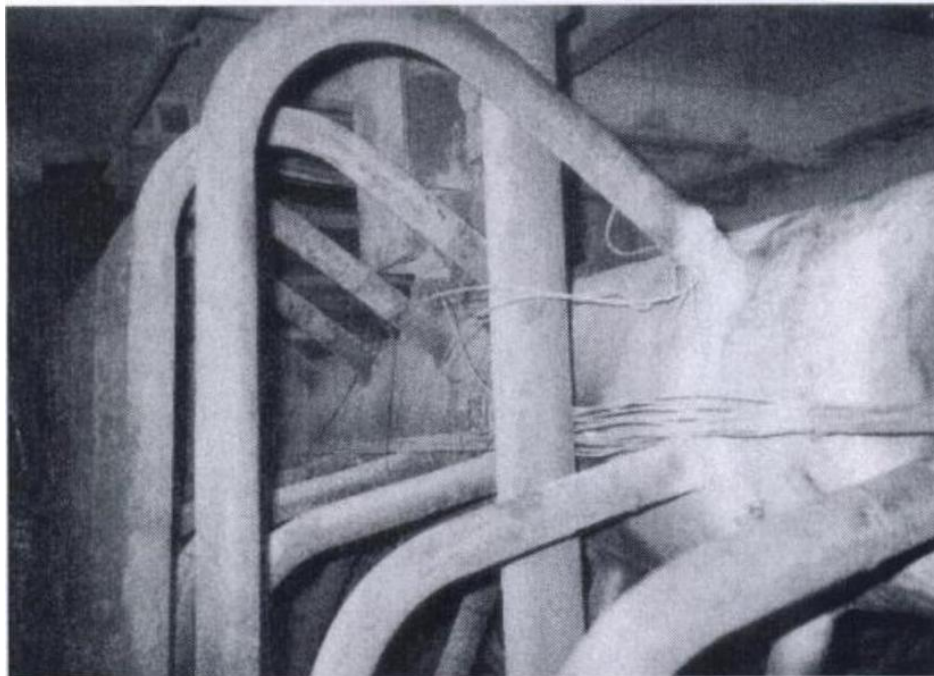


Fig. 1-1. Main steam tube and the arrangement of stubs of the header made of Mod.9Cr-1Mo steel [1-2].

Generally speaking the weldment of the ferritic steel such as Cr-Mo has the HAZ (heat affected zone) structure with the affected by the peak temperature about A_{c3} that shows considerably lower creep strength than the base metal. As pointed at the beginning it has been reported in the welded joints of ferritic steel a unique model of failure: Type IV cracking in the HAZ close to base metal. Voids nucleated in the weak zone in the HAZ close to base

metal were found in the weldment. The same failure cases were found mostly in the zone close to the base metal, which part also could be named as Type IV zone in the weldment. The involved failure cases were reported [1-3 ~ 1-5] in the middle of 1970s, the cracks in the Cr-Mo steels were classified [1-6], and four types of cracking in conventional low alloy ferritic steels were distinguished by their locations and orientation as follows:

Type I : Cracks are both transverse and parallel to the weld and are fully located within the weld metal;

Type II : Cracks are both transverse and parallel to the weld by can propagate into the HAZ and beyond into the base metal;

Type III: Cracks initiate in the coarse-grained HAZ close to and parallel to the fusion boundary and can propagate both in this region and also into the base metal;

Type IV: Cracks are located in the fine-grained HAZ or the intercritical HAZ adjacent to the base metal and run parallel to but offset from the fusion boundary.

The four cracks are indicated in the Fig 1-2.

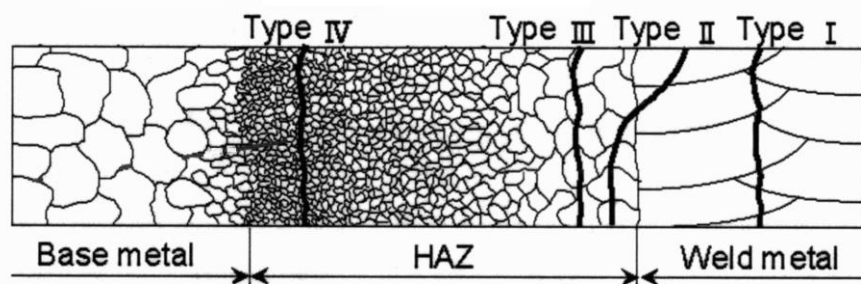
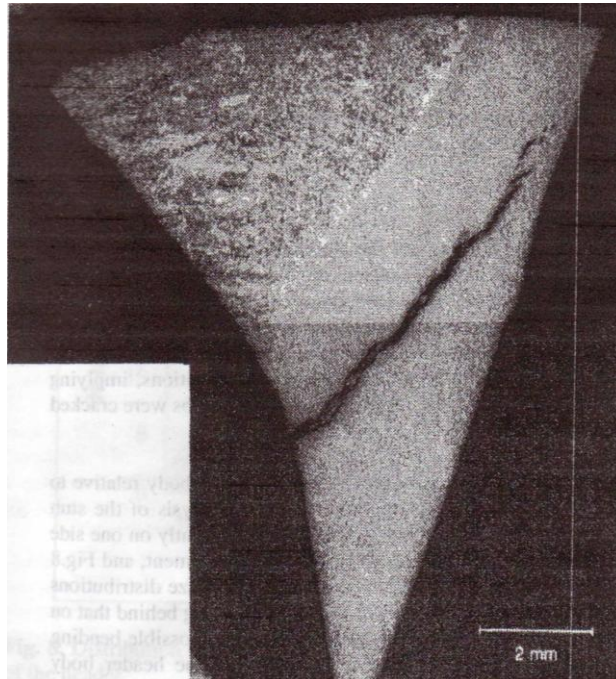


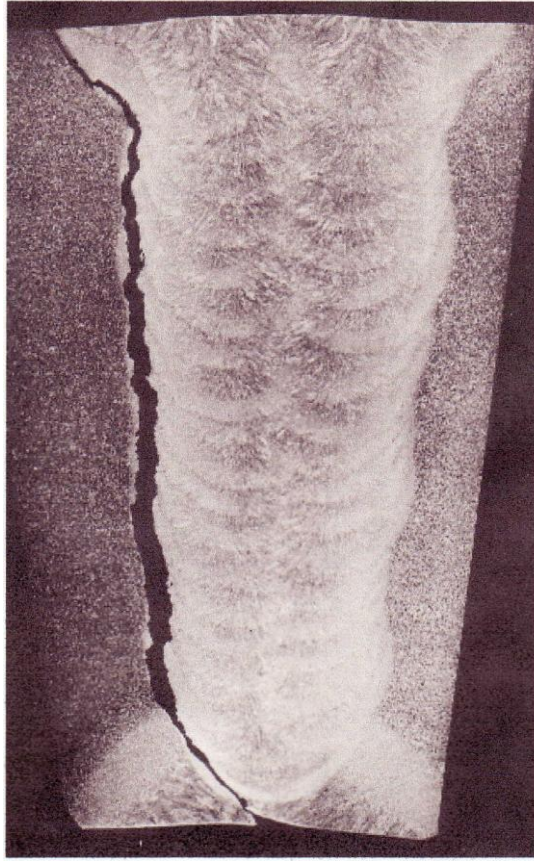
Fig. 1-2. Sketch map of the cracks in ferritic steel weldment [1-7].

Type IV cracking is of the prominent damage form of welded joint for the Mod.9Cr-1Mo ferritic heat resistant steel at high temperatures. Examples of the Type IV cracks in the welded joint of the Mod.9Cr-1Mo steel and 1.25Cr-0.5Mo steel were shown in the Fig 1-3a and b respectively. Important features of the Type IV failure are the following [1-8]:

- 1) The failure time is less than that for the wrought base metal. Type IV failure is often termed mid-life cracking because of its characteristic failure time. Typically, the loss in creep strength can be described as either a stress reduction factor or a life reduction factor with respect to the base metal.
- 2) The fracture has a macroscopic appearance typical of a low ductility failure but, significant creep deformations are measured in the narrow HAZ region indicating strain localization.
- 3) The susceptibility to Type IV damage is related to the ductility of the base metal.
- 4) The rupture life depends on the stress state and the applied loading direction, e.g., girth weld versus longitudinal seam weld.
- 5) Agreement between the theoretical predictions and experimental measurements for the effect of constraint and specimen size/component section size on the rupture life depend strongly on the material properties and multiaxial stress rupture criteria used in the analysis.



a)



b)

Fig. 1-3. Type IV cracking in the welded joint of a) Mod.9Cr-1Mo steel [1-2] and b) 1.25Cr-0.5Mo steel [1-9] after long-term high-temperature exposure.

In 1997, Ellis gave a reviews on the Type IV damage in the Cr-Mo heat resistant steel [1-9], in which he concluded the causes on the damage in the Type IV zone of the welded joint. They are listed in the following lines:

- 1) Type IV cracking is the results of a microstructural zone of material that has low creep strength surrounded by materials that are stronger in creep. Type IV cracking has been found in the fine-grained HAZ associated with exposure to temperatures around the A_{c3} temperature and in the intercritical region of the HAZ. Because cracking occurs in service, it is often termed mid-life cracking.
- 2) Type IV cracking is caused by thermal softening of the HAZ due to the welding thermal recycle. For Cr-Mo steel, creep strength is a function of grain size,

substructure, solid solution and particle strengthening. For the fine-grained HAZ and intercritical regions of the HAZ, metallographic examination reveals changes in the dislocation substructure from high density laths to equiaxed subgrains and larger carbide size/interparticle spacing that is expected to result in lower creep strength of the material.

- 3) Creep rupture tests on cross welds and simulated HAZ samples indicate premature failure as compared to base material for samples that fail by the Type IV mechanism. The degree of creep strength reduction can be expressed either as a life reduction factor or a stress reduction factor. For Cr-Mo steels, the weldment lives vary from approximately equal to values of 1/5 of that for minimum strength base material. Hence, failures in service may be expected at life fractions as low as 0.2, consistent with service experience.
- 4) For the low alloy ferritic steels, the susceptibility to Type IV cracking and the degree of life reduction appears to depend on the specific alloy, and based on Ontario Hydro experience with girth welds increases in the following order; 2-1/4Cr-1Mo to 1-1/4Cr-1/2Mo to Cr-MoV.
- 5) Factors that affect creep ductility such as multiaxial stresses, PWHT and inclusion content/matrix strength for the parent or base material may be important in determining susceptibility to Type IV cracking. In addition, the content of residual carbide formers – Nb, Ti and V that affect the creep strength of the base material may also play an important role in determining susceptibility to Type IV cracking and the accuracy of life reduction.
- 6) The local failure strain for the Type IV mechanism is relatively large, i.e., greater than 10%, consistent with the physical interpretation of strain localization in a narrow, creep-ductile, low creep strength zone. Thus, damage detection and life assessment using capacitance strain gages, grids, or optical deformation measurements may be

useful.

- 7) For Cr-Mo weldments that failure by Type IV mechanism, the rupture life increases as the specimen size increases. However, the effect of specimen size and the use of the data in component life assessment should be studied in more detail.

That what is the damage mechanism on earth is still the argument topic on high chromium steel weldment in elevated temperature service. The accurate location of the Type IV zone is the fine-grained HAZ and intercritical HAZ supported by two-group researchers, respectively. Still further continuous work on these is necessary.

1.2 Reviews on the Previous Work

1.2.1 Development of High Chromium Ferritic Steel

The material in the present study was the 9Cr-1Mo-V-Nb ferritic heat resistant steel, and the historical development is reviewed in this section. The first high chromium ferritic steels appeared in Europe in the mid 1960s. A 9Cr-2Mo steel was developed in France primarily for tubing and subsequently named as EM12. This steel had a duplex microstructure containing δ -ferrite, giving poor impact toughness [1-10]. During much of the same time a 12Cr-1Mo steel was developed in Germany with the designation X20CrMoV12-1 and applied throughout the EU for superheated tubes and pipes. While this steel benefited from a fully martensitic microstructure, it exhibited inferior creep strength to EM12 at temperatures higher than 520°C and was difficult to weld, primarily owing to higher carbon content [1-11]. These two steels had the 100,000h creep strength of 35MPa at 600°C. The evolution of the 9-12 Cr ferritic steels is illustrated in Fig 1-4 [1-12].

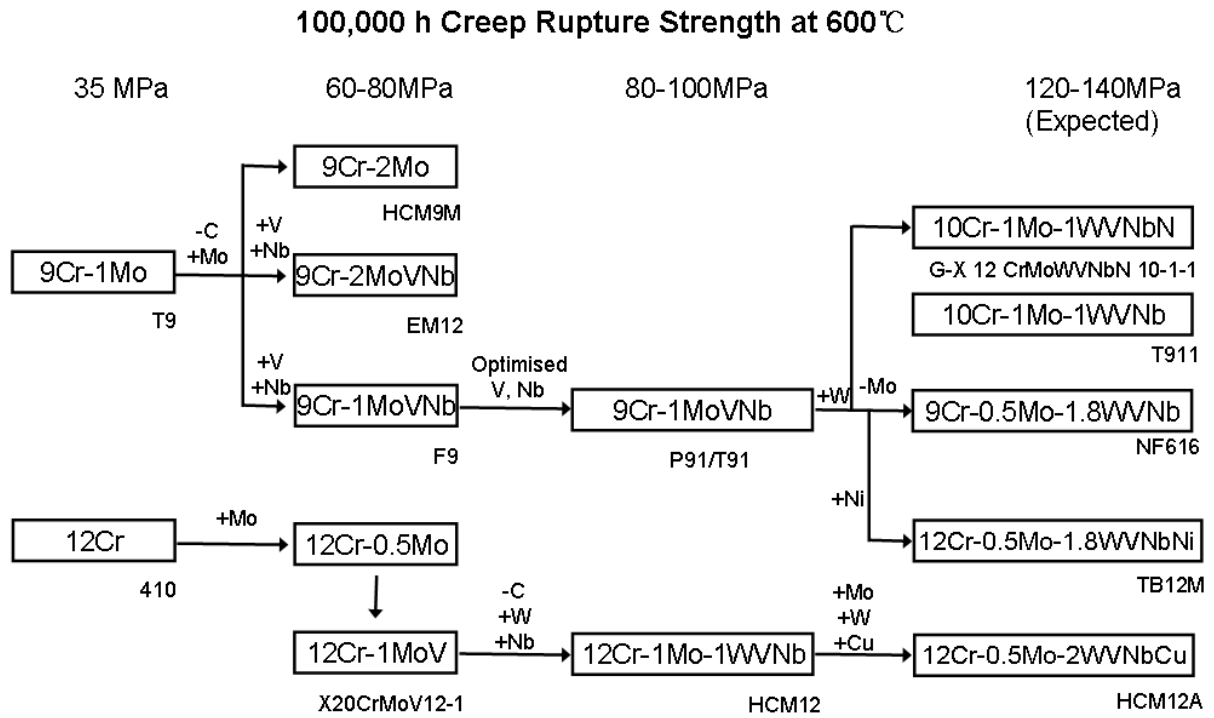


Fig. 1-4. Evolution of high Cr ferritic heat resistant steels [1-10].

In the 1970s the Oak Ridge National Laboratory (ORNL) in USA developed the modified 9Cr-1Mo steel [1-11], leading to T91 for pressure tube applications and Alloy P91 for piping and headers. The F9 is composed of the 9%Cr and 1Mo as the primary alloy elements, has a creep strength in the range 60-80MPa at 600°C while the T91/P91 developed on the base of modification on the composition of F9 steel and apparent improvement in creep strength (80-100MPa) was obtained. This superseded EM12 and X20CrMoV12-1. This alloy relies on a tempered martensitic microstructure stabilized by $M_{23}C_6$ carbides, with further strengthening owing to molybdenum in solid solution and a fine distribution of vanadium/niobium rich carbonitride (MX) precipitates [1-12]. LowC9Cr1MoVNb [1-13], 9Cr2MoVNb [1-14] and 9Cr1MoVNb (T91) [1-15] are the modified 9Cr-1Mo steels with high temperature strength enhanced by adding carbonitride-forming elements such as V and Nb. Of these modified 9Cr-1Mo steels, T91 developed in the US has higher allowable stress and had already been used extensively worldwide not only for superheater tubes but also for

thick walled components such as headers and main steam pipes [1-1, 1-2 and 1-16]. Meanwhile, improved 12%Cr steels for boilers, 12Cr1Mo1WVNb (HCM12) [1-17] was developed by eliminating the drawbacks of conventional 12%Cr steels. Namely, it is a 12%Cr steel of dual phase structures consisting of tempered martensite and δ -ferrite with weldability and creep rupture strength being markedly improved. As shown in Fig 1-4, we classified it into the same level to the T91/P91 in term of the creep strength at 600°C.

Further improvements in creep strength have been achieved with the advent of steels such as NF616 (T92) and HCM12A (T122), where tungsten enhances the long term creep strength (in the range of 120-140MPa) through solid solution hardening [1-18] and retards the coarsening of $M_{23}C_6$ carbides (which stabilized the martensite lath structure) [1-19]. However, with tungsten concentrations in excess of 2 wt-%, the formation of coarse laves phase (Fe_2W) can lead to a deterioration of creep properties [1-20]. Tungsten also promotes the formation of δ -ferrite, so its use has to be balanced, either by reductions in the concentrations of other ferrite promoting solutes such as molybdenum, or by adding austenite stabilizers such as cobalt [1-21]. An effect of silicon on steam oxidation was investigated using 9%Cr steels with 0.05 to 0.5%Si to make clear the temperature dependence of the silicon effect and microstructures of the scales. For NF616 steel, silicon effectively reduces the steam oxidation rate due to the formation of protective amorphous SiO_2 films [1-22]. It can be seen that many of the modern steels contain tungsten in the range 1-2 wt-%. Furthermore, E911 [1-23] (9Cr1Mo1WVNb) having a higher allowable stress than that of the T91 have been developed in the late 1990s. The high strength of T911 and T92 (NF616) were obtained based on steels with Mo content replaced by addition of tungsten. Mo was decreased to 0.5% and 1.8% of W added to T91 in case of T92, while 1% W was added to T91 in the case of T911.

It should be emphasized here that many of the new alloys which exhibited improved creep rupture strength in short term tests have disappointed when 100,000h data became available. As a result, the focus of research had shifted to understanding the factors that affect the long

term stability of $M_{23}C_6$ and MX precipitates. In creep tested steels a ‘modified Z-phase’, Cr(V, Nb)N seems to precipitate at the expense of $M_{23}C_6$ and vitally, the MX precipitates [1-21 and 1-24]. Recent studies have examined the effect of carbon concentration and controlled additions of boron on the $M_{23}C_6$ and MX precipitation behavior [1-25 and 1-26].

Table 1-1 shows the nominal chemical compositions of 9% and 12% Cr ferritic heat resistant steels. If the material is assumed to be used for temperature up to 650°C, 9%Cr would be insufficient in terms of oxidation resistance while 12%Cr steel could meet the requirements [1-16]. All the steels and alloys containing with 9 and 12%Cr content have chemical compositions with Co added and W content increased. 11Cr2.6W2.5CoVNbBN [1-27] contains Co of 2.5% and W of 2.6%, with B addition slightly increased in comparison with conventional steels. The steel of 11Cr3W3CoVNbTaNdN has 3% of both Co and W, characterized by the addition of Ta and Nd. It was reported that both Ta and Nd form fine, stabilized nitrides, which can enhance creep strength in the temperature range of 600°C to 650°C [1-28]. Thus developed 11%Cr ferritic heat resistant steels have a creep strength of 180MPa in 10⁵h at 600°C.

Chromium is the basic alloying element for heat resistant steels, and increased Cr content improves oxidation and corrosion resistance. Although Cr per se does not exhibit a marked effect on creep strength, high strength is more likely to be obtained neat Cr percentages of 2% and 9 through 12% in ferritic steels, and strength declines at compositions between the two overages. The reason for this remains unknown.

Molybdenum, tungsten and rhenium are all elements useful to solution strengthening, and molybdenum and tungsten have long been used for heat resistant steels. Also, these elements further enhance the creep strength of heat resistant steels when added in greater quantities. If their additions exceed a certain limit, however, δ -ferrite precipitates and reduces the strength, and precipitation of the Laves phase decreases toughness. Furthermore, the effect of tungsten on creep strength is approximately half that of Molybdenum, and, as described later,

the combined addition of molybdenum and tungsten can be effective for strength improvement. Rhenium is reported to raise creep strength if added in account of around 0.5%, and this effect is similar to the actions of molybdenum and tungsten [1-29].

The effects of vanadium, niobium titanium and tantalum all combine with carbon and/or nitrogen to produce carbides, nitrides, which finely and coherently precipitate on the ferritic matrix to exhibit a marked effect of precipitation strengthening. Among these, vanadium and niobium are found to exhibit particularly optimal contents, about 0.2% and 0.05% respectively, and as described later, the effect of their combined addition can be great. This suggests that the formations of precipitations composed by vanadium and niobium are associated with each other [1-16].

Because carbon and nitrogen are austenite formers, they are useful in inhibiting δ -ferrite. Also, their contents relate to the precipitation and coarsening of chromium carbides and nitrides. For carbon particularly, if addition exceeds 0.1%, the creep strength often declines, and it is believed that there should be an optimal addition according to the types and contents, etc. of carbide-forming elements. Nitrogen is believed to be an element essential for raising creep strength in 9% Cr steels. Additions of nitrogen are often at about 0.05%, and it is believed that there should be an optimal content relative to other nitride-forming elements such as boron [1-16].

Boron improves hardenability and enhances grain boundary strength, and can greatly improve creep strength. Furthermore, a publication indicates that it exhibits the effects of stabilizing carbides by penetrating into $M_{23}C_6$ [1-30]. A weld filler, with contain the boron of 90-130 ppm in combination with minimized nitrogen, for welding P92 and P122 ferritic steels was developed, and its welded joint produced had the best creep resistance. Kondo *et al* contributed the reason to the large size grain formation in the temperature of A_{c3} point since the fine-grained HAZ was always weak than the coarse-grain HAZ when materials serviced in long term at high temperatures [1-31].

With respect to silicon and manganese addition, silicon is a ferrite former, whereas manganese is an austenite former. These actions are viewed as being contradictory to each other, the reduction of the contents of both of these elements can improve creep strength. Also, silicon works to decrease toughness by promoting the Laves phase, whereas manganese, though useful for toughness improvement, can impair the high temperature stability of the ferrite structure in the same manner as nickel [1-16].

Nickel, copper and cobalt are all austenite formers, and if added as alloy elements, they inhibit the formation of δ -ferrite by decreasing the chromium equivalent, but they simultaneously decrease the A_1 transformation temperature. However, level of this decrease varies among these elements, and the decline seen with addition of nickel. Therefore, if copper and/or cobalt are added, the effect of the inhibition of δ -ferrite formation can be expected, making high-temperature tempering possible [1-16].

Table 1-1. Nominal chemical composition of high Cr ferritic steels.

Steel Name	Specification		Chemical Composition (mass %)											
	ASME	JIS	C	Si	Mn	Cr	Mo	W	Co	V	Nb	B	N	Others
9Cr1Mo	T/P9	STBA26	0.12	0.60	0.45	9.0	1.00	-	-	-	-	-	-	-
9Cr2Mo	-	STBA27	0.07	0.30	0.45	9.0	2.00	-	-	-	-	-	-	-
9Cr1MoVNb	T/P91	STBA28	0.10	0.40	0.45	9.0	1.00	-	-	0.20	0.08	-	0.05	-
9%Cr	T/P92	STBA29	0.07	0.06	0.45	9.0	0.50	1.80	-	0.20	0.05	0.004	0.06	-
	T/P911	-	0.11	0.30	0.45	9.0	1.00	1.00	-	0.20	0.08	0.003	0.06	-
LowC9Cr1MoVNb	-	-	0.06	0.50	0.60	9.0	1.00	-	-	0.25	0.40	0.005	-	-
9Cr2MoVNb	-	NFA49213	0.10	0.40	0.10	9.0	2.00	-	-	0.30	0.40	-	-	-
12Cr1MoV	DIN X20CrMoV121	-	0.20	0.40	0.60	12.0	1.00	-	-	0.25	-	-	-	0.5Ni
12Cr1MoWV	DIN X20CrMoWV121	-	0.20	0.40	0.60	12.0	1.00	0.50	-	0.25	-	-	-	0.5Ni
12Cr1Mo1WVNb	-	SUS410J2TB	0.10	0.30	0.55	12.0	1.00	1.00	-	0.25	0.05	-	0.03	-
12%Cr	T/P122	SUS410J3TB	0.11	0.10	0.60	12.0	0.40	2.00	-	0.20	0.05	0.003	0.06	1.0Cu
	12Cr2.6W2.5CoVNbN	-	0.08	0.20	0.50	11.0	0.20	2.60	2.50	0.20	0.07	0.004	0.05	-
11Cr3W3MoVNbTaNdN	-	-	0.10	0.30	0.20	11.0	-	3.00	3.00	0.20	0.07	-	0.04	0.07Ta,0.04Nd

1.2.2 Investigation on Mechanical Properties with Finite Element Analysis

In the design analysis and failure investigation the finite element method (FEM) has been widely used to ensure the soundness of the structures such as spacecraft, chemical plants, medical equipments, power plants and nuclear reactors. For the weldment servicing at elevated temperatures, we also utilized this method to simulate the analyzing the evolution and distribution of the mechanical parameters since the welded joint includes heterogeneous properties due to the weaker zone produced during welding. The software such as MARC, ANSYS, ABAQUS and DEFORM *etc.* can be adopted for conducting the FEM analysis. The software we used was the MARC operated under the Linux system. We believe the FEM could provide the useful tools to investigate mechanical behavior, and it is a valid method to clarify the mechanical behavior of the materials during servicing at a certain conditions. Particularly, our use of the FEM is primarily to investigate the mechanism of the creep damages in the weldment during the high temperature long-time service.

Using the FEM to investigate the mechanical behavior of welded joints, there are many forerunners before us [1-32 ~ 1-41]. Eggeler *et al* conducted a 2-D longitudinal sectional area of a pipe FE modeling with single groove was conducted in two models, and they are the classical Norton minimum creep strain rate model and the logistic creep strain prediction (LCSP). With the same FE modeling, Holmström *et al* compared the calculated results from the two models and showed the differences, the Norton law appears inferior to the LCSP in the third stage of creep [1-33]. Eggeler *et al* ever conducted a 3-dimension FE modeling in three material states (weld metal, intercritical HAZ and base metal) under uniaxial tension. The elastic modulus of P91 was measured and the uniaxial creep behavior of the three material states was characterized and represented by the Norton law and in terms of the Robinson model. A welded pressure vessel was creep tested and hoop and axial strains were measured for three welds in the vessel. A creep stress analysis of welded pressure vessel was performed based on Norton's law and the Robinson model concentrating on the accumulated

hoop and axial strains in the welds. As a result, the calculated axial and hoop strains were found to be in good agreement with the measured ones [1-32]. With this modeling, the distribution of the strains and stresses were investigated in the whole welded pressure vessel which might be the earliest and systemic FE analysis example utilized in resistant ferritic steel to simulate the mechanical behavior during creep. Albert analyzed the stress and strain distributions within the bar specimen during creep deformation using the FE method. Though they conducted the simple 3-D FE modeling composed of 5 components (The creep properties of the relative 4 components were from the material simulated at 1000, 950, 900, 850°C with welding simulator respectively, and the fifth component was from the base metal.) without groove, the results indicated that creep deformation and fracture were influenced by the multiaxial stress state produced in the specimen due to the existence of different microstructures varying significantly in their creep properties [1-34]. Watanabe *et al* also conducted the 3-dimension (3-D) FE modeling composed of 3 components (weld metal, fine-grained HAZ and base metal) with single U groove with comparing with the final damage distribution in plate, enhancing the theory of the negative effects of the stress triaxiality factor on the creep damage [1-38]. Ogata *et al* conducted a 3-material (weld metal, HAZ and base metal) and 3-D bar FE modeling to simulate the micro creep damages (sizes and numbers of void in welded joint) with time. It is indicated that creep strain accumulated in the HAZ preferentially resulting in Type IV failure of the weld joint specimen [1-37]. Hyde *et al* described some issues concerning weld modeling and failure prediction with conducting a 3-D FE modeling of pipe with single groove, which was quiet systemic modeling [1-40]. Bauer *et al* analyzed the stress-strain situations and multiaxial stress state in various pipe models (with the changing of angle of the single groove) including welds for clarifying the effect of creep strength of weld metal [1-35]. The FEM modeling was investigated focusing on the mechanical parameters such as Von Mises stress, equivalent creep strain and the factor of multiaxiality in two directions including of along the HAZ and along the longitudinal

direction of the welded joint. The 3-D FEM modeling was composed of 5 components, such as the components of weld metal, HAZ1 (coarse-grained HAZ), HAZ2 (fine-grained HAZ), HAZ3 (transformed intercritical HAZ) and base metal. The calculation results from the longitudinal direction of the welded joint modeling could be studied quite with comparing the actual creep rupture results. Along the HAZ, however the investigated parameters had no actual results for comparing. The components for constructing the modeling of welded joint were much detailed.

Shinozaki *et al* performed a set of FEM simulations including of a welded joint model and a matrix/precipitation model. The 2-D welded joint model without groove was composed of 4 components (weld metal, coarse-grained HAZ, fine-grained HAZ and base metal), and the 3-D matrix/precipitation model included a precipitation for consideration of its role on the vacancy nucleation. With comparing the creep rupture tests and the void observations, the large equivalent creep strain had a good agreement with the high density of creep void in fine-grained HAZ comparing with the other components in the welded joint. Moreover, the precipitation in the matrix acts a role of nucleation site in creep vacancy occurrence with the creep deformation [1-41].

Up to now, the development of the FEM analysis has been studied systemically. The FEM modeling designed more and more complicated, such as from 2-D to 3-D, simple plate modeling to bar and then the pipe, without groove to groove done, and 2, 3 to 5 components of the modeling. In summarizing the previous FEM applications to the creep behavior of weldment, it seems to us that there still remain the lack of the direct comparison with the calculation (FEM) and the experiment (creep testing). In our work, in addition to the FEM computation we observed wholly the evolution and distribution of damage (mainly vacancies, voids and Type IV cracks) in the weak zone of the thick welded joint by several interrupting of creep tests.

1.2.3 Review on Creep Damage Evaluation

In order to save energy and reduce the output of carbon dioxide gas, it becomes the most important to improve the energy efficiency of high-temperature structures used in fossil power plants and jet engines, etc. The materials tend to be improved to meet the more serious requirements since its structural components would work at much higher temperatures and bear much longer times. Moreover, in view of the recent economic considerations, the plants might be operated longer times often exceeding its predicted life. Therefore, more accurate prediction for the life of used component at high temperatures becomes very important.

1.2.3.1 Macroscopic Continuum Damage Mechanics

Beside of the methods mentioned above, there was also a predicting method using the constitutive equations with the continuum damage mechanics (CDM) at a certain temperature. The original idea utilized in uniaxial creep tension was firstly proposed by Kachanov in 1958 [1-42], and subsequently by Rabotnov [1-43]. The idea of Kachanov-Rabotnov will be described here in some details because the concept of the creep damage is one of central themes of the research. Kachanov observed that in uniaxial creep specimens, cracks and voids formed on the planes across which the applied tension force was transmitted and which he considered as the areas of damage. By defining a damage parameter, ω , as that fraction of the original cross-sectional area occupied by cracks and voids he defined the local net stress as,

$$\sigma_n = \frac{\sigma}{1 - \omega} \quad (1.1)$$

where σ is the stress applied to the initially undamaged area. The rate of change in damage is given in terms of the nominal stress σ and the current value of ω by

$$\dot{\omega} = f(\sigma, \omega) \quad (1.2)$$

In order to make the prediction of the creep strain, different methods were essentially the

same and involve the usage of a single state damage variable theory in which the creep strain rate $\dot{\varepsilon}$ is given by Equation (1.3) [1-43 ~ 1-45].

$$\dot{\varepsilon} = g(\sigma, \omega) \quad (1.3)$$

Under the uniaxial conditions, the damage rate (1.2) and strain rate (1.3) equations could be given by

$$\dot{\varepsilon} = G \left(\frac{\sigma}{1 - \omega} \right)^n \quad (1.4)$$

$$\dot{\omega} = C \frac{\sigma^\chi}{(1 - \omega)^\phi} \quad (1.5)$$

where G , C , n , χ and ϕ are material constants and could be solved after integrating the equations (1.4) and (1.5). The damage parameter ω represents the scalar quantity of damage in the range from 0 at the beginning of damage formation to 1 at failure, ε is the strain, and σ is the local stress equal to the effective stress to rupture under the uniaxial stress state. The stress σ presents mostly contributing to the damage during service of the material. Two extreme material classifications were made by Hayhurst according to the results of several multiaxial stress creep-rupture tests in order to solve the constitutive equations under the multiaxial stress states [1-46]. In the first category the rupture time is governed by a maximum principal tension stress criterion; the behavior of copper and Nimonic alloys (nickel based) is approximately described by this criterion. In the second classification the rupture time is dependent upon the maximum effective stress. For the maximum principal stress criterion σ is expressed by the maximum principal stress σ_1 ($\sigma_3 < \sigma_2 < \sigma_1$) and for the maximum effective stress criterion the corresponding term is σ_{eq} . Where σ_{eq} is the Von Mises stress. However, a number of materials, including austenitic stainless steels, obey mixed criteria, in these situations σ can be expressed by

$$\sigma = \alpha \sigma_1 + (1 - \alpha) \sigma_{eq} \quad (1.6)$$

In this expression the factor of α , obtained by carrying two sets of creep tests with different multiaxial stress state, is dependent on the material properties at a certain temperature. The factor α is normally named as the multiaxial stress rupture criteria. It is in the range from zero when the material belongs to the first category to unity for the material in the second classification.

Under the uniaxial and biaxial creep tension conditions, cracks and voids formed on planes across which the applied tension force was transmitted and the imaginary or hypothetical areas of damage was considered as the damage parameter of ω . Kachanov and Rabotnov have discussed the practical importance of accurately predicting the rupture life of structural components which have operated for long period within the temperature range 0.4-0.6 T_m (T_m is the melting point of the material) [1-47]. The suitable working stresses are low fractions of the material yield stress of the material. On the basis of these, Hayhurst *et al* conducted the evaluation of creep damage on the uniaxial tension plate containing a hole. The effect of the multiaxiality stress system decreased the uniaxial rupture life of the material by as much as 50% according to experiences in practice. The reasons for that were investigated. As a result he pointed out that the understanding of the multiaxial behavior of the material upon the rupture is imperative [1-46 and 1-48]. Tu and Sandström proposed a model of an inherent discrete process of material degradation by a continuous variable [1-49]. After the work of Kachanov was described in detailed by Hayhurst in 1973, the damage was generalized as an internal state variable in the context of irreversible thermodynamics later in 1970s by Lemaitre and Chaboche [1-50]. The systematic CDM equations were constructed to evaluate the creep behavior by Hayhurst *et al* [1-51]. The constitutive equations are given by

$$\dot{\varepsilon}_{ij} = \frac{\partial \varphi^{n+1}(\sigma_{kl})}{\partial \sigma_{ij} (1-\omega)^n (n+1)} \cdot G \cdot f(t) \quad (1.7)$$

$$\dot{\omega} = \frac{C [\alpha \sigma_1 + (1-\alpha) \sigma_{eq}]^\chi}{(1-\omega)^\phi} \quad (1.8)$$

where $f(t)$ is a function of time (usually of the form t^m), G , n and m are material constants and $\varphi(\sigma_{kl})$ is a homogeneous potential function of degree one in the components of stress σ_{kl} .

With consideration the complicated multiaxial structure, the FEM was adopted to solve the rupture life in the CDM approach by Hayhurst group [1-52]. The tested specimens were aluminium and copper plates containing central circular holes, the force applied on which was the simple tension. In this case, the virtual stress distribution was simulated by the FEM. Though the importance of the multiaxial state of stress in the actual structures, the relation between of the damage and the rates of creep strain was studied in uniaxial state continuously, leading to that the CDM conversional equations could be applied to not only the macroscopic observations but also that of the physical damage growth in the material [1-53]. Furthermore the CDM approach was introduced to study the creep behavior of weldment in the beginning of 1990s [1-54 ~ 1-56], and they give an evaluation on the failure history of the pipe weldment. In Hall's model, he obtained the creep properties of the coarse-grained and fine-grained HAZ comparing their bainitic microstructures fraction with that of weld metal. Moreover, the factor of α was obtained with carrying the biaxial creep rupture tests. Hyde *et al* developed a subroutine with collaborating the CDM constitutive equations and FEM simulation for creep behavior evaluation [1-57]. They tested the evaluation work with conducting a set of creep tests on P91 material at 625°C. The experimental results showed that the damage location prediction was in good agreement with the experimental, while the rupture lifetime was conservative with 80% of the actual rupture life under the stress of 105MPa [1-58]. Tu and Sandström took the CDM constitutive equations for design considerations with understanding the histories [1-59]. Perrin extrapolated the evaluation on

creep behavior on much higher temperature with the CDM equations given below under the uniaxial stress state [1-60]:

$$\dot{\varepsilon} = \frac{d\varepsilon}{dt} = A \sinh \left[\frac{B\sigma(1-H)}{(1-\phi)(1-\omega)} \right] \quad (1.9)$$

$$\frac{dH}{dt} = \frac{h}{\sigma} \dot{\varepsilon} \left(1 - \frac{H}{H^*} \right) \quad (1.10)$$

$$\frac{d\phi}{dt} = \frac{K_c}{3} (1-\phi)^4 \quad (1.11)$$

$$\frac{d\omega}{dt} = C \dot{\varepsilon} \quad (1.12)$$

where A , B , C , h , H^* and K_c are constitutive constants to be determined and H , ϕ are the two state variables. The factor H represents the strain hardening that occurs during primary creep; initially H is zero and, as strain is accumulated, increasing to a value H^* . The second state variable, ϕ , describes the evolution of spacing of carbide precipitations which is known to lead to a progressive loss in the creep resistance of particle-hardened alloys such as ferritic steels. In the CDM constitutive equations, the global features of creep behavior, such as the minimum creep strain rates, lifetimes and failure strains were used to solve the constants of the constitutive equations. Later, Perrin reported that both the maximum principal stress and the effective stress affected the rupture lives of a weldment with combining the CDM evaluation and FEM simulation [1-61]. The evaluation of the creep behavior was conducted comparing with a failure within the Type IV zone. The value of 2.8 for the stress state index of 0.5Cr-0.5Mo-0.25V ferritic steel was calculated, which is closed to the results of the stress triaxial factor from in our calculation. Using the same CDM constitutive equations to predict the components rupture lives in a pipe welded joint, the predicting results showed in closed agreement with the experimental results. A three-dimensional solver was developed [1-62]. Base on the CDM evaluation model proposed by Hayhurst in 1983, Becker

et al developed a user-subroutine for simulating the creep behavior in the terms of creep damage, strain and stress in uniaxial stress state and multiaxial stress state [1-63]. However, the true stress level is not constant due to the plastic straining during test, which leads to no full convincing results from the conventional CDM constitutive equations. The relation of plastic strain and the true stress was found by Xu, and then he constructed the integration on them in the CDM model [1-64]. The CDM constitutive equations were introduced to study the life reduction due to the presence of a weld and the effect of weld repair [1-65]. A cycle jumping numerical technique was used to analyze a multi-bar model of the slag tap using viscoplastic constitutive equations embodying softening due to combined cyclic plasticity and creep damage [1-66]. Hayhurst demonstrated how computational CDM could be used to predict the behavior of structural components, ranging from modest stress concentrators to the growth of cracks by creep [1-67]. However, Kinugawa *et al* found the local variability in the transverse welded joint with the aids of FEM simulation, i.e. along the thickness direction of welded joint the mechanical parameters are variable [1-68]. It is inevitable that the effective stress and the maximum principal stress are all changing with locations, which reach the difficulties to conduct the CDM constitutive equations for evaluating the creep behavior of the thick welded joint. In present study we are trying to solve this problem.

On a global view, the phenomenological evaluation on the creep behavior had been developed much perfectly. However, the mechanical parameters in the weldment are changing with the local variations during creep, which makes it difficult to extract the effective value to conduct the calculation with the conventional constitutive equations. The materials constants defined in the previous methods might not reflect the creep behavior exactly.

1.2.3.2 Microscopic Continuum Damage Mechanics

The other evaluation with CDM constitutive equations was focusing on the microscopic damage evolution in material [1-69 ~ 1-71]. In early 1980s, Cocks and Ashby developed a set of evaluation constitutive equations in terms of the continuum damage mechanics, due to

controlled by different damage mechanism such as diffusion creep, by power-law creep, or by a coupling of diffusion and power-law creeps.

This model was base on the observation of micro-damage in the materials, and a set of brief formulas developed in 1980 could help understanding. They are given by

$$t_f = t_n + \frac{\alpha}{(n+1)\dot{\varepsilon}_{ss}} \cdot \ln\left(\frac{1}{(n+1)f_i}\right) \quad (1.13)$$

$$\frac{1}{\alpha} = \sinh\left[\frac{2\left(n - \frac{1}{2}\right)}{\left(n + \frac{1}{2}\right)} \cdot \frac{p}{\sigma_{eq}}\right] \quad (1.14)$$

where t_f is the time to fracture at constants stress, t_n is the time to nucleate voids and f_i presents the initial area fraction of holes. The factor $\dot{\varepsilon}_{ss}$ denotes the average steady-state creep state is given by Equation (1.15) without consideration of the voids in material.

$$\dot{\varepsilon}_{ss} = \dot{\varepsilon}_0 \left(\frac{\sigma_{eq}}{\sigma_0} \right) \quad (1.15)$$

In this formula the factor $\dot{\varepsilon}_0$ is the minimum creep rate.

Later, Yu took the CDM model into predicting the creep time for material with some modification on Equations (1.13 and 1.14), which showed that the calculated results in good agreement with the experimental [1-71]. However, the damage observation in his study, that was not basis of his own work systemically, should be continuously investigated. The set of constitutive equations are also facing the problems that the stress fluctuation along the cross-sectional lays under the multiaxiality stress state. Much critical microstructural observations are required for fitting these evaluation equations.

1.2.3.3 Prediction of Creep Life

There are two types of methods for creep rupture life prediction: the one is the constitutive equation and the other one is time-temperature parameter (TTP) methods [1-72]. As Expressed in equation (1.16), a polynomial of logarithmic stress can be used for the logarithmic of the creep rupture times at a temperature.

$$\log t_R = a_0 + a_1 \log \sigma + a_2 (\log \sigma)^2 + \dots + a_k (\log \sigma)^k \quad (1.16)$$

where t_R is the time to rupture and σ denotes the applied stress. $a_0, a_1, a_2, \dots, a_k$ are the constants. To predict the creep rupture strength the direction solution is commonly used to extrapolate from shorter databases, by which a number of experimental data are necessary at the same temperature. The prediction of life with CDM constitutive equations at a certain temperature belong to this method. However, it is difficult to conduct the evaluation because the servicing material tends to deteriorate and leads to reducing the creep strength in long term at elevated temperatures.

As given in Equation (1.17), the TTP method gives a relation of the creep life and the applied stress with taking the temperature dependency into account, i.e. it can extrapolate from the data of elevated temperatures and short creep life.

$$P(t_R, T) = F(\sigma) \quad (1.17)$$

Comparing with the direction method, the TTP method was popular of evaluating the creep during long term service. Fujida *et al* gave a detailed procedure on the TTP method relative to the prediction of creep life in long term [1-73]. There have been many proposals for the TTP concept. The followings are major ones widely used:

$$\text{Larson-Miller: } P = T(\log t_R + C) \quad (1.18)$$

$$\text{Orr-Sherby-Dorn: } P = \log t_R - Q/(2.3RT) \quad (1.19)$$

$$\text{Manson-Haferd: } P = (\log t_R - \log t_a) / (T - T_a) \quad (1.20)$$

where T is the absolute temperature, t_R represents the creep-rupture to time, Q is the creep activation energy and R denotes the gas constant. C , t_a and T_a are materials constants. Moreover, among the equations listed above, although the Larson-Miller equation is the most commonly used to predict the creep life in long term, it is known Larson-Miller could not give conservative prediction. The Manson-Haferd parameter with two materials constants is more flexible. A software package of time-temperature parameter for creep-rupture data analysis (ECRTTP) was published from the ISIJ in 1994 [1-73].

1.3 Objective of the Research

The purpose of this research is to clarify the creep damage mechanism of Type IV cracking in Mod.9Cr-1Mo steel weldment. On the basis of creep-rupture testing and microscopic observation by SEM and LASER microscope, the mechanical parameters to be used in the FEM simulation are evaluated.

The macroscopic CDM approach combined with the microscopic voids nucleation and growth in the fine-grained HAZ and in the intercritical HAZ should give a new insight into the understanding of the creep damage in the ferritic steel.

As Hayhurst and his coworkers pointed out we think the triaxiality under creep exposure and the evolution of the microstructural changes, particularly the void formation in the weak zone, must be clarified in order to avoid the failure of Type IV cracking.

References of Chapter 1

- [1-1] S. J. Brett, D. J. Allen, J Pacey: **CHIFI International Conference**, (Milan, 1999) pp. 873-884.
- [1-2] S. J. Brett, D. L. Oates, C. Johnston: **ECCC Creep Conference**, (London, 2005) pp. 563-572.
- [1-3] L. H. Toft and D. E. Yeldham: **CEGB' Proc. Conf.**, (1972) pp. 5-19.
- [1-4] D. Cheetham and M. Jagger: *CEGB Report SSD/NE/N118*, (1975).
- [1-5] D. Cheetham and M. Jagger: *CEGB Report SSD/NE/N134*, (1976).
- [1-6] H. J. Schüller, L. Hagn and A. Woitscheck: *Der Maschinenschaden*. **47**(1974) 1-13.
- [1-7] W. Chan, R. L. McQueen, J. Prince and D. Sidey: **Service Experience in Operation Plants**, (ASME, NY, NY, 1991) pp. 97-105
- [1-8] S. T. Kimmins, M. C. Coleman and D. J. Smith: **Proceeding of Fifth International Conference on Creep and Fracture of Engineering Materials and Structures**, UK, 1993, 681-694.
- [1-9] F. V. Ellis: *Review of Type IV cracking in piping welds*, (Tordonato Energy Consultants, Inc., Chattabooga, 1997) pp. 3-11.
- [1-10] C. D. Lundin, P. Liu and Y. Cui: *Welding Res Council Bull* **454**(2000) 1–36.
- [1-11] V. K. Sikka and P. Patriarca: *Technical report*, Metals and Ceramics Division, Oak Ridge National Laboratory, USA, 1984.
- [1-12] K. Haarmann, J. C. Vaillant, B. Vendenberghe, W. Bendick and A. Arbab: *The T91/P91 book*, (Vallourec & Mannesmann Tubes, (2002).
- [1-13] K. Kinoshita: *NKK Tech. Rep.*, **62**(1973) 602.
- [1-14] M. Ivenel: *Revue Générale Term*, (1964) 555.
- [1-15] V. K. Sikka, C. T. Ward and K. C. Thomas: **ASM Int. Conf. Production, Fabrication, Properties and Applications of Ferritic Steels for High-Temperature Applications**, Warrendale, PA, (1981).

- [1-16] F. Masuyama: ISIJ International. **41**(2001) 612-625.
- [1-17] A. Iseda, H. Teranishi, K. Yoshikawa, F. Yasuyama, T. Daikoku and H. Haneda: Therm. Nucl. Power. **39**(1988) 897.
- [1-18] K. Iwanaga, T. Tsuchiyama and S. Takaki: Key Engineering Material. **171-174**(2000) 477-482
- [1-19] F. Abe: Key Engineering Material. **171-174**(2000) 395-402.
- [1-20] Y. Hasengawa, T. Muraki, M. Ohgami and H. Mimura: Key Engineering Material. **171-174**(2000) 427-436.
- [1-21] C. Berger, A. Scholz, Y. Wang and K. H. Mayer: Z. Metallkd. **96**(2005) 667-674.
- [1-22] T. Ishitsuka, Y. Inoue and H. Ogawa: Oxidation of Metals. **61**(2004) 125-142.
- [1-23] H. Cerjak, E. Letofsky, G. Feigl and P. Pichler: **Materials for Advanced Power Engineering**, Part I , ed. by J. Lecomte-Beckers *et al.*, Jülich GmbH, Forschungszentrum, Jülich, (1998) 401.
- [1-24] E. Letofsky and H. Cerjak: Science and Technology of Welding & Joining. **9**(2004) 31-36.
- [1-25] M. Taneike, K. Sawada and F. Abe: Metallurgical and Materials Transactions A. **35A** (2004) 1255-1262.
- [1-26] S. K. Albert, M. Kondo, M. Tabuchi, F. Yin, K. Sawada and F. Abe: Metallurgical and Materials Transactions A. **36A**(2005) 333-343.
- [1-27] M. Ohgami, Y. Hasegawa, H. Naoi and T. Fujita: **IMechE Conf. Trans.**, 1997-2, Advanced Steam Plant, (IMechE, London, 1997) pp. 115.
- [1-28] M. Igarashi and Y. Sawaragi: **Proc. Int. Conf. Power Engineering'97**. (1997) pp. 107.
- [1-29] M. Morinaga, R. Hashizume and Y. Murata: **Materials for Advanced Power Engineering**, Part I , ed. by D. Coutoursadis *et al.*, (Kluwer Academic Publishers, Dordrecht, 1994) pp. 319.
- [1-30] L. Lundin: P hD Thesis, Chalmers Univ. of Tech., 1995.

- [1-31] M. Kondo, M. Tabuchi, S. Tsukamoto, F. Yin and F. Abe: Science and Technology of Welding and Joining. **11**(2006) 216-223.
- [1-32] G. Eggeler, A. Ramteke, M. Coleman, B. Chew, G. Peter, A. Burblies, J. Hald, C. Jefferey, J. Rantala, M. deWitte and R. Mohrmann: International Journal of Pressure Vessels and Piping. **60**(1994) 237-257.
- [1-33] S. Holmström, A. Laukkanen and K. Calonius: **Proceedings of 3rd International Conference on Integrity of High Temperature Welds**. (London: IOM Communications, 2007) pp. 245-255.
- [1-34] S. K. Albert, M. Matsui, H. Hongo, T. Watanabe, K. Kondo and M. Tabuchi: International Journal of Pressure Vessels and Piping. **81**(2004) 221-234.
- [1-35] M. Bauer, A. Klenk, K. Maile and E. Roos: **Proceedings of 3rd International Conference on Integrity of High Temperature Welds**. (London: IOM Communications, 2007) pp. 257-266.
- [1-36] T. Ogata, T. Sakai and M. Yaguchi: **Proceedings of 3rd International Conference on Integrity of High Temperature Welds**. (London: IOM Communication, 2007) pp. 285-294.
- [1-37] H. P. Leeuwen: Engineering Fracture Mechanics. **9**(1977) 951-974.
- [1-38] T. Watanabe, M. Tabuchi, M. Yamazaki, H Hongo and T. Tanabe: International Journal of Pressure Vessels and Piping. **83**(2006) 63-71.
- [1-39] H. Mae: Journal of the Society of Materials Science. **57**(2008) 1173-1178.
- [1-40] T. H. Hyde: **Proceedings of 3rd International Conference on Integrity of High Temperature Welds**. (London: IOM Communication, 2007) pp. 227-243.
- [1-41] K. Shinozaki, D. J. Li, H. Kuroki, H. Harada and K. Ohishi: ISIJ International. **42**(2002) 1578-1584.
- [1-42] L. M. Kachanov: Izvestiya Akademii Nauk SSR Otdelenie Technicheskikh Nauk. (1958) 26-31.

- [1-43] Y. N. Rabotnov: *Creep Problems in Structural Members*, (John Wiley & Sons, New York, 1969) pp. 359-382.
- [1-44] D. R. Hayhurst and F. A. Leckie: *J. Mech. Phys. Solids*. **21**(1973) 431-446.
- [1-45] F. A. Leckie and D. R. Hayhurst: *Proc. R. Soc. Lond. A*. **340**(1974) 323-347
- [1-46] D. R. Hayhurst: *J. Mech. Phys.* **20**(1972) 381-390.
- [1-47] L. M. Kachanov: **Chs. IX, X**. (National Lending Library, Boston, Spa. English translation edited by A. J. Kennedy, 1960). and Y. N. Rabotnov: Ch. 6. North-Holland, Amsterdam, (English translation edited by F. A. Leckie, 1969).
- [1-48] D. R. Hayhurst: *Journal of Applied Mechanics*. **40**(1973) 244-250.
- [1-49] S. T. Tu, R. Wu and R. Sandström: *International Journal of Pressing Vessel and Piping*. **58**(1994) 345-354.
- [1-50] J. Lemaitre and J. L. Chaboche: **Mecanique des Materiaux Solides**. Paris: Dunod, 1985.
- [1-51] D. R. Hayhurst, P. R. Dimmer and C. J. Morrison: *Philosophical Transactions of the Royal Society of London. Series A, Mathematical and Physical Sciences*. **311**(1984) 103-129.
- [1-52] D. R. Hayhurst, P. R. Dimmer and M. W. Chernuka: *J. Mech. Phys. Solids*. **23**(1975) 335-355.
- [1-53] F. A. Leckie and D. R. Hayhurst: *Acta Metallurgica*. **25**(1977) 1059-1070.
- [1-54] F. R. Hall and D. R. Hayhurst: *The Royal Society*. **433** (1991) 383-403.
- [1-55] D. R. Hayhurst, I. J. Perlin: **Proc. Tenth Conf. Engng. Mech.**, (ASCE, 1995) pp. 393-396.
- [1-56] T. H. Hyde, W. Sun and A. A. Becker: *Int. J. Pressure Vessels & Piping*. **78**(2001)765-771.
- [1-57] T. H. Hyde, H. A. Williams and W. Sun: *Int. J. Pressure Vessels & Piping*. **76**(1999) 515-525.

- [1-58] T. H. Hyde, A. A. Becker, W. Sun, A. Yaghi, A. Thomas and P. Seliger: **5th international Conference on Mechanics and Materials in Design**, (2006) pp. 1-12.
- [1-59] S. T. Tu and R. Sandström: **Proceedings of fifth International Conference on Creep Fracture of Engineering Materials and Structures**, (edited by In: Wilshire B, Evans RW, Institute of Materials, 1993) pp.695-704.
- [1-60] I. J. Perrin and D. R. Hayhurst: Int. J. Pressure Vessels & Piping. **68**(1996) 299-309.
- [1-61] I. J. Perrin and D. R. Hayhurst: Int. J. Pressure Vessels & Piping. **76**(1999) 599-617.
- [1-62] D. R. Hayhurst, M. T. Wong and F. Vakili-Tahami: JSME International Journal, Series A. **45**(2002) 90-97.
- [1-63] A. A. Becker, T. H. Hyde, W. Sun and P. Andersson: Computational Material Science. **25**(2002) 34-41.
- [1-64] Q. Xu and D. R. Hayhurst: Int. J. Pressure Vessels & Piping. **80**(2003) 689-694.
- [1-65] S. T. Tu, P. Segle and J. M. Gong: Int. J. Pressure Vessels & Piping. **81**(2004) 199-209.
- [1-66] D. R. Hayhurst, J. Makin, M. T. Wong and Q. Xu: Philosophical Magazine. **85**(2005) 1701-1728.
- [1-67] D. R. Hayhurst: Arch. Mech.. **57**(2005) 103-132.
- [1-68] J. Kinugawa, Y. Monma, H. Hongo, M. Yamazaki and T. Watanabe: Creep Behaviour of 304 Stainless Steel Welded Joints Composed of Different 308 Weld Metals, **Proc, IUTAM Symposium on Mechanical Effects of Welding**, (Springer-Verlag, 1992) pp.231-238.
- [1-69] A. C. F. Cocks and M. F. Ashby: Metal Science. (1980) 395-402.
- [1-70] A. C. F. Cocks and M. F. Ashby: Progress in Materials Science. **27**(1982) 189-244.
- [1-71] T. Yu, M. Yatomi and H. J. Shi: **6th Japan-China Bilateral Symposium on High Temperature Strength of Materials**, (The Society of Materials Science Japan, 2007) pp. 137-142.
- [1-72] K. Kimura: *Tetsu-to-Hagané* (Ferrum) **13**(2008) 17-22.

[1-73] T. Fujita, Y. Monma, A. Matsuzaki, S. Kihara, M. Shiga and K. Kasahara: *Manual of Creep-Rupture Data Extrapolation in Accordance with ISO6303*, ISIJ (1983).

Chapter 2

Experimental Procedures

In this chapter we cover the experimental procedures. They are:

- 1) Specimen supplying and preparation from the weldment;
- 2) Creep testing of welded joint, base metal and welded joint;
- 3) Hardness profile before and after the creep tests;
- 4) Simulated specimen for the weak zone in the welded joint;
- 5) Observation of microstructure by SEM and LASER microscope;
- 6) Counting of void density and distribution.

The weaker zone in the welded joint was found in the HAZ close to the base metal, which was produced by the fast temperature raising and cooling during the welding process. The temperature of the zone was close to the temperature point of Ac_3 phase transformation, so that the fine grains formed in the pre-austenite lattice matrix during the rapid cooling [2-1]. In order to simulate the thermal process we conducted the Gleeble tests at several temperatures above Ac_3 point. However, the overheating occurs during weld due to the rapid thermal input, therefore it is difficult to locate the weak zone such as fine-grained HAZ and inter-critical HAZ. Also we observed the voids in the HAZ near to base metal of the thick welded joint by interrupting during the creep tests. We believe this is most detailed procedures of damage observation for evaluating the damage evolution in the welded joint.

2.1 Material and Welding Processing

The material investigated in the present study is a Mod.9Cr-1Mo steel plate of 25mm in thickness as shown in Fig 2-1. The Mod.9Cr-1Mo steel was developed in the USA in 1970s, and designated P91/T91 in the ASME/ASTM standards. The chemical compositions of the

base metal and the welding filler are given in Table 2-1. The plates were welded by using gas tungsten arc welding (GTAW) method with double U grooves as shown in Table 2-2. The post weld heat treatment (PWHT) adopted was to keep temperature at 745°C for 1 hour.



Fig. 2-1. As received GTAW joint of Mod.9Cr-1Mo steel plate with 25mm thickness.

Table 2-1. Chemical compositions of the base metal and welding filler (mass%).

Compositions	C	Si	Mn	P	S	Cr	Mo	V	Nb	N	Al	Cu	Ni
Base metal	0.1	0.25	0.43	0.006	0.002	8.87	0.93	0.19	0.07	0.06	0.014	0.012	0.06
Weld filler	0.08	0.12	1.02	0.005	0.004	8.99	0.9	0.18	0.04	-	-	0.12	0.71

Table 2-2. Welding procedure of GTAW for the Mod.9Cr-1Mo steel plate with 25mm thickness.

Positions	Passes	Current (A)	Voltage (V)	Velocity (mm/min)	Wire Supplying (mm/min)	Temperatures of Preheat and Interpass (°C)	PWHT
Lower Part	1	180/160			540		745°C x1h
	2~3	180/140	9~9.5	9~9.5	700	210~220	
	4~5	220/180			720		
	6~13	230/190			750		
Upper Part	14	230/190					745°C x1h
	15~16	230/180	9~9.5	9~9.5	750	210~220	
	17~26	230/190					

2.2 Creep Testing of Welded Joint, Base Metal and Welded Joint

Figure 2-2 shows the specimen geometry for the creep tests. The round bar specimens with 4mm in diameter and 15mm in gauge length for simulated HAZ (Fig 2-2a), those with 6mm in diameter and 30mm in gauge length for base metal (Fig 2-2b), and smooth thin plate specimens for the welded joint (Fig 2-2c) were machined from the welded plate and crept in long term at 550, 600 and 650°C with several stress levels from 40MPa to 240MPa. Several thick plate specimens shown in Fig 2-2d were also machined from the welded joint. These thick plate specimens were subjected the creep tests at 600°C under the applied stress of 90MPa. The thick welded joints were interrupted at several time intervals for the void observation that are explained in details later. The applied stresses, creep-rupture times, elongation, reduction of cross-sectional area, minimum strain rate and damage locations are listed in Tables 2-3, 2-4 and 2-5 for the base metal, the simulated HAZ and the welded joints, respectively.

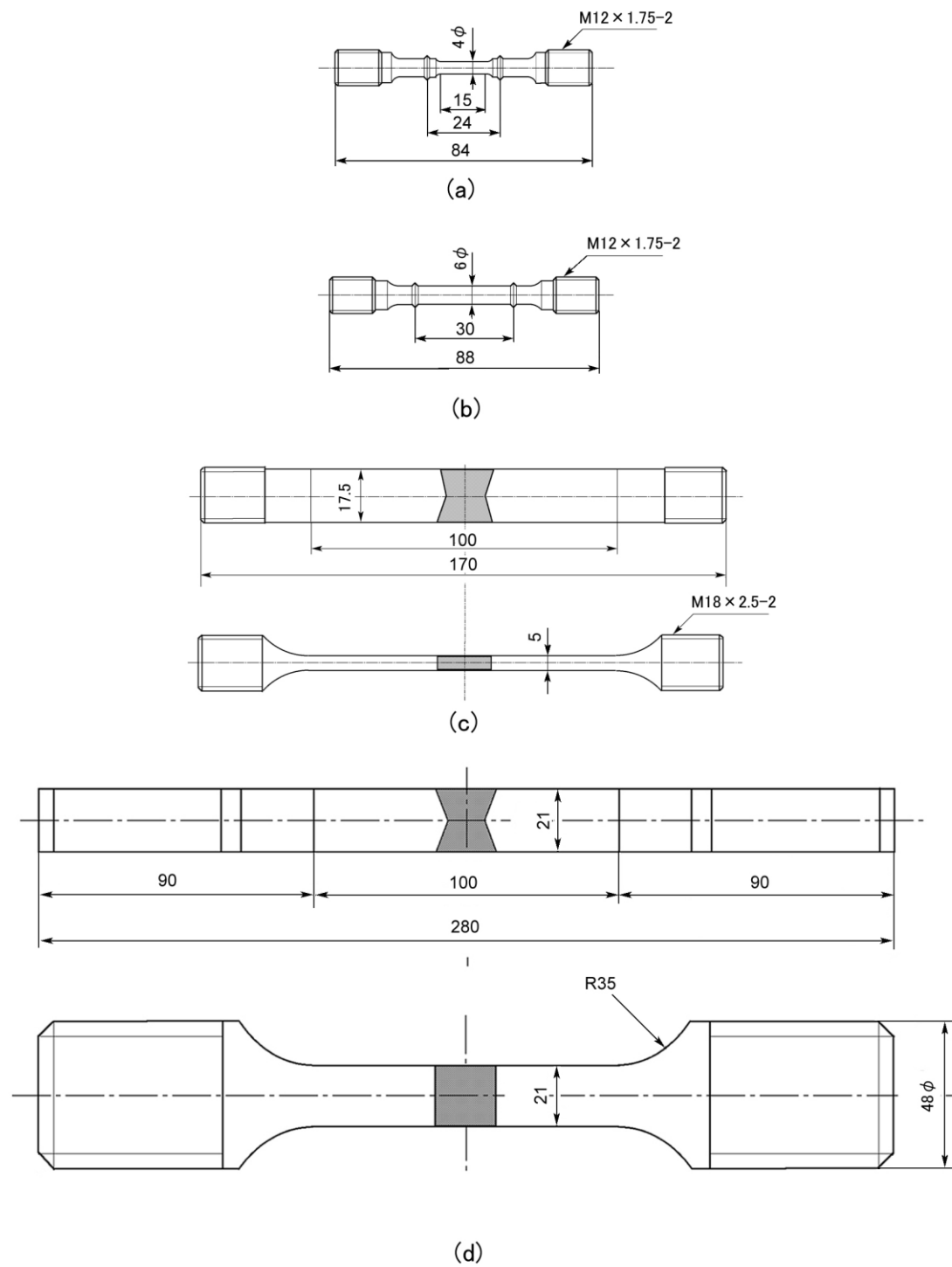


Fig. 2-2. Dimensions of the creep specimens for (a) the simulated HAZ, for (b) base metal, for (c) thin plate welded joint, and for (d) thick plate welded joint. (All dimensions in mm).

Table 2-3. Results of creep tests on the base metal.

Temperatures (°C)	Stress (MPa)	Time to rupture (h)	Elongation (%)	Reduction of Area (%)	Minimum strain rate (h ⁻¹)
550	240	290.7	31.0	88.0	1.79E-02
	220	2392.5	28.6	88.1	1.77E-03
	200	10432.9	26.4	86.2	3.24E-04
	190	18514.7	27.2	82.9	1.45E-04
600	160	501.4	34.9	89.3	9.57E-03
	140	2550.2	32.1	89.0	1.63E-03
	130	6036.8	30.7	83.0	5.31E-04
	110	19907.5	23.7	79.8	9.60E-05
650	90	928.0	32.2	87.9	3.59E-03
	80	2726.1	34.6	80.7	1.16E-03
	70	8385.6	32.8	81.6	4.57E-04

Table 2-4. Results of creep tests on the simulated heat affected zone.

Temperatures (°C)	Stress (MPa)	Time to rupture (h)	Elongation (%)	Reduction of Area (%)	Minimum strain rate (h ⁻¹)
550	200	289.7	26.6	89.2	1.72E-02
	190	960.4	31.6	88.7	5.14E-03
	170	6147.6	22.1	86.7	4.81E-04
600	140	63.5	43.7	93.3	1.49E-01
	120	155.0	38.6	92.9	6.13E-02
	100	1271.9	42.8	91.3	4.48E-03
	80	6295.0	35.3	89.0	2.46E-04
650	70	167.5	47.8	91.3	7.14E-02
	50	1536.2	35.2	82.0	5.08E-03
	40	6948.5	29.1	80.4	7.59E-04

Table 2-5. Results of creep tests on the welded joint (thin and thick).

Welded joints	Temperatures (°C)	Stress (MPa)	Time to rupture (h)	Elongation (%)	Rupture locations
Thin welded joints	550	240	451.6	14.4	in BM
		220	1783.9	11.4	in BM
		200	8662.6	7.6	in HAZ
		170	20460	2.8	in HAZ
	600	140	983.9	2.9	in HAZ
		130	1341.7	2.6	in HAZ
		100	4324.8	2.2	in HAZ
		90	7147.1	0.9	in HAZ
		80	10330.5	1.3	in HAZ
	650	80	349.9	2.1	in HAZ
		70	862.3	1.6	in HAZ
		50	3568.2	1.3	in HAZ
Thick welded joints	600	90	8853.4		in HAZ

2.3 Hardness Profile in the Welded Joint

In terms of cost performance, the hardness measurement can be even better than the tensile test for evaluating the strength. We can use a hardness profile to identify the local variability of strength in a welded joint, particularly the weak position in the HAZ. Thus, the Micro-Vickers hardness measurement was conducted on the welded joint specimens in the longitudinal direction. The location is about 1/4 in the thickness direction paralleling to the welded joint as shown in Fig 2-3. With regard to the hardness welded joints under the conditions of as weld and crept were measured in Hardness. The specimens were crept with the rupture time of 20,460h and 3,568h at 550°C and 650°C respectively.

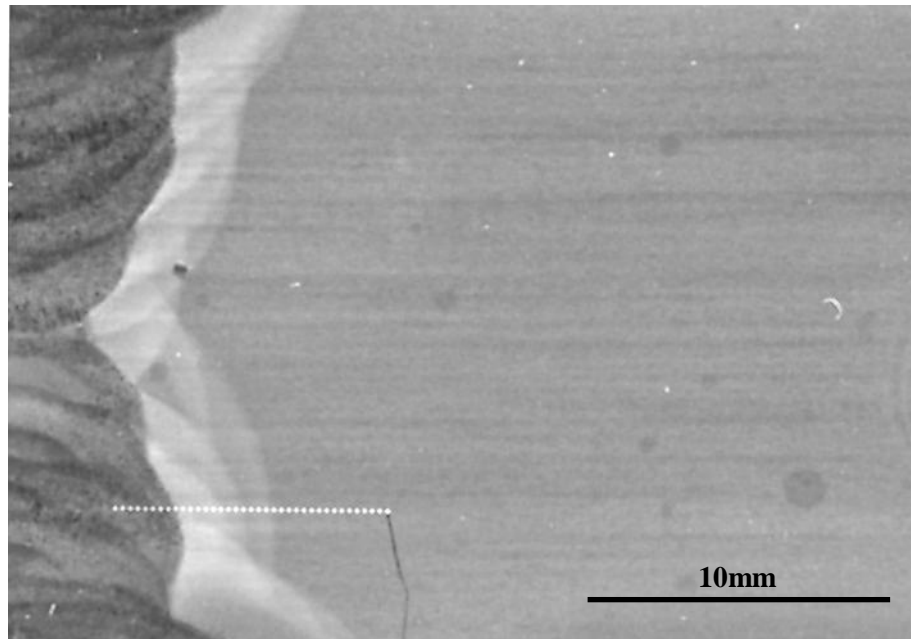


Fig. 2-3. Hardness checking path denoted with the white dots in the diagram.

2.4 Specimens of Simulated HAZ

The specimens for the weak zone were fabricated from the base metal of the thick plate of the Mod.9Cr-1Mo steel. Gleeble is a thermo-mechanical simulator, which can give the weld thermal cycles to specimens by supplying current directly into the specimen (direct resistance heating) under the mechanically constrained condition. The specimens were preheated at 200°C, and then were simulated by rapid heating to the peak temperature with the speed of 60°C/s and followed by the gas cooling with the speed of 40°C/s to the temperature of 430°C using weld a simulator. After that, the specimens were cooled in air. The thermal history profile is shown in the Fig 2-4.

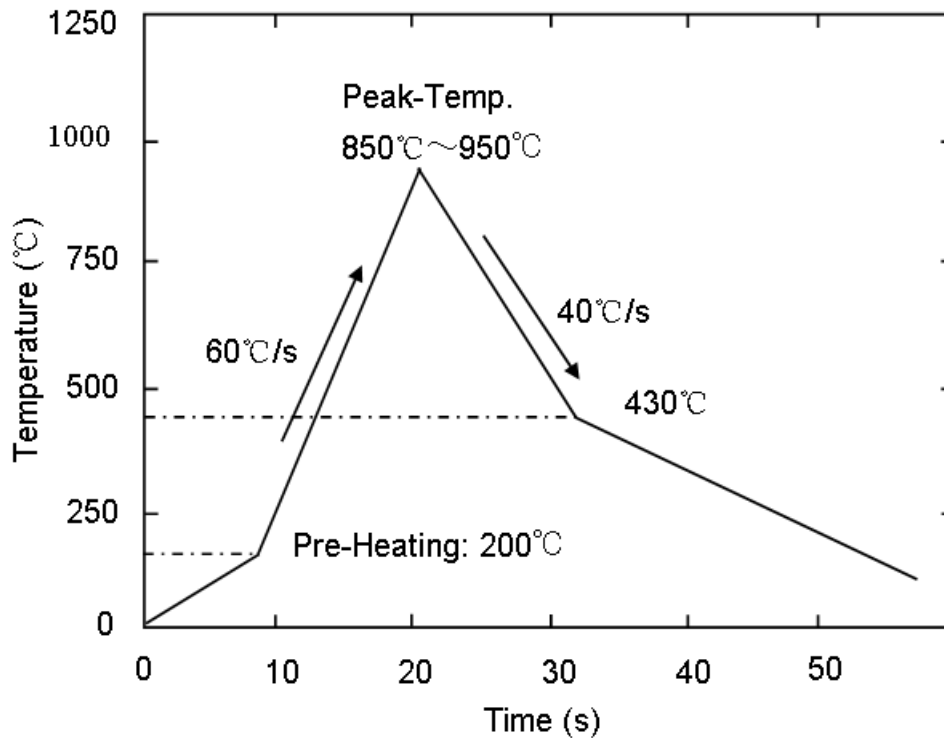


Fig. 2-4. Simulated processing used for the simulated heat affected zone of the welded joint in the weld simulator.

The peak temperatures were selected in the ranges around A_{c3} point of the Mod.9Cr-1Mo steel, and the temperatures of 850°C, 870°C, 900°C, 925°C and 950°C were selected as the peak temperature. After the finished up the procedure in the weld simulator, the specimens were tempered at 745°C for 1 hour. Figure 2-5 shows the photographs of the base metal and the simulated HAZ observed by scanning electron microscope (SEM). Comparing with the six photographs, the base metal has the larger grain size while the specimen simulated with the peak temperature at 900°C has the smaller grain size. The several specimens of the simulated weak zone were investigated in the hardness and crept under the two stress levels of 120MPa and 140MPa at 600°C. The Vickers hardness was lower for the specimens simulated with the peak temperatures of 850°C and 870°C in Fig 2-6, which should be the tempering zone of the HAZ that localized in the part between the inter-critical HAZ and base metal in a

welded joint as shown in Fig 2-2. The creep testing results are shown in Fig 2-7, and the specimen with the peak temperature of 925°C was the weakest under the stress of 140MPa while the specimen with the peak temperature of 900°C was the weakest under the stress of 120MPa. The specimen of the base metal was the stronger comparing with the simulated HAZ specimens with different temperatures under the two stress levels. At high stress range, the creep strength of the simulated HAZ was decreasing with the applied stresses, and the weakest zone of the HAZ was the tempering zone under the applied stress of high levels.

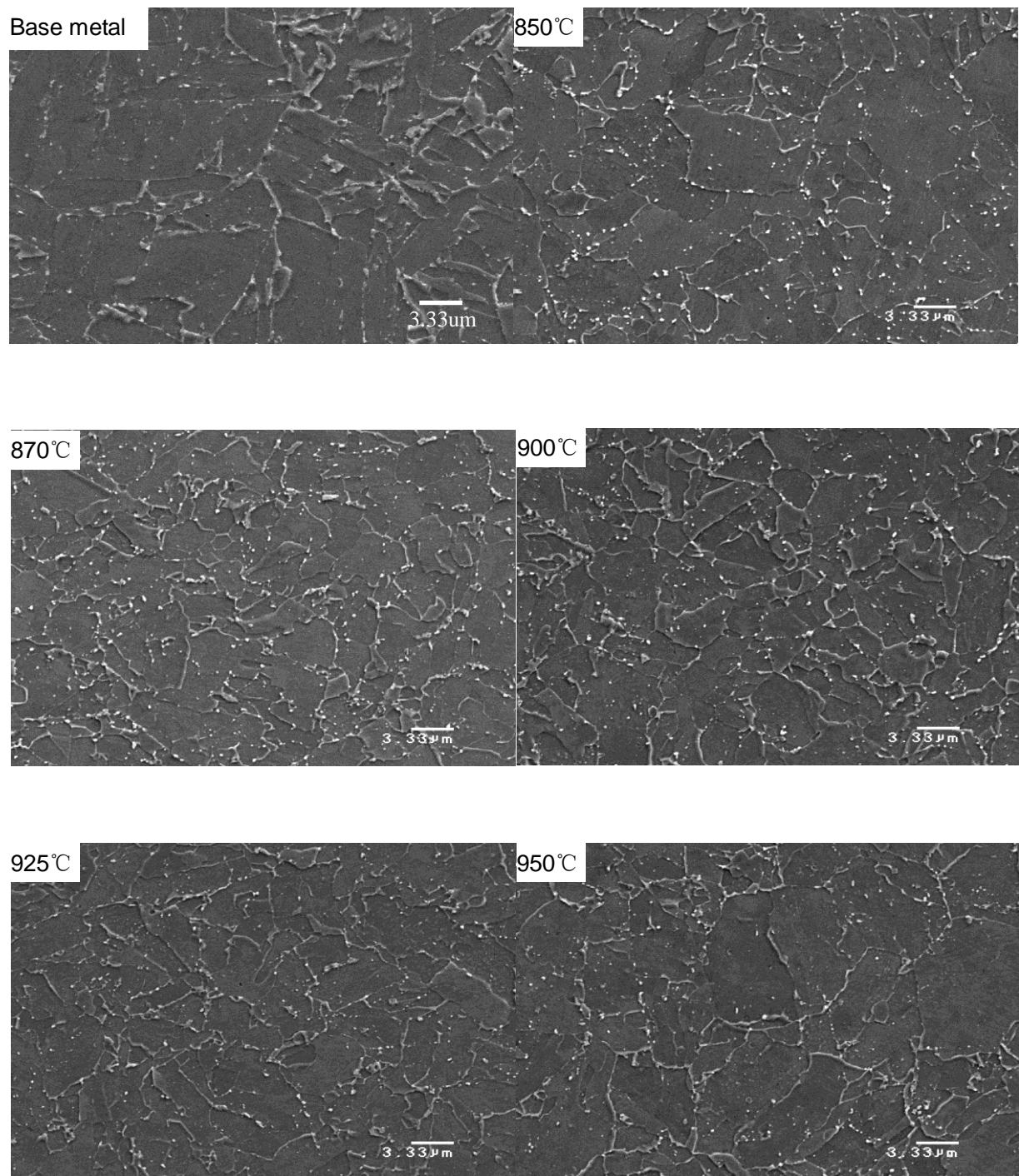


Fig. 2-5. Observation the grain size of the base metal and the simulated weak zone with different peak temperatures by SEM.

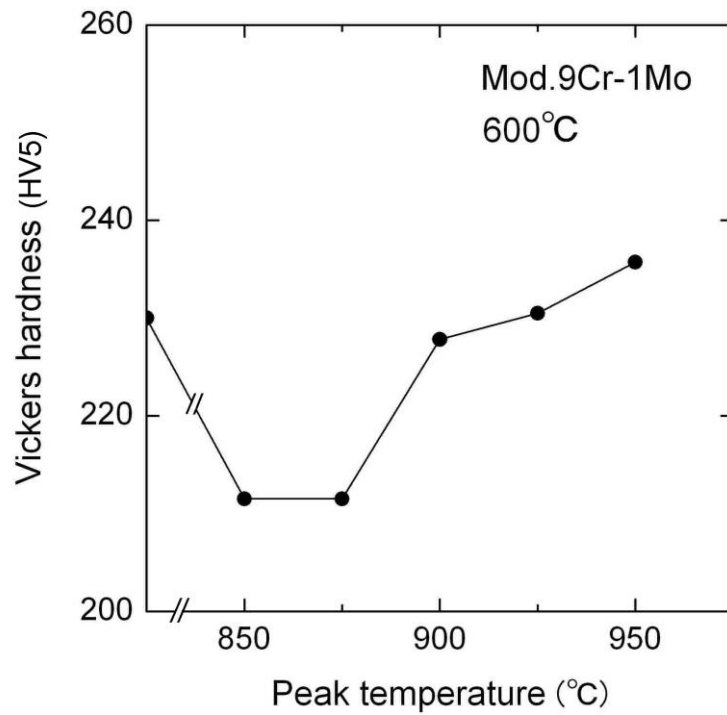


Fig. 2-6. Changes in Vickers hardness for the base metal and weak zone with simulated at different peak temperatures.

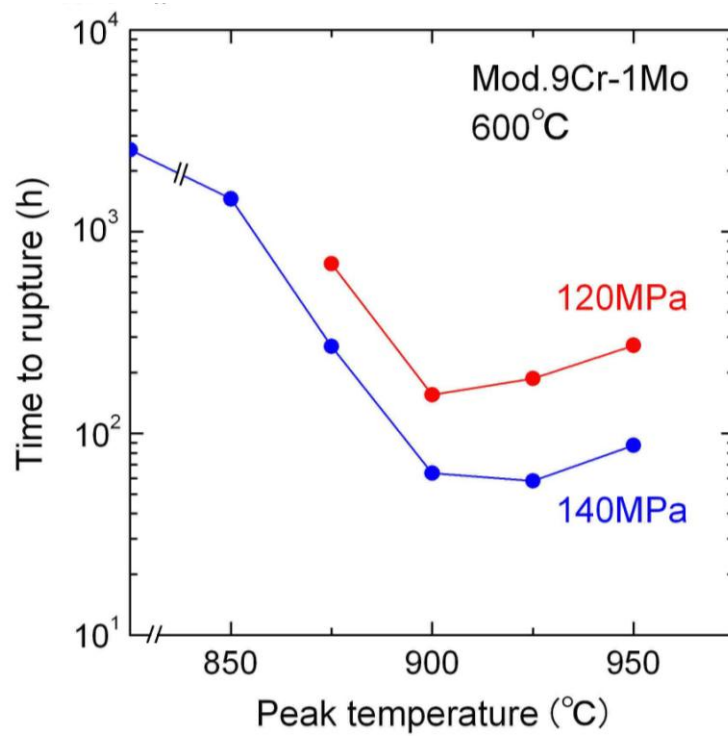


Fig. 2-7. Rupture life of the base metal and the simulated weak zone with simulated at different peak temperatures.

Thus we used the base metal specimens for the simulated weak zone with the peak temperature of 900°C in the weld simulator. The microstructures of the simulated weak zone and base metal were observed with using the optical microscope (OM) and transmission electron microscopy (TEM) as shown in Fig 2-8. From the photographs, the grain diameter is about 3μm for the simulated HAZ and lath martensite phase was not found.

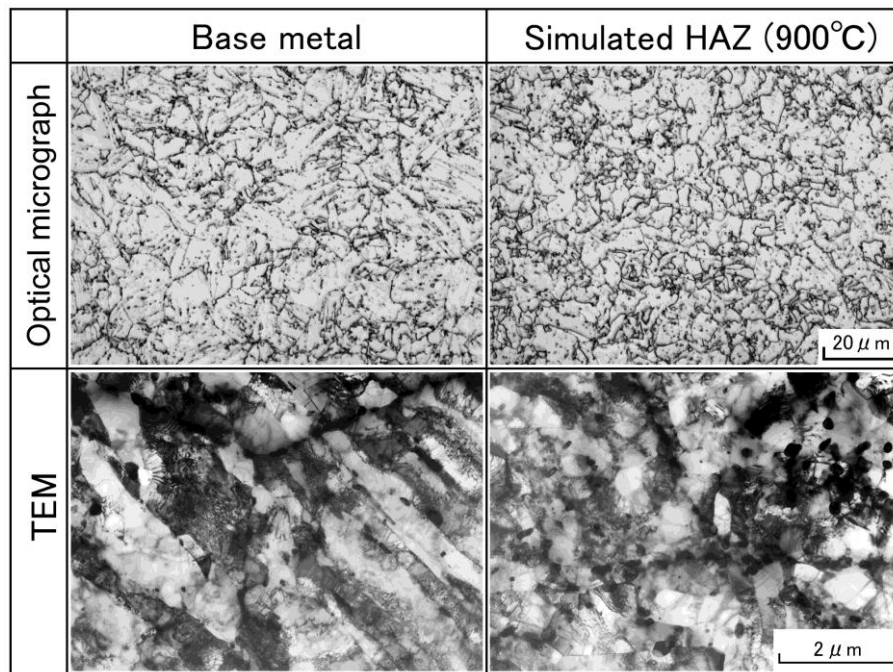


Fig. 2-8. Microstructures of base metal and simulated HAZ heated to the peak temperature of 900°C.

2.5 Measurement of the Voids in Thick Welded Joint

Normally the Type VI cracking was found in the fine-grained HAZ or inter-critical HAZ of a weldment during long term creep exposure at elevated temperatures, which is believed to be produced by the connection of voids after formation and growth. We are interested in the evolution of void process in the thick welded joint of Mod.9Cr-1Mo steel during creep. The void observation in the HAZ was made for the interrupted specimens crept under 90MPa at 600°C.

2.5.1 Observation of Voids in HAZ of Welded Joint

These thick plate specimens whose dimensions and shape are shown in Fig 2-3d were crept at 600°C under the applied stress of 90MPa, the creep testing machine has a maximum capacity of 50 ton shown in Fig 2-9. The creep tests were interrupted at about 1010h, 2000h, 4425h, 6000h, 7040h and 7970h during creep in order to investigate the damage processes as shown in Fig 2-10. The figure indicates that several specimens of the thick welded joint creep at the same conditions at the temperature of 600°C and the stress of 90MPa. All the creep tests except one were interrupted before rupture. The rupture life (t_r) for the thick welded joint in present condition was 8,853h and the thick welded joint specimen shown in Fig 2-11 was taken after rupture at 600°C.



Fig. 2-9. 50t heavy-loading creep testing machine used for testing the specimens of the thick welded joint.

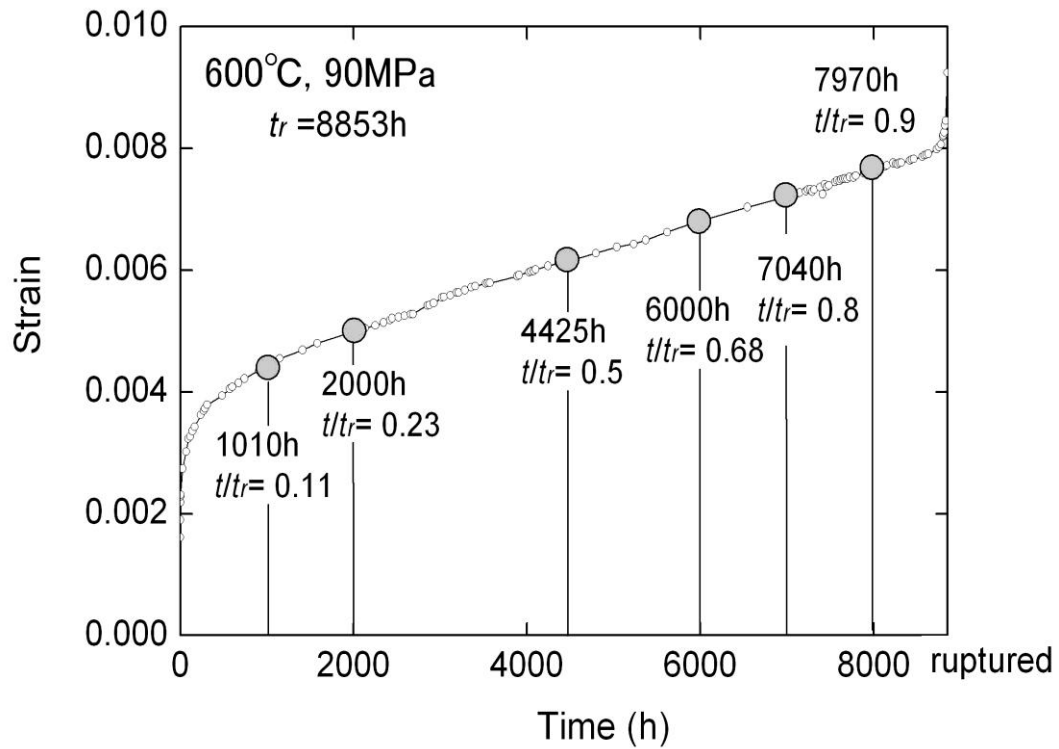


Fig. 2-10. Sketch map for the interrupted times of the different thick welded joints at 1010, 2000, 4425, 6000, 7040 and 7970h with the creep conditions of 600°C and 90MPa.

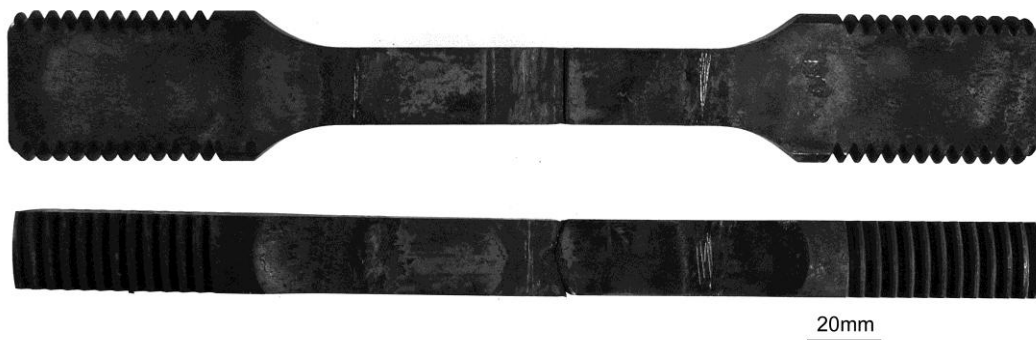


Fig. 2-11. The ruptured thick welded joint crept under 90MPa at 600°C.

After each interruption of creep tests of the thick welded joint at 600°C under 90MPa, those specimens were cut in order to observe the creep damages on the central cross section of the welded joint. Figure 2-12 illustrates the procedures for fabricating the specimens in a thick

plate welded joint after the creep interruptions. The chemical etching was carried out for about 1h in a solution of 4% nitric acid and ethanol after automatic polishing machine. Before we observed the specimens, the etched specimen should be cleaned in the ethanol solution with an ultrasonic cleaner. As shown in Fig 2-12, along the HAZ, the cutting specimen was divided into 10 equal parts by 11 locations to be observed, with the resolution of 2mm in y-direction. On the every location, the voids were measured in an rectangular area with 0.2×2mm using a LASER microscope (VK-8500 by KEYENCE Japan with the minimum resolution of 0.01 μ m).

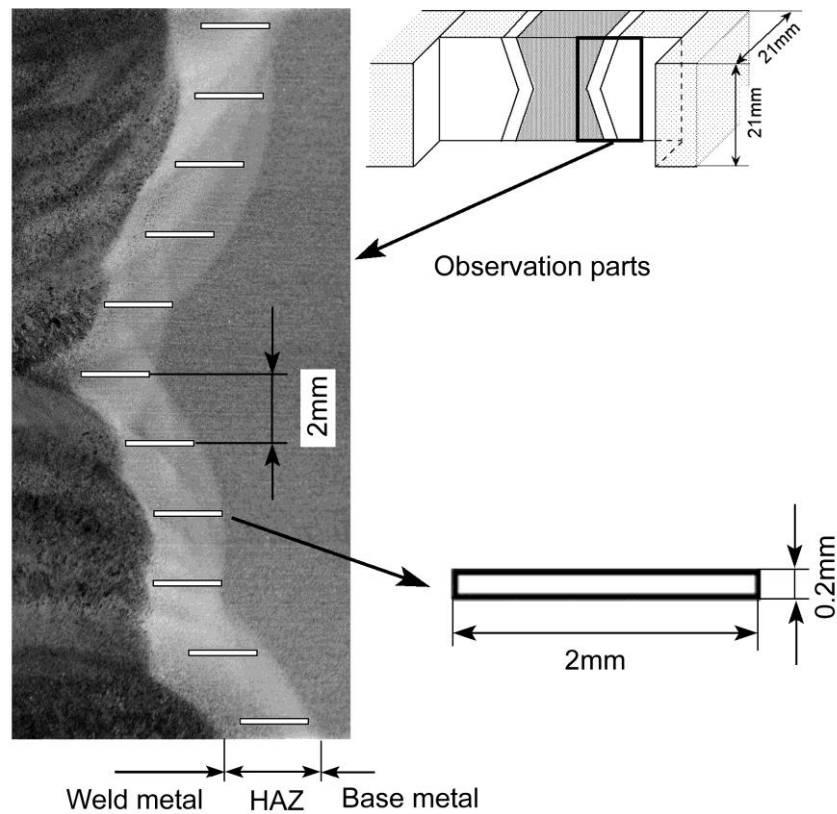


Fig. 2-12. Procedures for measurement of creep voids in a thick plate welded joint after interruption of creep test.

At every rectangular area, more than 25 photographs were taken for covering the weak zone containing the voids with using the LASER microscope. The photographs taken from the

HAZ of the thick welded joint were pieced together and then formed the large one as shown in Fig 2-13 that was taken for the specimen at 7970h interruption. The photographs for observing the voids in HAZ at other interruptions were listed in the appendix. As shown in Fig 2-12, the rectangular areas actually cover the whole HAZ in the longitudinal direction of the welded joint specimen. Therefore, one area as shown in Fig 2-13 would take about photographs from 25 to 30 pieces so that it took about 275~330 photographs at a interruption during creep.

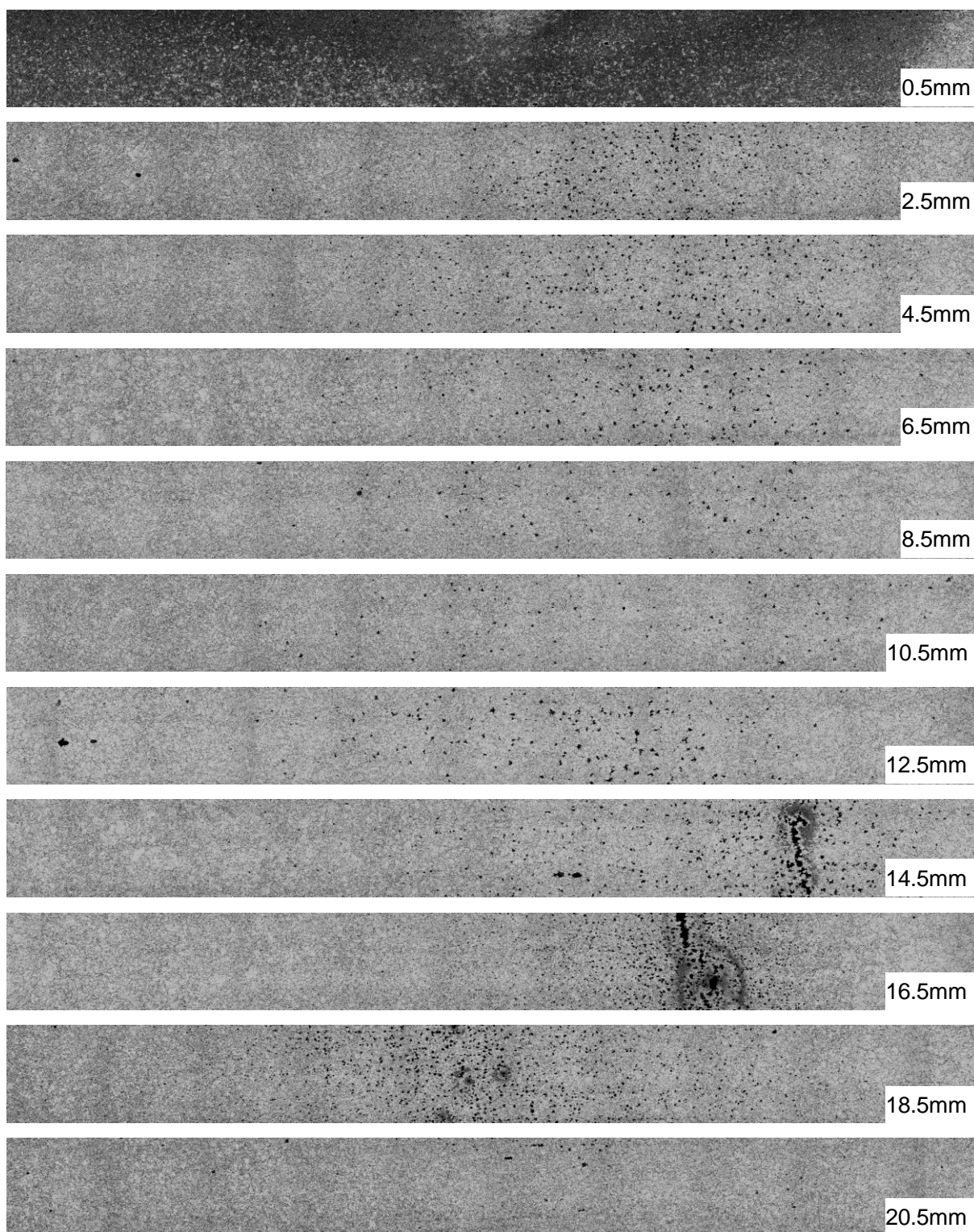


Fig. 2-13. Photographs pieced together for the rectangular area with 0.2×2mm at 11 coordinates at the interruption of 7,970h.

Apparently, large Type IV cracking and a number of voids are found in 4.5, 16.5, 18.5 mm location from the top surface at this time step. After interruptions at 2,000, 6,000, 7,040 and 7,970h, the photographs of the full profile view of the specimens were also pieced together as shown in Fig 2-14. After imaging processing, the black dot image indicates the evolution of void process. In Fig 2-14, the voids were found prominently tending to form in the narrow zone in HAZ of the thick welded joint. The voids distribute in the zone like a saddle along the fusion line within the HAZ of the thick welded joint after long term exposure at this temperature.

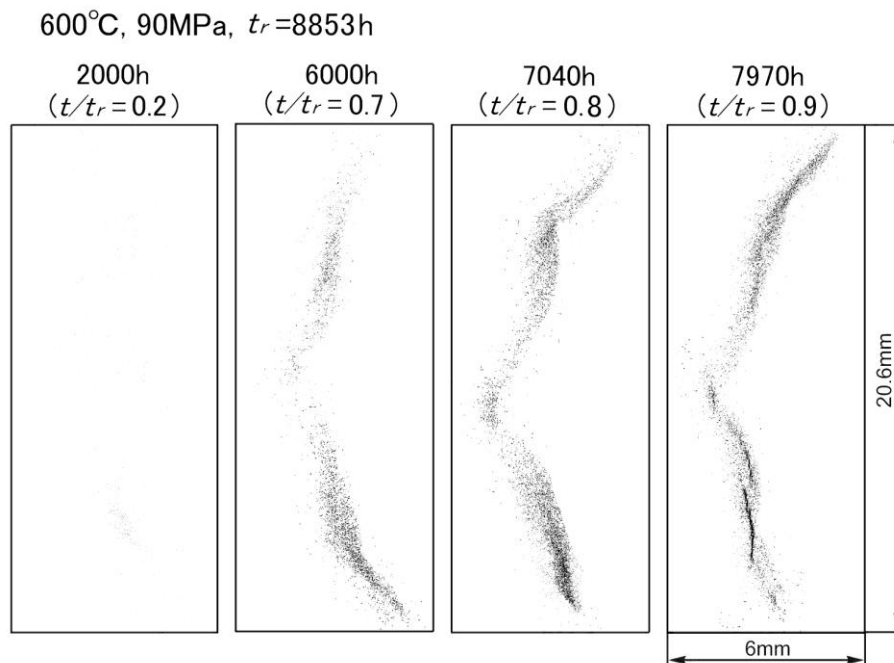


Fig. 2-14. Binary images of creep voids and cracks observed in the central cross section of HAZ of different thick plate welded joint after interruptions of creep test at 2000, 6000, 7040 and 7970h.

2.5.2 Void Counting Using Image-Pro Plus Software

We checked every photograph and the voids were counted by an image processing software , Image-Pro Plus Version 6.2 from MediaCybernetics, after the format of the

images were changed into *.JPEG. The software can give us state-of-the art imaging and analysis capability for acquire, enhancing and analyzing our images [2-2]. Followings are the feature of Image-Pro PLUS software:

- (1) Acquire image data from a camera, microscope, vertical redundancy check (VRC), or scanner;
- (2) Read and write data in all the standard image file formats including, TIFF, JPEG, BMP, TGA, and many others;
- (3) Perform image enhancement using powerful color and contrast filters, including Fast Fourier Transforms (FFT), morphology, field flattening, background subtraction and other spatial and geometric operations;
- (4) Trace and count objects manually or automatically (We selected the target voids manually in this studies.). Measure object attributes such as: area, angle, perimeter, diameter, roughness and aspect ratio (The terms of area and diameter of voids were selected.).
- (5) View collected data numerically, statistically or in graphic form, save the operation recorder which could be folded with the software so that some other terms to be checked could be conducted again.

The counting interface when we were selecting the area of interest (AOI) using the Image-pro software is shown in Fig 2-15.

We counted the voids in the 11 locations taken from the HAZ of the thick welded joint at the listed creep time steps. The voids counted are no less than 1 micron in size. The results are shown in the Table 2-6, Table 2-7, Table 2-8 and Table 2-9 for observing the interruptions at 2000h, 4425h, 6000h and 7970h respectively. The voids could not found in the HAZ at the earliest interruption of 1000h. We have to note that the experimental data for the voids counting were all from one side of HAZ of the thick welded joint.

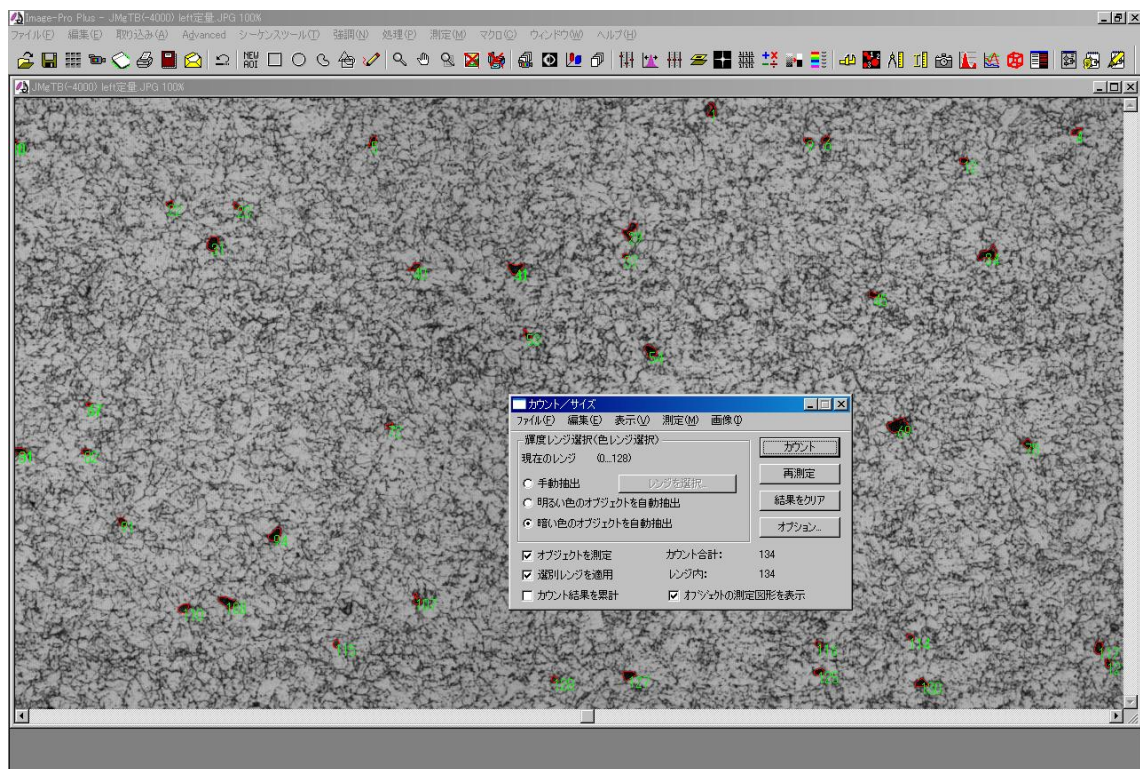


Fig. 2-15. The counting interface of the Image-Pro software.

Table 2-6. Void counting at 2,000h interruption in left side of the HAZ of the thick welded joint crept at 600°C and 90 MPa.

Locations in the Machine	Distance from Back Side (mm)	Numbers	Fraction of Area	Average Diameter (μ m)
10000	0.5	46	0.0004	2.0332
8000	2.5	298	0.0014	1.5240
6000	4.5	298	0.0017	1.6176
4000	6.5	102	0.0005	1.5740
2000	8.5	46	0.0004	1.9822
0	10.5	37	0.0002	1.5710
-2000	12.5	53	0.0003	1.7915
-4000	14.5	96	0.0005	1.7021
-6000	16.5	292	0.0016	1.6296
-8000	18.5	43	0.0003	1.8922
-10000	20.5	59	0.0007	2.1802

Table 2-7. Void counting at 4,25h interruption in left side of the HAZ of the thick welded joint crept at 600°C and 90 MPa.

Locations in the Machine	Distance from Back Side (mm)	Numbers	Fraction of Area	Average Diameter (μ m)
10000	0.5	16	0.0003	2.7921
8000	2.5	758	0.0096	2.3661
6000	4.5	560	0.0082	2.5327
4000	6.5	118	0.0018	2.6124
2000	8.5	55	0.0009	2.6081
0	10.5	23	0.0003	2.4213
-2000	12.5	40	0.0005	2.4596
-4000	14.5	134	0.0025	2.8485
-6000	16.5	440	0.0045	2.1533
-8000	18.5	148	0.0017	2.2735
-10000	20.5	21	0.0004	2.9309

Table 2-8. Void counting at 6,000h interruption in left side of the HAZ of the thick welded joint crept at 600°C and 90 MPa.

Locations in the Machine	Distance from Back Side (mm)	Numbers	Fraction of Area	Average Diameter (μ m)
10000	0.5	19	0.0004	2.8852
8000	2.5	841	0.0150	2.7599
6000	4.5	892	0.0133	2.5360
4000	6.5	399	0.0070	2.7417
2000	8.5	111	0.0032	3.4312
0	10.5	102	0.0021	3.0098
-2000	12.5	76	0.0011	2.5711
-4000	14.5	181	0.0040	3.3532
-6000	16.5	591	0.0089	2.5593
-8000	18.5	128	0.0020	2.5664
-10000	20.5	15	0.0004	3.5124

Table 2-9. Void counting at 7,970h interruption in left side of the HAZ of the thick welded joint crept at 600°C and 90 MPa.

Locations in the Machine	Distance from Back Side (mm)	Numbers	Fraction of Area	Average Diameter (μ m)
10000	0.5	33	0.0009	3.3965
8000	2.5	908	0.0222	3.1561
6000	4.5	923	0.0207	3.0919
4000	6.5	357	0.0123	3.8232
2000	8.5	137	0.0048	3.8429
0	10.5	160	0.0055	3.8597
-2000	12.5	141	0.0030	3.0555
-4000	14.5	219	0.0063	3.5081
-6000	16.5	628	0.0090	2.4791
-8000	18.5	185	0.0036	2.8094
-10000	20.5	43	0.0007	2.6285

Table 2-10 summarizes the void counting to yield the area fraction and the void density.

Table 2-10. Summation of the voids in the 11 locations along left side of the HAZ of the thick welded joint at every interruption.

Time (h)	Number of Void	Area Fraction of Void	Density of Void ($1/\text{mm}^2$)
2000	1370	0.0007	498
4425	2313	0.0028	841
6000	3355	0.0052	1220
7040	3808	0.0061	1385
7970	3734	0.0081	1358

2.6 Summaries

By use of the base metal, the simulated HAZ and the welded joint specimens we obtained the grain size, hardness, and the effects of the peak temperatures on the creep-rupture times. The thick welded joints subjected to the creep testing under 90MPa at 600°C were interrupted at six different time intervals and subsequently measured the void distribution and density (the number of voids, the fraction of area, and the average of diameter) in 0.22mm area at 11 coordinates transverse to the HAZ.

In the following chapters we would use these data in the FEM analysis and the creep damage evolution based on the CDM.

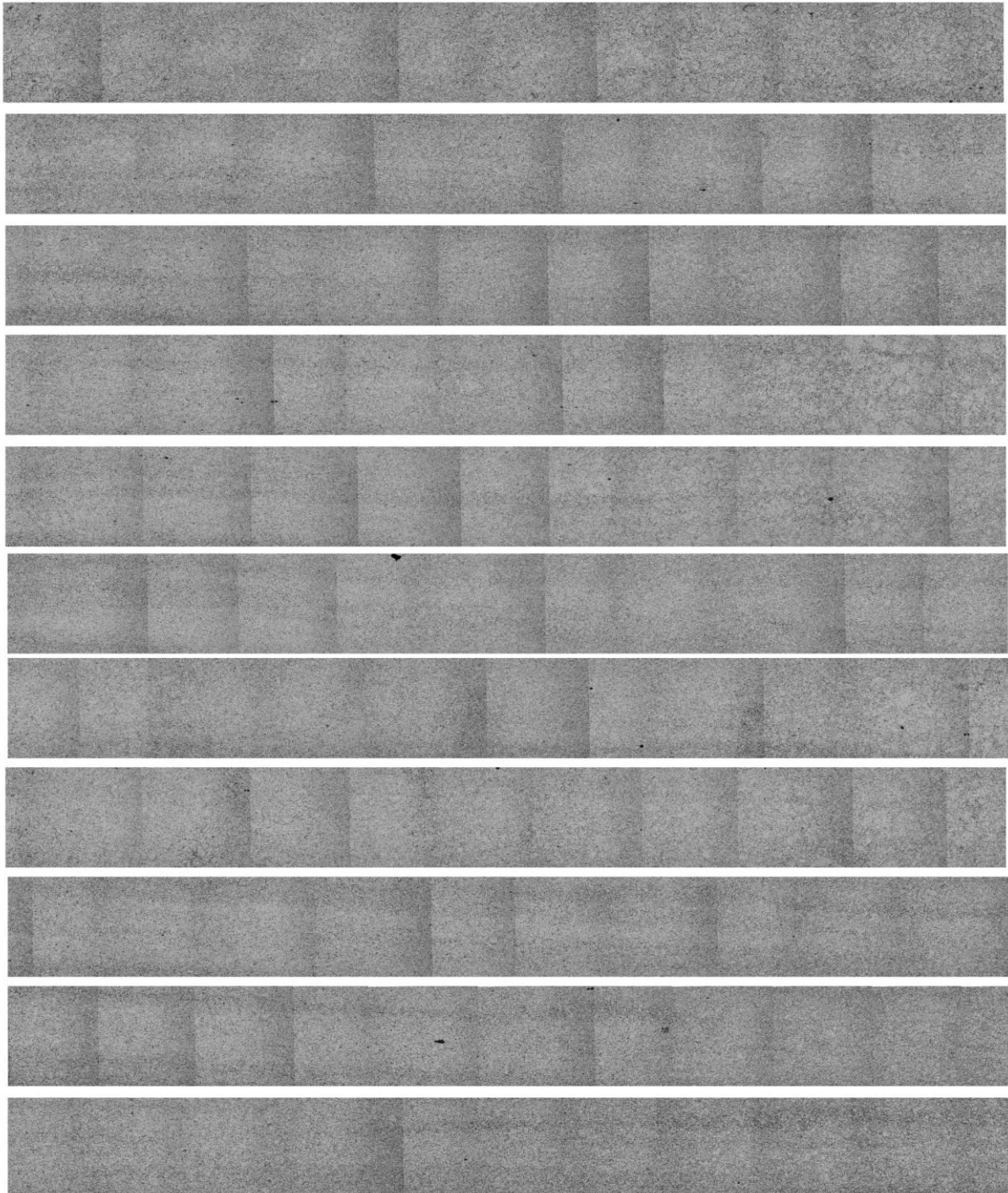
References of Chapter 2

- [2-1] S. Fujibayashi and T. Endo: Creep behavior at the intercritical HAZ of a 1.25Cr-0.5Mo steel, ISIJ International 42(11), pp.1309-1317
- [2-2] *Image-Pro Plus Version 6.2 for WindowsTM*. (Media Cybernetics, Inc. Georgia Avenue, 2006)

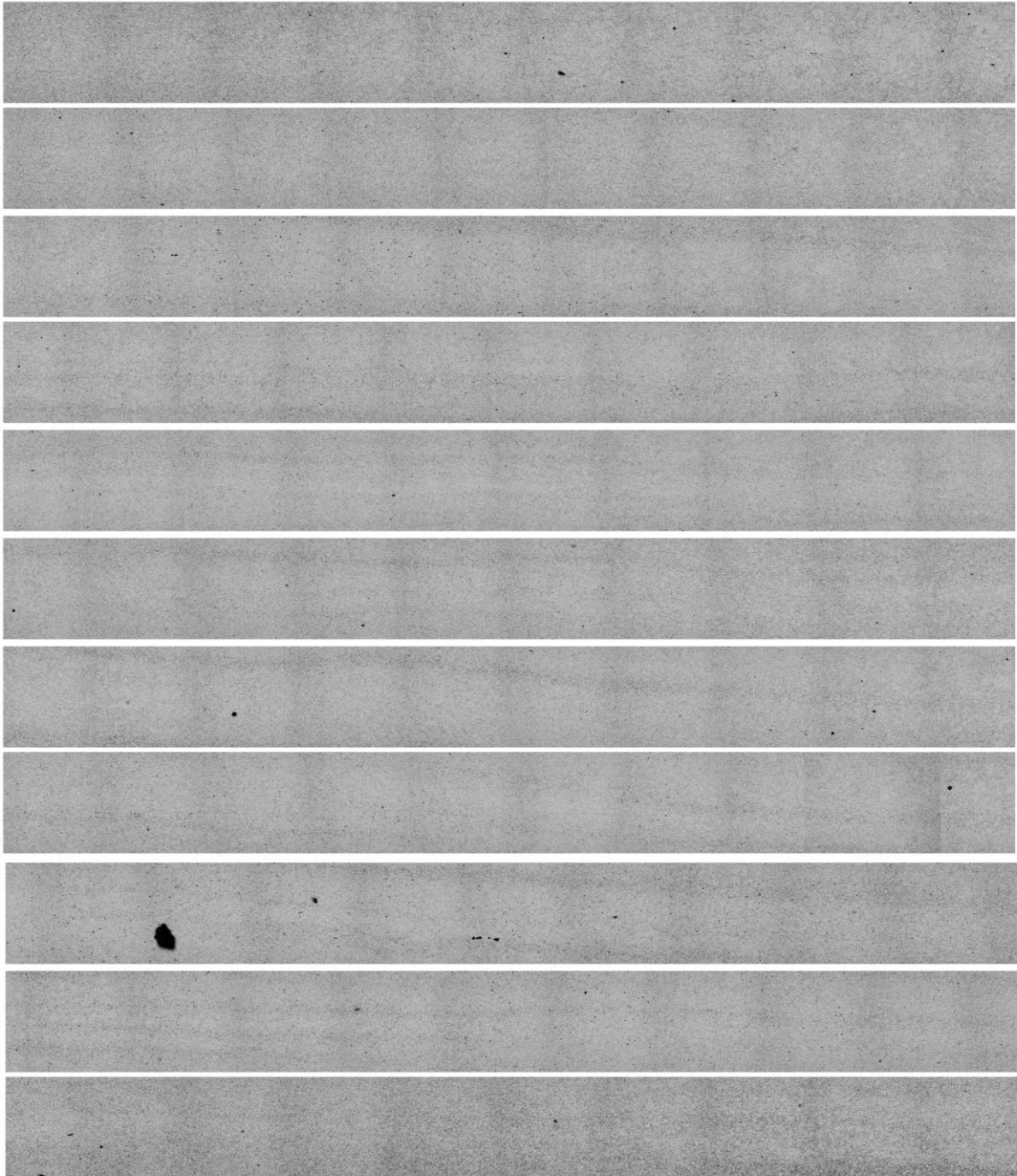
Appendix A

Microphotographs of 0.2mm×2mm areas in the HAZ of the thick specimens creep tested at 600 and 60 MPa.

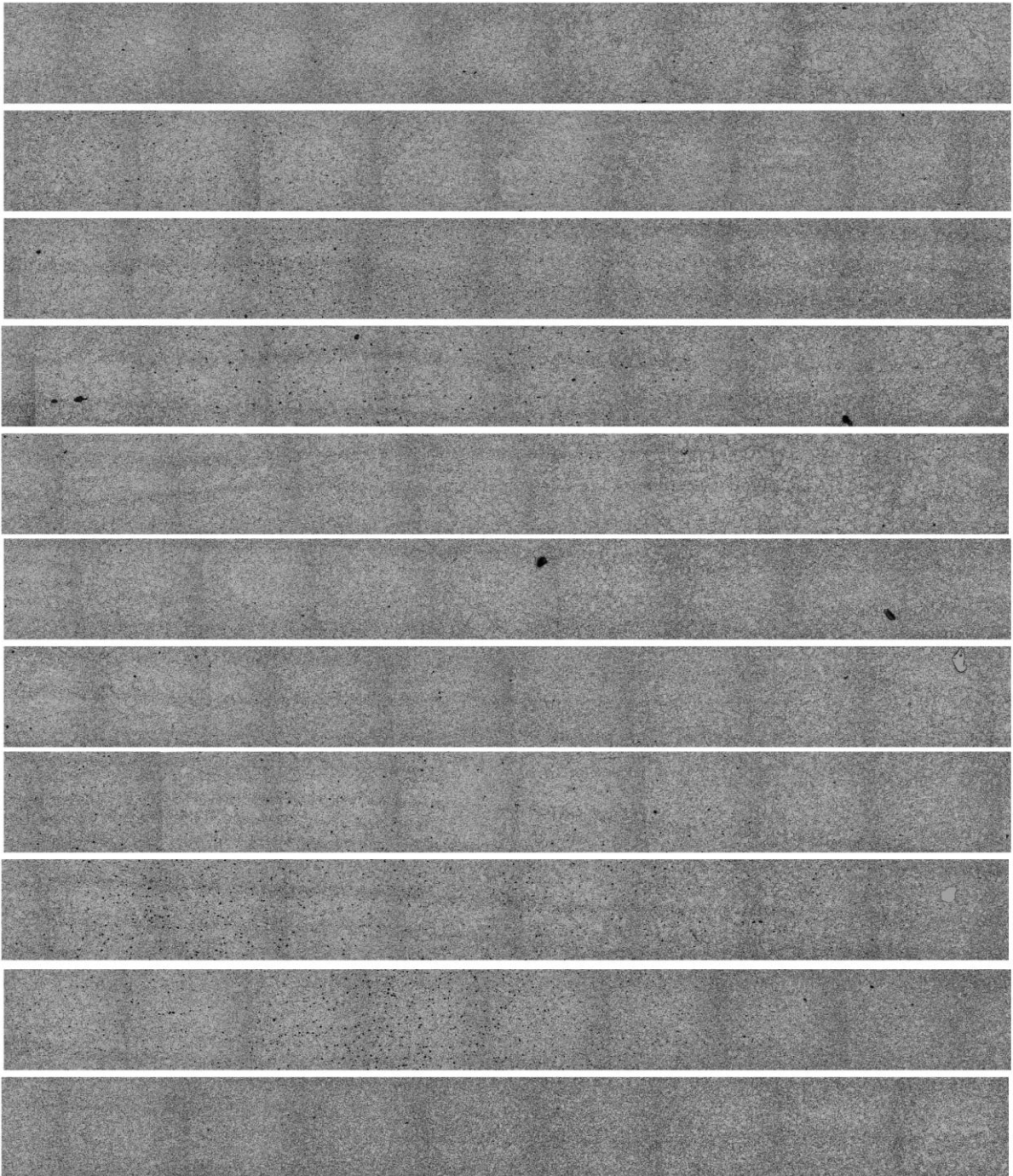
1) Interrupted at 1,000h



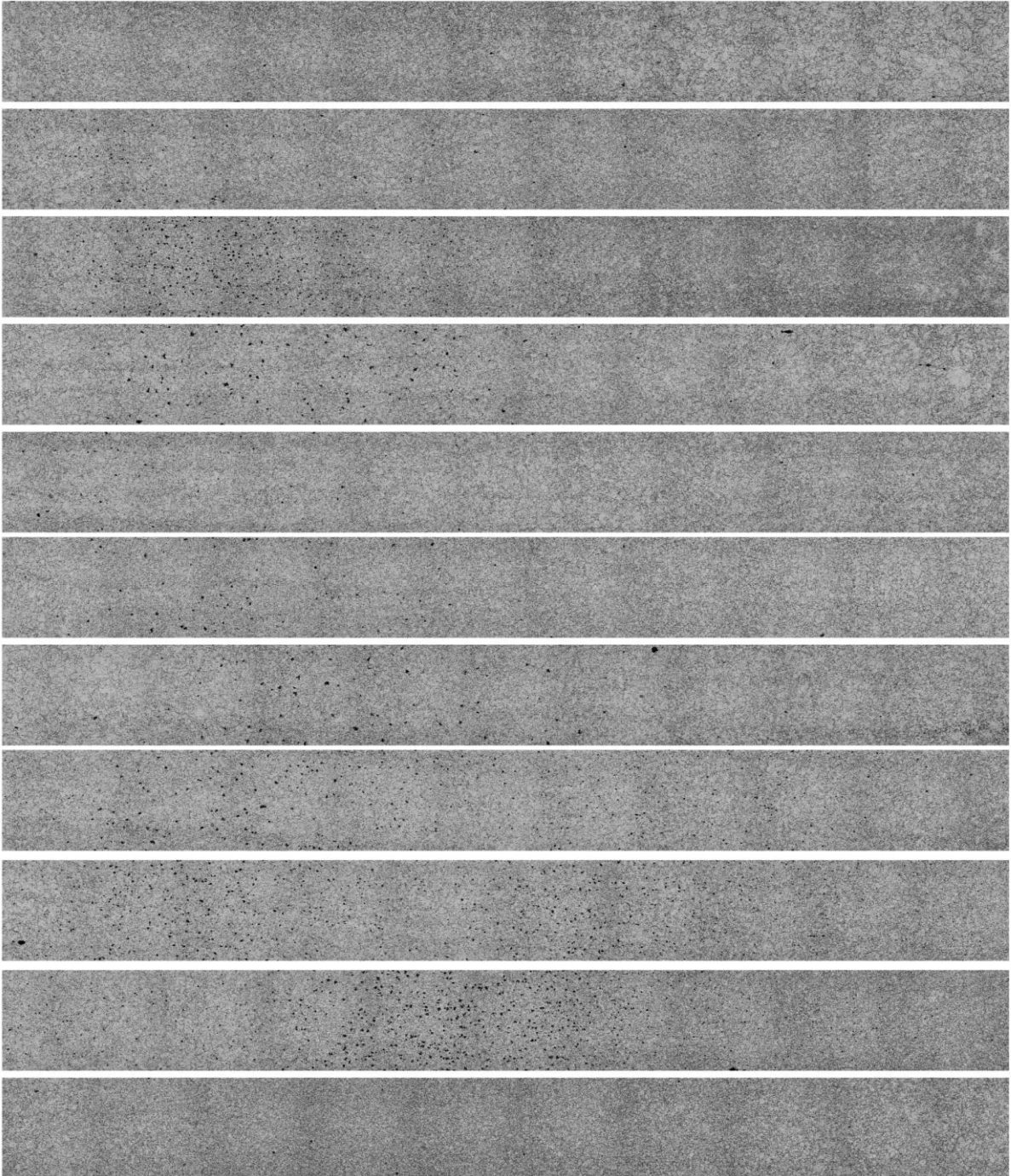
2) Interrupted at 2,000h



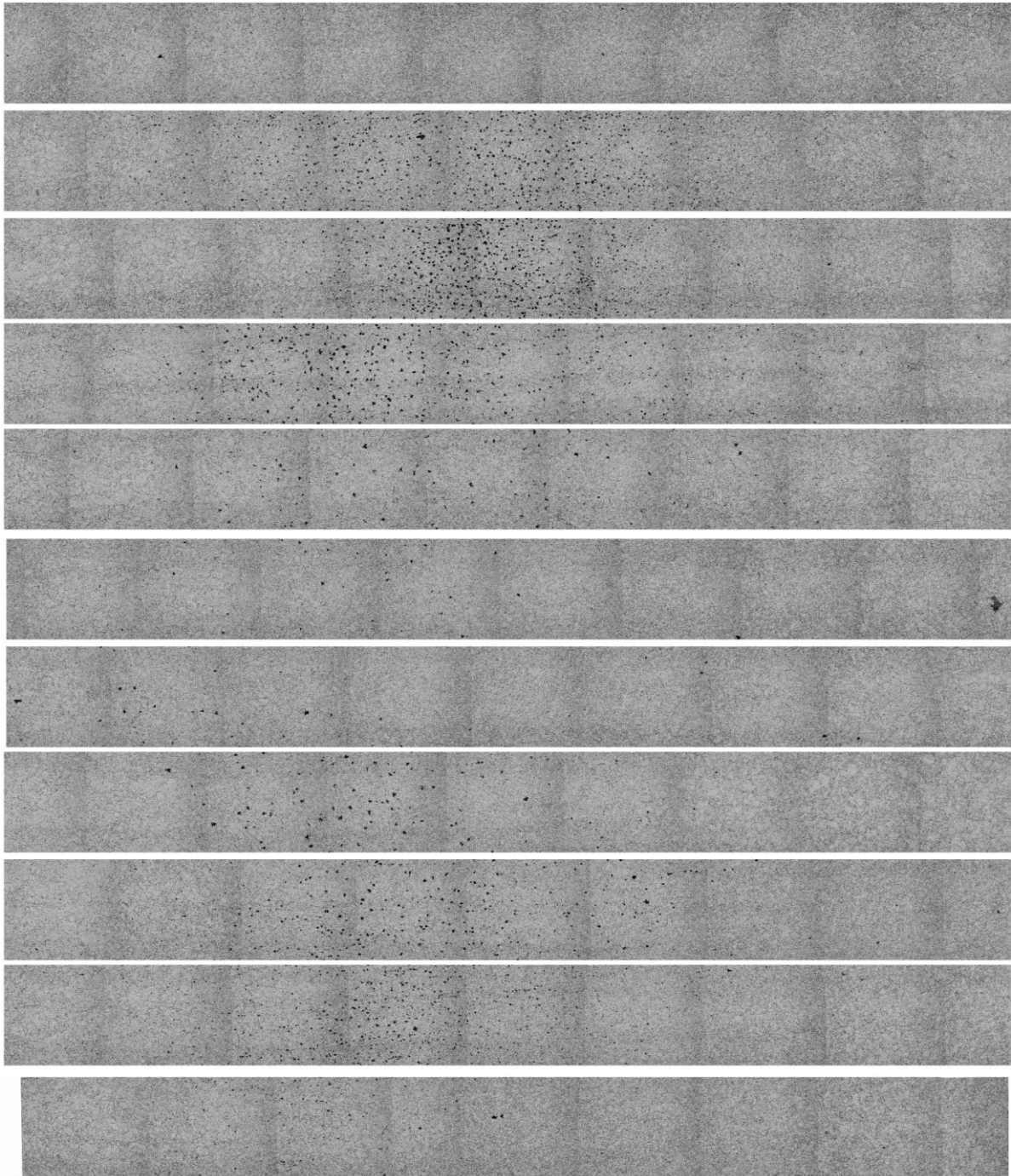
3) Interrupted at 4,425h



4) Interrupted at 6,000h



5) Interrupted at 7,040h



Chapter 3

Evaluation of Creep Damages in HAZ of Welded Joint

3.1 Introduction

Mod.9Cr-1Mo steel has been widely used for high temperature structures such as boiler components in ultra-supercritical (USC) thermal power plants operating at about 600°C. It is also a candidate material for a steam generator, intermediate heat exchanger and secondary piping of the liquid metal faster breeder reactor (LMFBR), and a pressure vessel and some internal structures of the high-temperature gas cooled reactors (HTGR) due to its high creep strength. However, it has been reported that the creep properties of the welded joints are inferior to those of the base metal and weld metal because of the Type IV cracking in the fine-grained HAZ paralleling to the fusion line at high temperature [3-1, 3-2]. Researcher and engineers have been investigating the mechanisms of Type IV fracture both from the microstructural approaches and mechanical approaches [3-3, 3-4 and 3-5]. However, the mechanisms of Type IV cracking have not been fully understood, where the Type IV cracking took place is still a confused problem. We will discuss the mechanism in details in Chapter 5. The complicated stress state distributed in the welded joint affects the formation and growth of creep voids prior to the crack growth in the Type IV zone, which occupies a large fraction of the creep life.

During the past years, several creep damage models were proposed in order to describe the nonlinear creep behavior of initially isotropic solids at high temperatures. After Kachanov first proposed the continuum damage mechanics to evaluate the creep life of a structure in 1958 [3-6], the damage mechanics has been applied for predicting creep damages and lives of components under complicated stress conditions [3-7]. Hyde *et al* predicted the creep damage

distributions and crack growth life of circumferential pipe welds by damage mechanics using creep data of parent, weld and HAZ of new and serviced materials [3-5]. Eggeler *et al.* investigated the effect of hoop, axial and radial stress distributions of a P91 pressure vessel with welds using the creep data of base metal, weld metal and simulated intercritical HAZ [3-4]. Bauer *et al.* analyzed the stress-strain situations and multiaxial stress state in various pipe models including welds for predicting creep life, and clarified the effect of creep strength of weld metal [3-8]. The works referred here were all conducted with the aid of the FEM. The FEM was popular to solve the evaluation on creep damage and deformation during creep because of no testing costs.

The experimental creep damage distributions and evolutions of high Cr steel welds, however, were scarcely investigated, and the comparison between experimental creep damage evolutions and numerical analysis is very limited conducted. In the present paper, we want to investigate the formation and growth processes of Type IV creep damages (voids and cracks) quantitatively using a full-thickness welded joint with double U grooves of the Mod.9Cr-1Mo steel. The failure mechanism is discussed comparing the experimental results with the stress-strain distributions and stress triaxial condition in the welded joint calculated by the FEM using.

3.2 Experimental Procedure

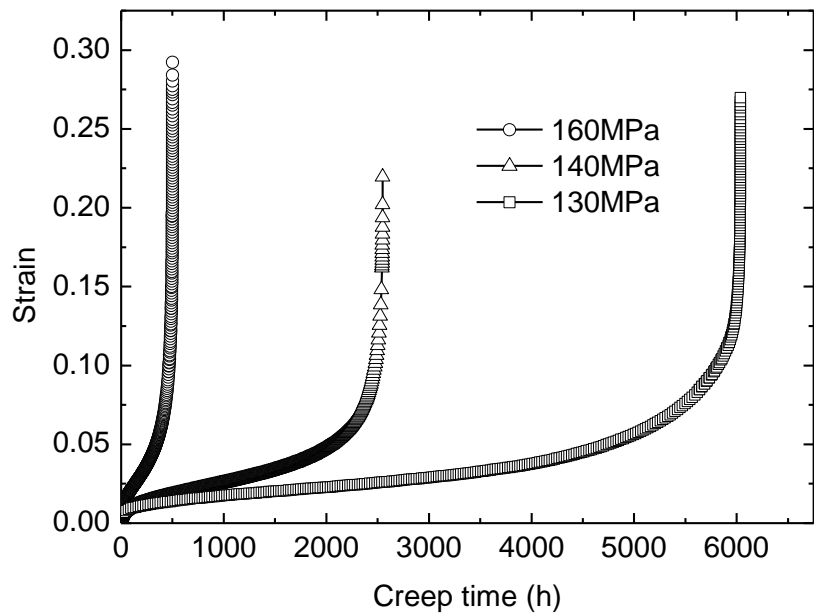
The creep tests and the specimens had been explained detailedly in Chapter 2. We present here the results of creep tests and measurement of creep voids are described briefly in the following sections. The creep properties and the FEM modeling are described in section of 3.2.3.

3.2.1 Creep Tests

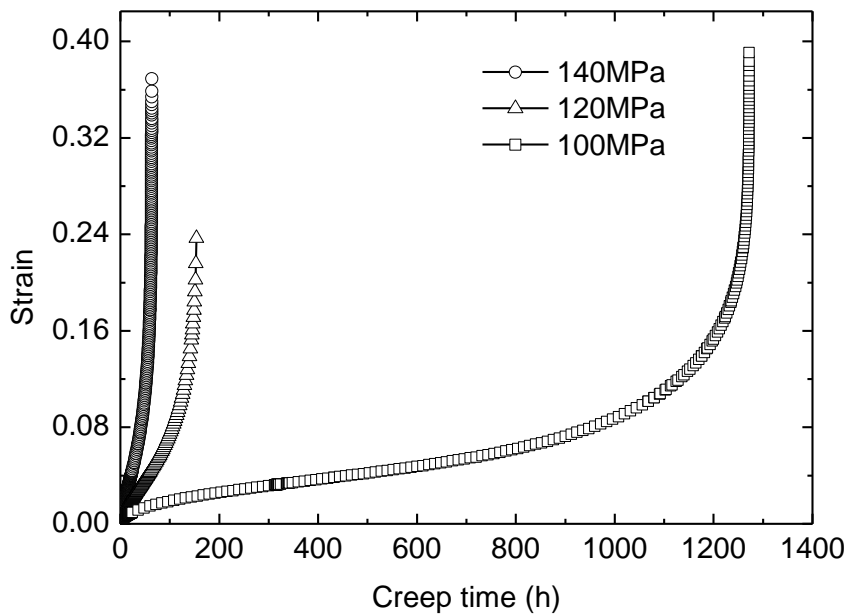
The material investigated in the present study is a Mod.9Cr-1Mo steel plate of 25mm in

thickness. The chemical compositions of base metal and the welding filler were given in Table 2-1 in Chapter 2. The plates were welded by using gas tungsten arc welding (GTAW) method with double U grooves. The post weld heat treatment (PWHT) adopted was to keep temperature at 745°C for 1 hour. The simulated HAZ specimens were produced by rapid heating (60°C/s) to the peak temperature 900°C and followed by the gas cooling (40°C/s) using weld simulator (Gleeble test).

The dimensions of the creep test specimens were indicated in Fig 2-2 in Chapter 2. The round bar specimens with 4mm in diameter and 15mm in gauge length for simulated Type IV zone (Fig 2-2a), those with 6mm in diameter and 30mm in gauge length for base metal (Fig 2-2b), and smooth thin plate specimens for the welded joint (Fig 2-2c) were machined and crept in long term at 550, 600 and 650°C with several stress levels from 40MPa to 240MPa. The strain-time curves for the base metal and simulated weak zone are shown in Fig 3-1. Several thick plate specimens shown in Fig 2-2d were also machined from the welded joint. These thick plate specimens were crept at 600°C under the applied stress of 90MPa, and the creep tests were interrupted at about 0.1, 0.2, 0.5, 0.7, 0.8, 0.9 of the rupture life in order to investigate damage processes. The interrupted conditions of creep tests were shown in Fig 2-10.



a)



b)

Fig. 3-1. Creep curves for a) base metal and b) simulated HAZ at 600°C.

3.2.2 Measurement of Creep Voids

Procedures for the measurement of creep voids in a thick plate welded joint after creep interruption were explained in Fig 2-10. After the interruption of each creep test of the thick welded joints at 600°C under 90MPa, those specimens were cut as shown in Fig 2-12 in order to observe the creep damages on the central cross section of the welded joint. The chemical etching was carried out for about 1h in a solution of 4% nitric acid and ethanol after automatic machine polishing. As shown in Fig 2-12, along the HAZ, the welded joint was divided into 10 equal parts by 11 locations. On the every location, the voids were measured in an area with $0.2 \times 2\text{mm}$ using a laser microscope and counted by an image processing software. The mean diameter of voids was in the range of from $1\mu\text{m}$ to $42\mu\text{m}$.

3.2.3 FEM Analysis

3.2.3.1 Constructing the Thick FEM Model

Comparing with the experimental measurement, a three-material (base metal, HAZ and weld metal) and three-dimensional finite element model shown in Fig 3-2 was constructed to calculate the stress-strain distributions in the thick plate welded joint specimen. Since the thick plate welded joint is a symmetrical structure according to the weld direction, half of the weldment was used to design the FEM meshing. The model has the dimensions of $21 \times 21 \times 50\text{mm}$, and composes of the 6660 elements and 8436 nodes.

The boundaries of the different components in the thick welded joint differentiate from the base metal, HAZ and weld metal in the Fig 3-2, which indicated the profile view of the thick welded joint. The boundary of C1-C2 is much clear, and separates the base metal from the HAZ in the thick welded joint. Therefore, C1-C2 was defined as the key line for measuring the coordinates in terms of the origin in the left and below the corner. The width of weak HAZ was fixed as 1.3mm according to the microstructural observation. Thus the two boundaries of the weaker zone in HAZ were decided, and the part on the left side of the weak zone was the

weld metal and the other side was the base metal. The consideration of the coarse-grained HAZ was ignored and was classified into the weld metal. The front surface of the welded joint was define as the plane containing the points of A2, B2, C2 and D2 as shown in Fig 3-3.

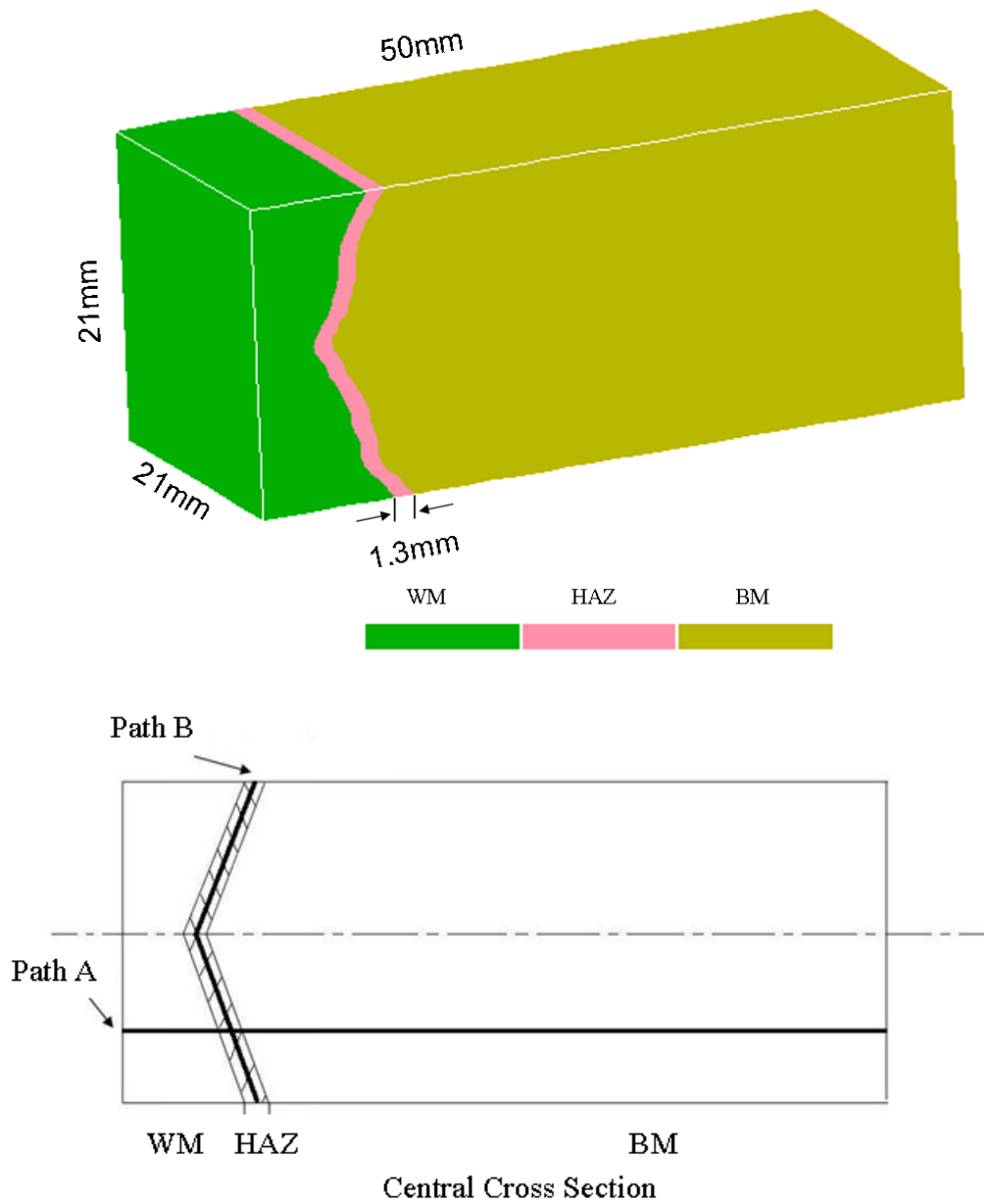


Fig. 3-2. Three-material and three-dimensional FEM model of thick plate welded joint specimen. Stress-strain distributions along Path A and Path B in the central cross section of the model are plotted in Fig 3-11 to Fig 3-19.

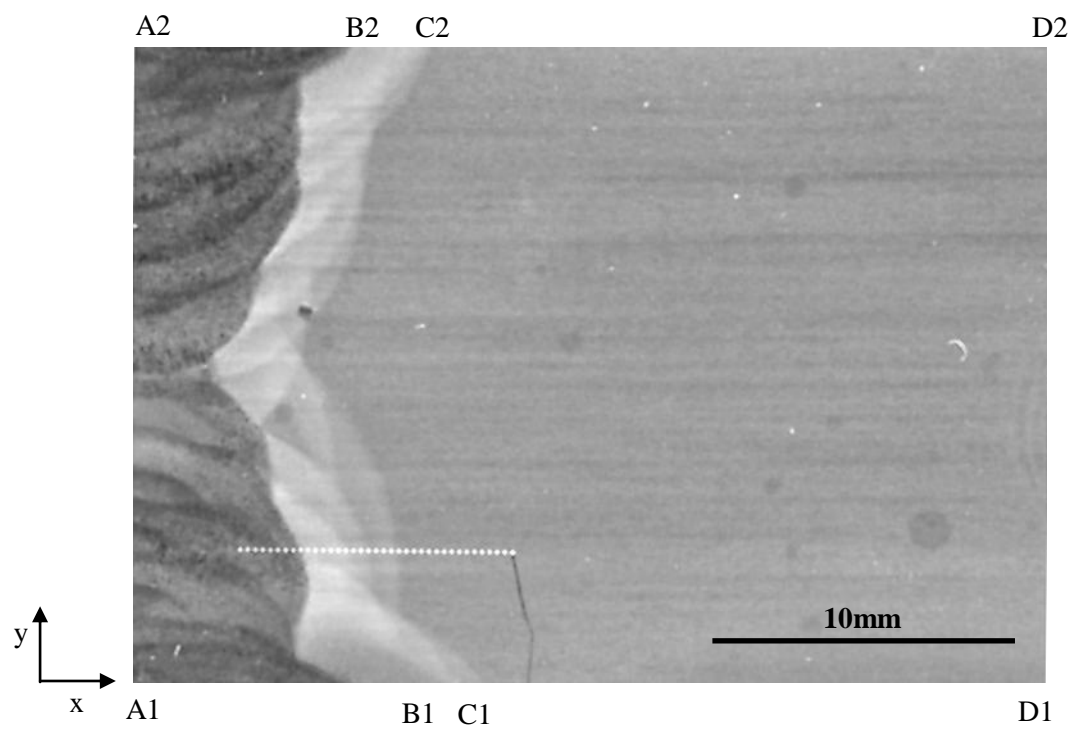


Fig 3-3. Profile view of the actual and macroscopic welded joint (where the area A1-B1-B2-A2 denoting the weld, the area C1-D1-D2-C2 representing the base metal, and between the two parts there is the HAZ).

Table 3-1. Key coordinates from profile view of the actual welded joint for FEM modeling. (Units: in mm)

y	x			
	A1-A2	B1-B2	C1-C2	D1-D2
0	0	8.3	9.6	50
0.5	0	8	9.3	50
1.1	0	7.5	8.8	50
1.6	0	7.3	8.6	50
2.1	0	6.9	8.2	50
2.8	0	6.5	7.8	50
3.3	0	6.3	7.6	50
4.1	0	6.1	7.4	50
4.7	0	6.1	7.4	50
5.2	0	6.1	7.4	50
5.8	0	6	7.3	50
6.3	0	5.8	7.1	50
6.9	0	5.6	6.9	50
7.4	0	5.4	6.7	50
8	0	5.2	6.5	50
8.6	0	4.7	6	50
9.1	0	4.5	5.8	50
9.5	0	4.2	5.5	50
9.9	0	4.1	5.4	50
10.3	0	4.2	5.5	50
10.8	0	4.5	5.8	50
11.4	0	4.9	6.2	50
12.1	0	5.1	6.4	50
12.7	0	5.5	6.8	50
13.3	0	5.8	7.1	50
13.8	0	6.1	7.4	50
14.2	0	6.3	7.6	50
14.7	0	6.5	7.8	50
15.5	0	6.6	7.9	50
16.1	0	6.8	8.1	50
16.7	0	7	8.3	50
17.3	0	7.1	8.4	50
17.9	0	7.1	8.4	50
18.5	0	7.3	8.6	50
19.1	0	7.7	9	50
19.6	0	8.4	9.7	50
20.3	0	8.9	10.2	50
21	0	9.5	10.8	50

The mechanical properties used for FEM analysis were shown in Table 3-2, which were obtained from the tensile and creep tests of the simulated HAZ and base metal of the present materials. A and n in Table 3-1 are the creep coefficient and exponent of the Norton's law:

$$\frac{d\varepsilon}{dt} = A\sigma^n \quad (3.1)$$

The relationship between the minimum creep rates vs. stress for Norton's law at 600°C are shown in Fig 3-4. Because the creep property of the weld metal was not obtained at the present work, it was substituted by that of base metal. This will not influence the trend of stress-strain distribution in base metal and the weak zone in HAZ significantly, since the weld metal normally have a lower minimum creep strain rate comparing with the base metal and HAZ [3-4]. Three-dimensional elastic-plastic-creep analysis was carried out under the applied stress of 90MPa at 600°C.

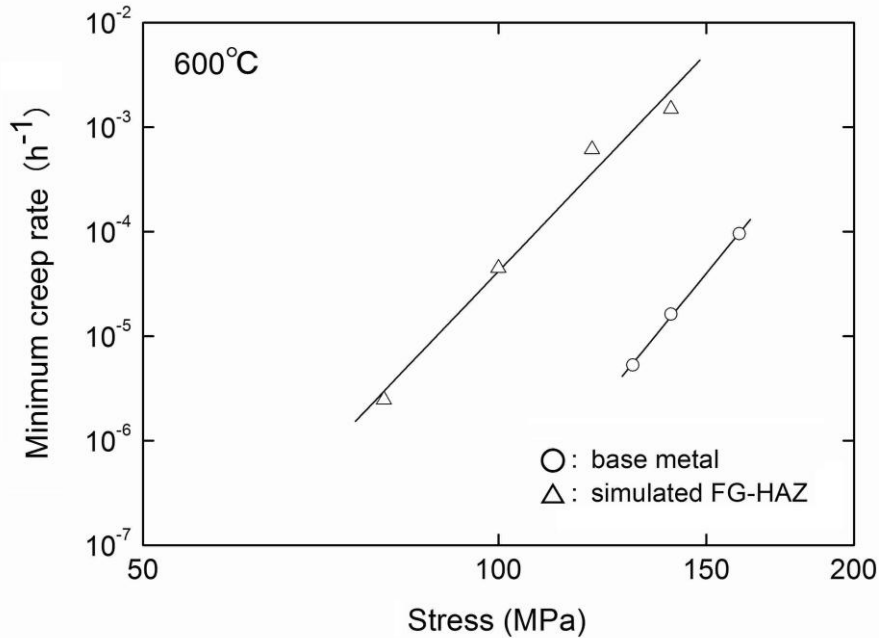


Fig. 3-4. Relationship between minimum creep rates versus stresses of the simulated HAZ and base metal at 600°C.

Table 3-2. Mechanical properties of the base metal and simulated HAZ of Mod.9Cr-1Mo steel at 600°C.

	Young's modulus (Gpa)	Yield stress (MPa)	Work hardening coefficient (MPa)	Work hardening exponent	A (MPa ⁻ⁿ h ⁻¹)	n
Simulated HAZ	100.2	136.7	310.1	0.051	1.44x10 ⁻²⁷	11.3
Base metal	117.4	140.8	377.4	0.047	1.22x10 ⁻³⁵	14

The stress triaxial factor TF is defined by the following equation:

$$TF = \frac{\sigma_1 + \sigma_2 + \sigma_3}{\sigma_{eq}} \quad (3.2)$$

where σ_1 , σ_2 and σ_3 indicate the three principal stresses, respectively. σ_{eq} is the equivalent stress (Von Mises stress) and is given by Equation (3.3).

$$\sigma_{eq} = \frac{\sqrt{2}}{2} [(\sigma_1 - \sigma_2)^2 + (\sigma_2 - \sigma_3)^2 + (\sigma_3 - \sigma_1)^2]^{1/2} \quad (3.3)$$

3.2.3.2 Constructing the Thin FEM Model

A thin 3-dimensional FEM model was also constructed comparing with the dimensions of the thin welded joint shown by Fig 2-2c in Chapter 2. The thin FEM model was also composed of three materials of the base metal, HAZ and weld metal, and it was indicated in Fig 3-5. The thin model was simulated under 90MPa at 600°C, and the creep properties listed in Table 3-2 were used again.

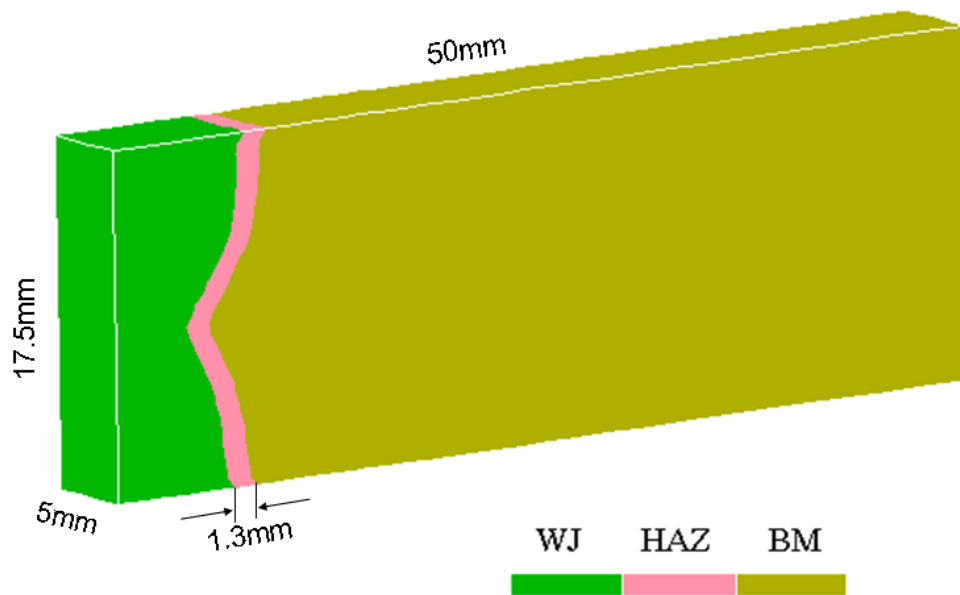


Fig. 3-5. FEM modeling for the thin welded joint conducted under 90MPa at 600°C.

3.3. Experimental and Numerical Results

3.3.1 Creep Properties of Welded Joint, Base Metal and Simulated HAZ

The creep test results for the welded joints, simulated HAZ and base metal (BM) of the Mod.9Cr-1Mo steel at 550, 600 and 650°C are shown in Fig 3-6. The failure location of welded joint is shown with subscript in this figure. The creep rupture times of the simulated HAZ were smaller more than one order than those of base metal at all temperatures. At 550°C, the fracture location of welded joint was base metal for the applied stress of 240 and 220MPa, and it shifted to HAZ (Type IV) at 200MPa. At high temperatures, 600 and 650°C, Type IV cracking became the dominating failure mode and all the welded joint specimens tested were fractured in HAZ. For the specimen fractured in HAZ, many creep voids on the grain boundaries were observed in the fine-grained HAZ and intercritical HAZ. Although the difference of creep strength between base metal and welded joint is small at 550°C, it became larger with increasing temperature and decreasing applied stress. The creep rupture times of welded joints approaches to those of simulated HAZ for lower stresses at 600 and 650°C.

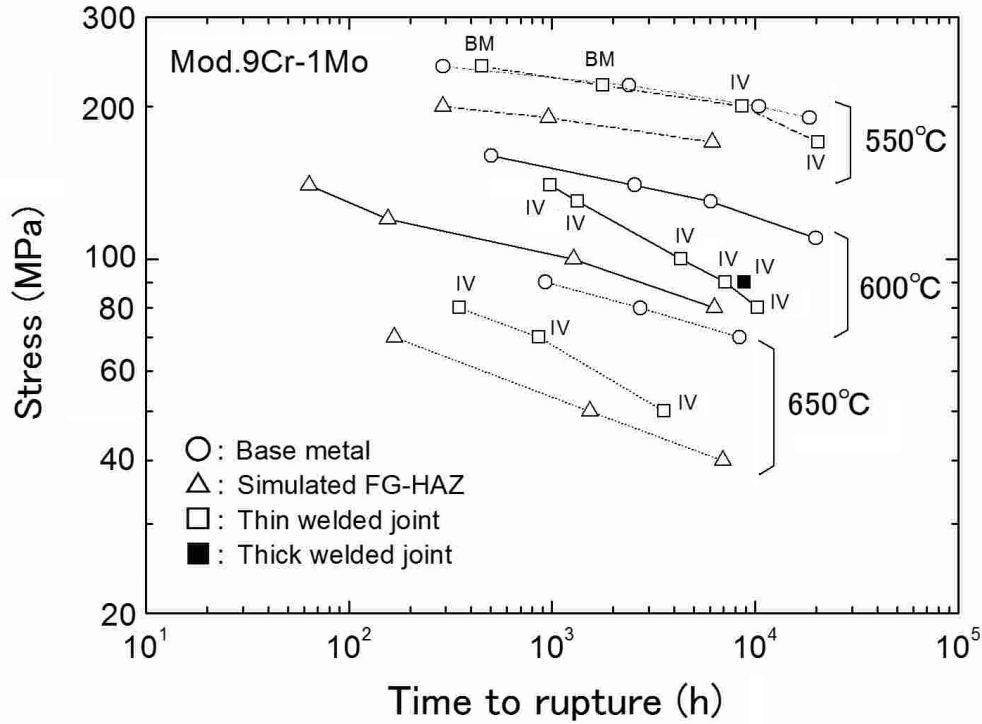


Fig. 3-6. Results of creep rupture tests for base metal, simulated HAZ, and welded joints of the Mod.9Cr-1Mo steel at 550, 600 and 650°C. The subscripts 'BM' and 'IV' attached to the data plots mean that the fracture location of welded joint is base metal and HAZ (Type IV), respectively.

3.3.2 Evolution and Distribution of Creep Voids in HAZ

Figure 3-7 shows the binary images of creep voids and cracks observed in HAZ of central cross section of creep interrupted thick plate specimens (Fig 2-11). Though this figure had been concerned in Chapter 2, we show it here for the convenience of comparison with the FEM results. It is found that the creep voids have already formed at 2000h (about 0.2 of rupture life) and grown into the crack between 7040h and 7970h (about 0.8-0.9 of rupture life). A crack with about 2mm in length was measured at a quarter depth of plate thickness in the fine-grained HAZ and intercritical HAZ at 7970h. The number and area fraction of these creep voids in the 11 areas with 0.2×2mm explained in Fig 2-12 were counted using laser microscope and image analysis. Figures 3-8 and 3-9 show the distributions of the number and

the area fraction of creep voids in the plate thickness direction in HAZ with creep time at 600°C for 90MPa, respectively. As shown in Fig 3-8 and Fig 3-9, two peaks are clearly observed at quarter depths from the specimen surfaces in the HAZ for both diagrams of number and area fraction of creep voids. The number of creep voids is fewer near the specimen surfaces and the center of thickness.

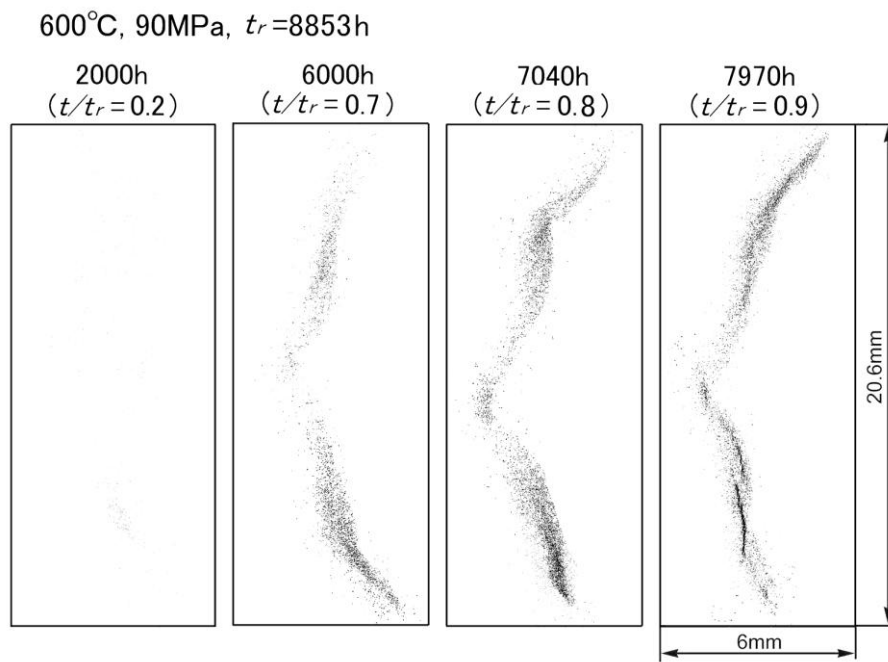


Fig. 3-7. Binary images of creep voids and cracks observed in the central cross section of HAZ of thick plate welded joint after interruption of creep test at 2000, 6000, 7040 and 7970h.

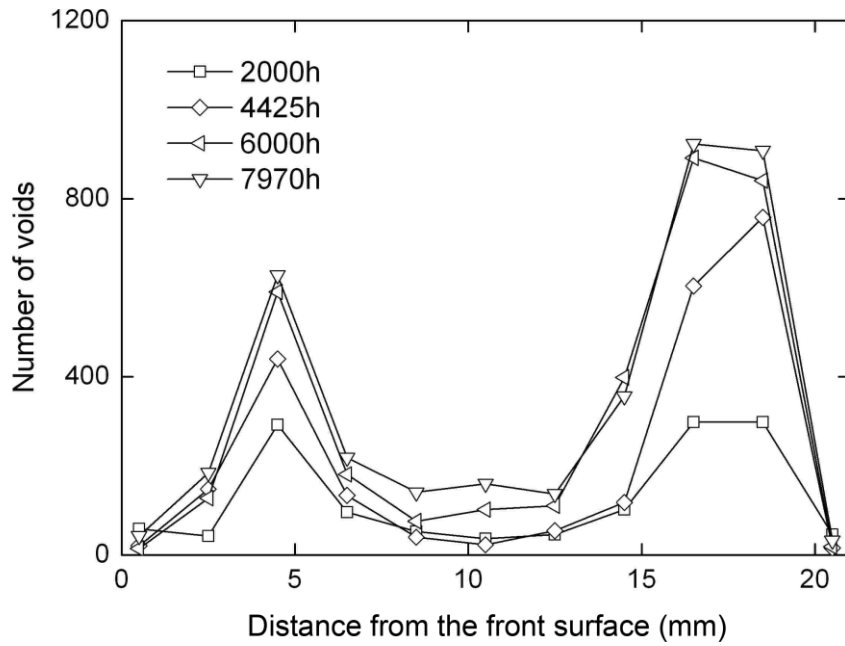


Fig. 3-8. Distribution of the number of creep voids along HAZ of the thick plate welded joint of Mod.9Cr-1Mo steel during creep at 600°C for 90MPa. The position of the front surface is indicated in Fig 3-2.

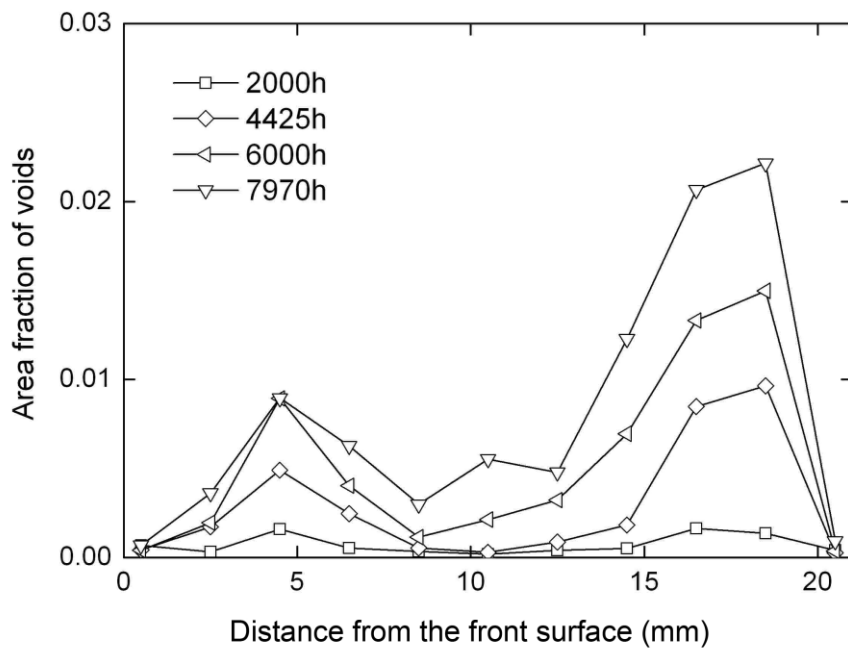


Fig. 3-9. Distribution of the area fraction of creep voids along HAZ of the thick plate welded joint of Mod.9Cr-1Mo steel during creep at 600°C for 90MPa. The

position of the front surface is indicated in Fig 3-2.

The number of creep voids increased with time till 6000h (0.7 of rupture life) and then saturated, while the area fraction of creep voids increased after 6000h, which is more obvious in Fig 3-10. In Fig 3-10, the total number of creep voids per 1mm^2 (void density) and average area fraction of creep voids in the 11 areas in HAZ was plotted against time normalized by creep rupture time (t/t_r). Because creep voids coalesced and grew to the crack, the number of voids was saturated at about 0.7 of rupture life, while the area fraction of voids was still accelerated after that. From these experiments, it was found that Type IV creep voids formed at the early stage of creep life inside the specimen, a quarter depths of thickness, number of voids increased with time, and voids coalesced into the macro crack after 0.8 of rupture life.

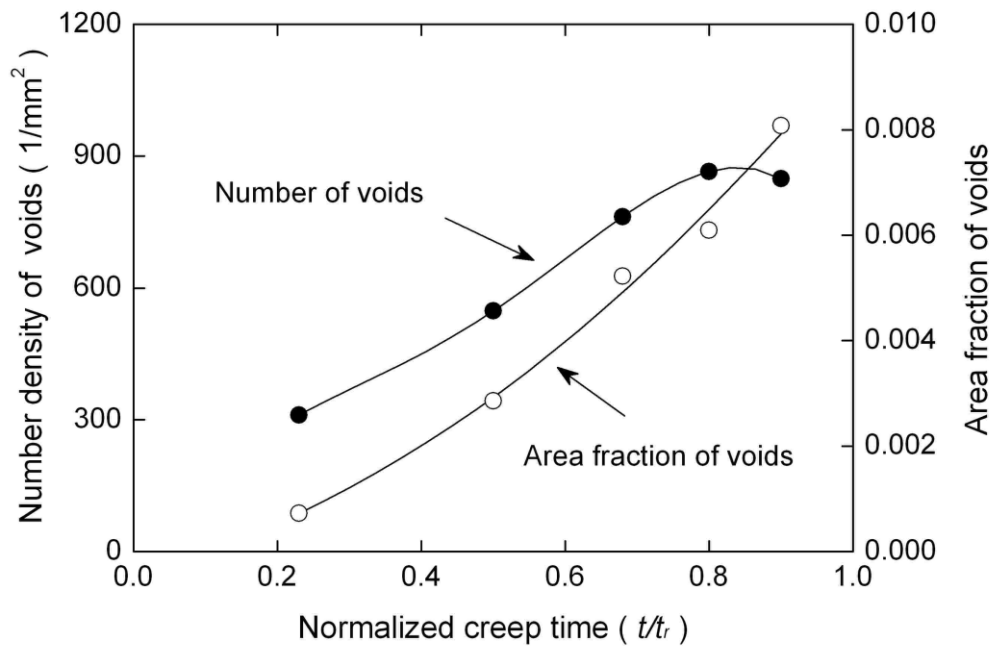


Fig. 3-10. Evolution of total number of creep voids per 1mm^2 (void density) and average area fraction of voids in HAZ of the thick plate welded joint during creep at 600°C for 90MPa.

3.3.3 Results of Numerical Analysis

By using FEM calculation, the stress-strain distributions of thick plate welded joints and of the thin welded joints were calculated. The evolution of the stress, strain and stress triaxial factor with time were investigated along the two paths in the central cross section of the three dimensional models. The two paths were defined as follows; Path A is along the longitudinal direction of the welded joint with 50mm length, while Path B is within the weak HAZ and along the bond line with 21mm vertical length as shown in Fig 3-2.

3.3.3.1 Stress-Strain Distribution and Evolution in Path A

In this section we discuss the simulation results of the thin and thick FEM models. The results of numerical analysis such as distributions of equivalent stress, equivalent creep strain and stress triaxial factor for Path A are shown in Figs 3-11, 3-12 and 3-13 from the thick FEM model, respectively. Figure 3-11 shows that the equivalent stress in weak HAZ is lower comparing with base metal/weld metal and decreases with time while it increases in base metal/weld metal in small scale. However, it appears inverse trends for the stress triaxial factor evolution in welded joint with time as shown in Fig 3-13. The stress triaxial factor shows the maximum value of about 3.5 in weak HAZ of the present welded joint at 8000h. There is no large changing in equivalent stress after 4000h creep for the weak HAZ and 500h for base metal. The equivalent creep strain in weak HAZ is always higher than that in weld metal and base metal in Fig 3-12. Obviously, the weak HAZ is weak to relieve the stress comparing with the base metal.

According to Eq. (3.2) the stress triaxial factor has a reversed linear relation with the Von Misses stress if the summation of the three principal stresses is invariable with the creep time. However, this is not realistic for the complicated structure. Also the Von Mises stress is the function of the three principal stresses in the Eq. (3.3), which are also changing with the simulated time. Therefore this makes their relation confused. From the FEM results such as Fig 3-11 and 3-13, that they are in the inversed trends with time can be observed.

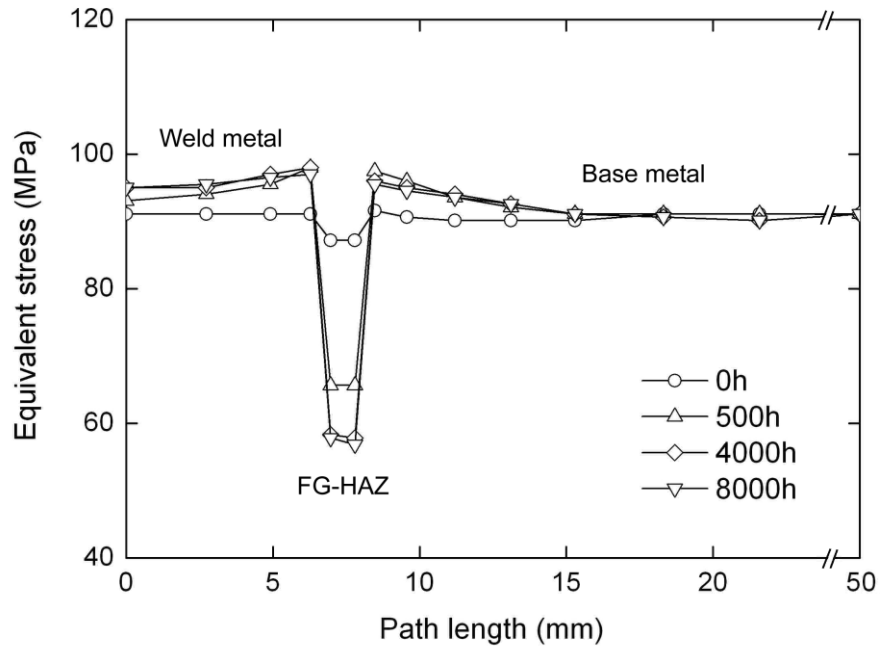


Fig. 3-11. Distribution of equivalent stress in Path A in thick welded joint during creep at 600°C for 90MPa calculated by FEM.

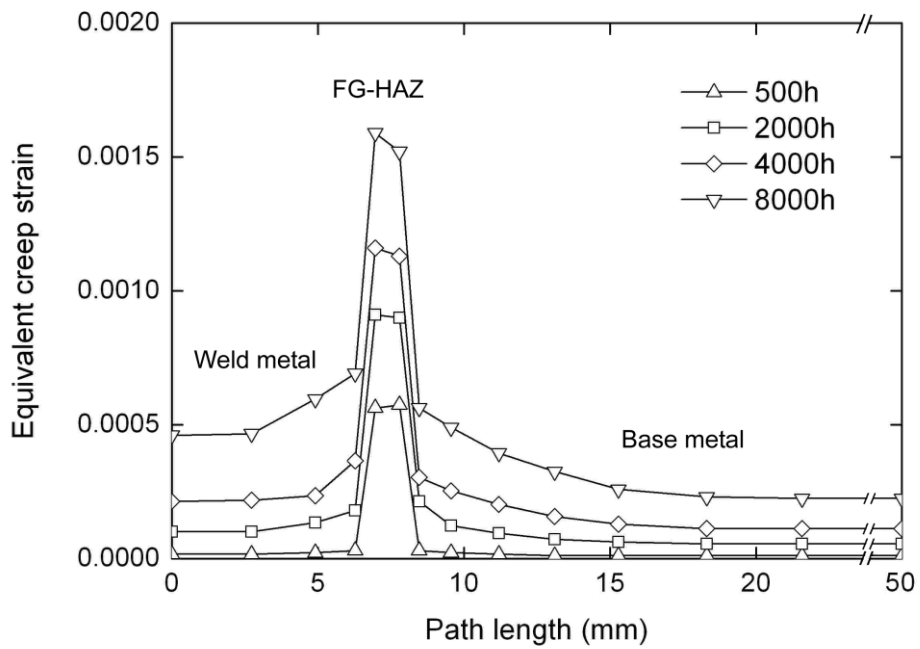


Fig. 3-12. Distribution of equivalent creep strain in Path A in thick welded joint during creep at 600°C for 90MPa.

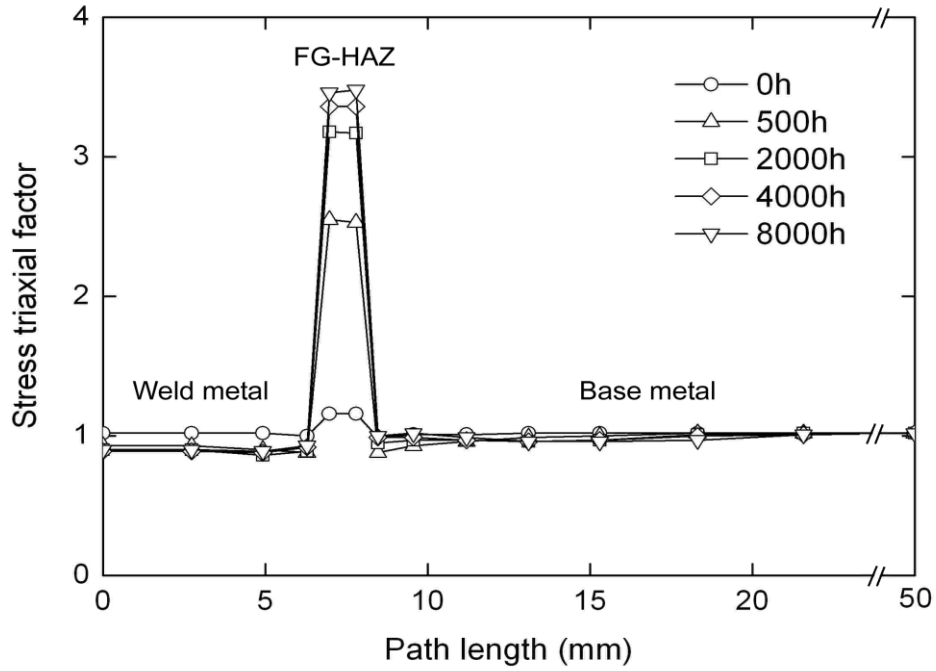


Fig. 3-13. Distribution of stress triaxial factor in Path A in thick welded joint during creep at 600°C for 90MPa.

The mechanical parameters such as stress triaxial factor and Von Mises stress were also investigated in the thin FEM model at some time steps during the simulation. They are shown in Fig 3-14 and Fig 3-15, respectively. The stress triaxial factor in the weak HAZ of the thin FEM model shown in Fig 3-14 is much smaller than that in the thick FEM model as indicated in the Fig 3-13. The stress triaxial factor in the base metal is almost same and equal to 1 in the two FEM models. It means that the constraints on the weak HAZ of the thin welded joint are smaller than in the thick welded joint while the constraints on the base metal are same for the two FEM models. The Von Mises stresses in the weak HAZ are larger in the thin FEM model than in thick FEM model at any time step. They are approximately equal to the applied stress (90MPa) in the base metal for both FEM model as indicated in Fig 3-11 and Fig 3-15. The equivalent creep strain in the thin FEM model (in Fig 3-16) is higher than in the thick welded joint (in Fig 3-12). Therefore, the constraints focusing on the weak zone in the large scale welded joint are higher than the small scale welded joint with same width of weak zone.

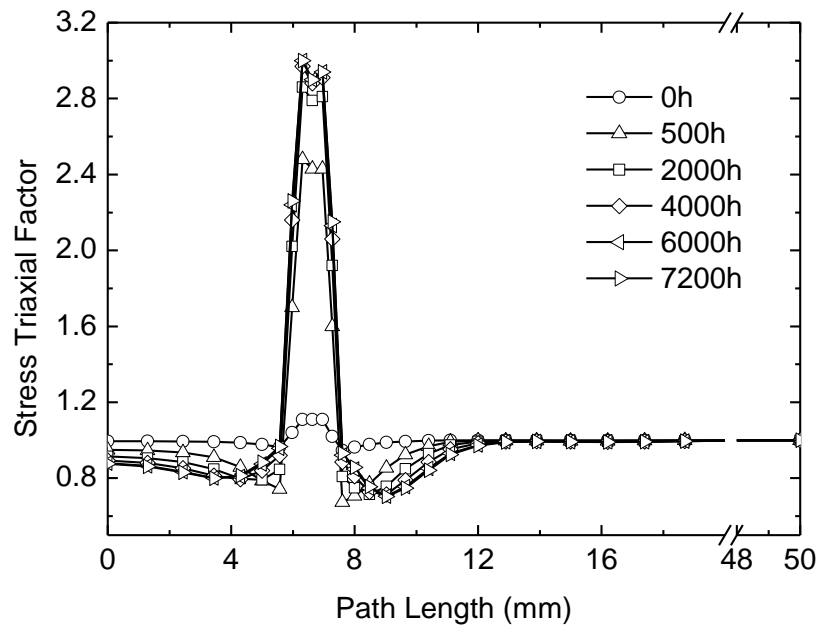


Fig. 3-14. Distribution of stress triaxial factor in Path A in thin welded joint during creep at 600°C under 90MPa.

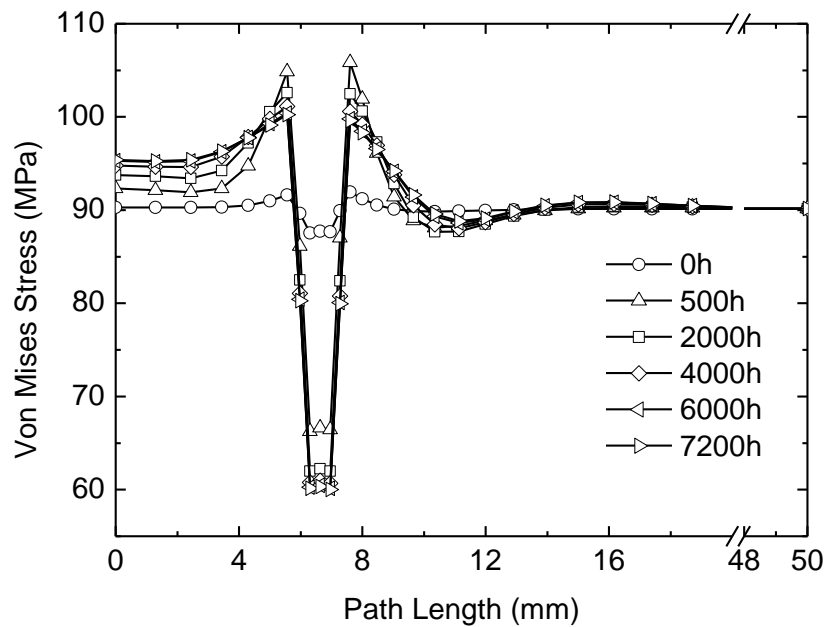


Fig. 3-15. Distribution of Von Mises stress in Path A in thin welded joint during creep at 600°C under 90MPa.

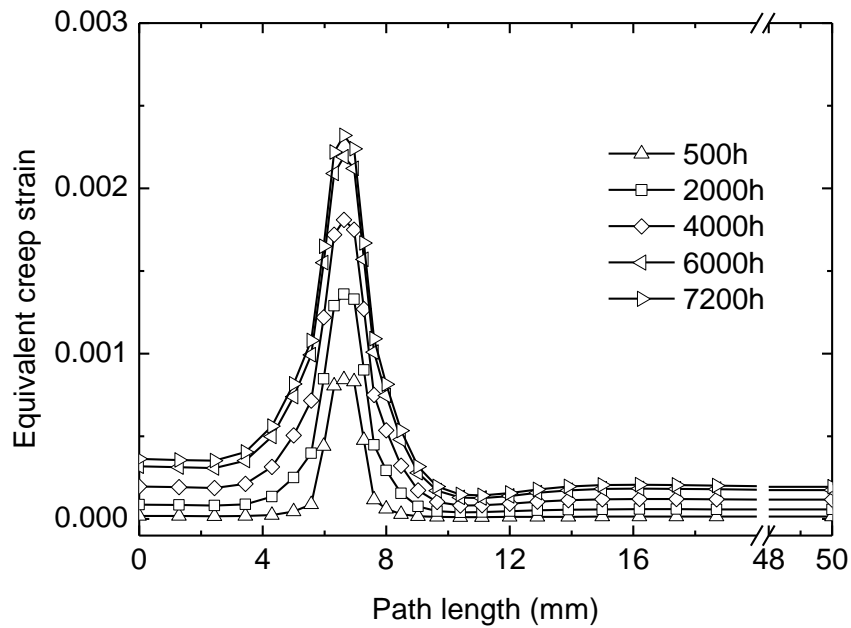


Fig. 3-16. Distribution of equivalent creep strain in Path A in thin welded joint during creep at 600°C under 90MPa.

3.3.3.2 Stress-Strain Distribution and Evolution in Path B

In order to clarify how the stresses, the stress triaxial factor and the strain distribute in the weak HAZ, they were calculated and examined along the Path B. The distributions of maximum principal/equivalent stress, stress triaxial factor, and equivalent creep strain for Path B are shown in Figs 3-17, 3-18 and 3-19, respectively. An inconspicuous fluctuation of equivalent stress with the locations in weak HAZ was observed and it was a little higher in the surface part than in the other parts after 500h. It decreases with time and almost invariable after 4,000h creep. There are no large changes with time for maximum principal stress, and it shows larger value at the parts from a quarter depths to the center of plate thickness in weak HAZ after 500h creep, which means that the distribution of maximum principal stress is much consistent with the experimental damage observation comparing with that of equivalent stress

(Fig 3-17). The stress triaxial factor increases with time inside the plate thickness. As shown in Fig 3-18, it is found that the stress triaxial factor is in high level from the 1/4 depths of thickness to the center of thickness in weak HAZ, while it is the smallest in the surface parts from 500h to 8,000h creep time.

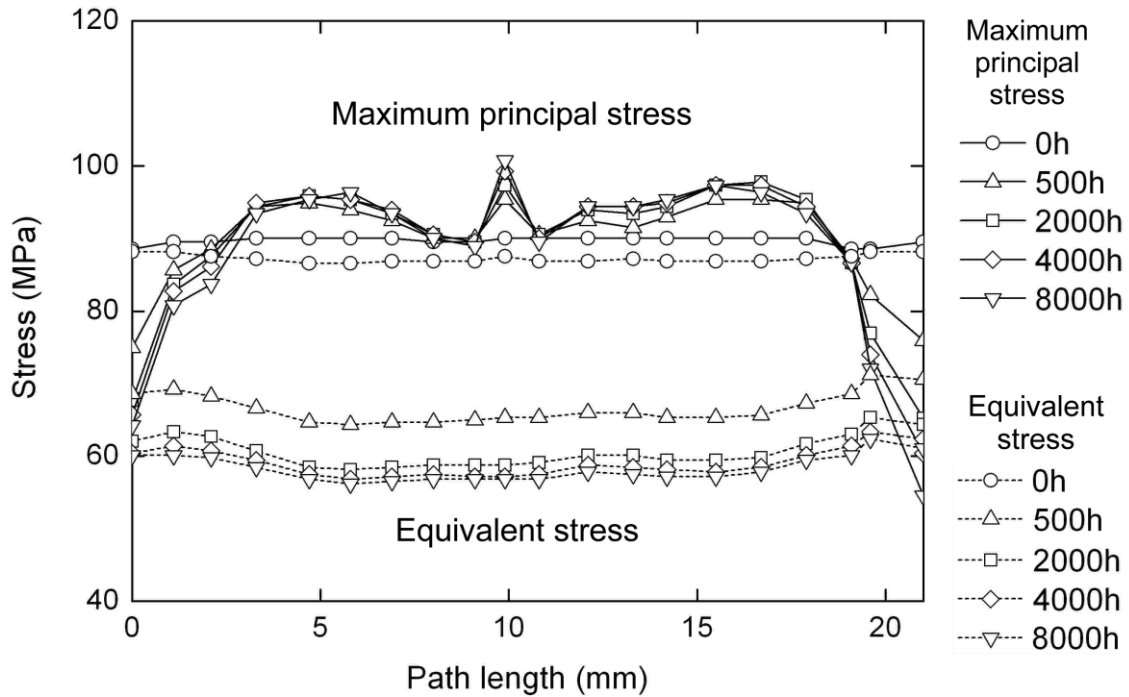


Fig. 3-17. Distribution of maximum principal stress and equivalent stress in Path B in weak HAZ of the thick welded joint during creep at 600°C for 90MPa.

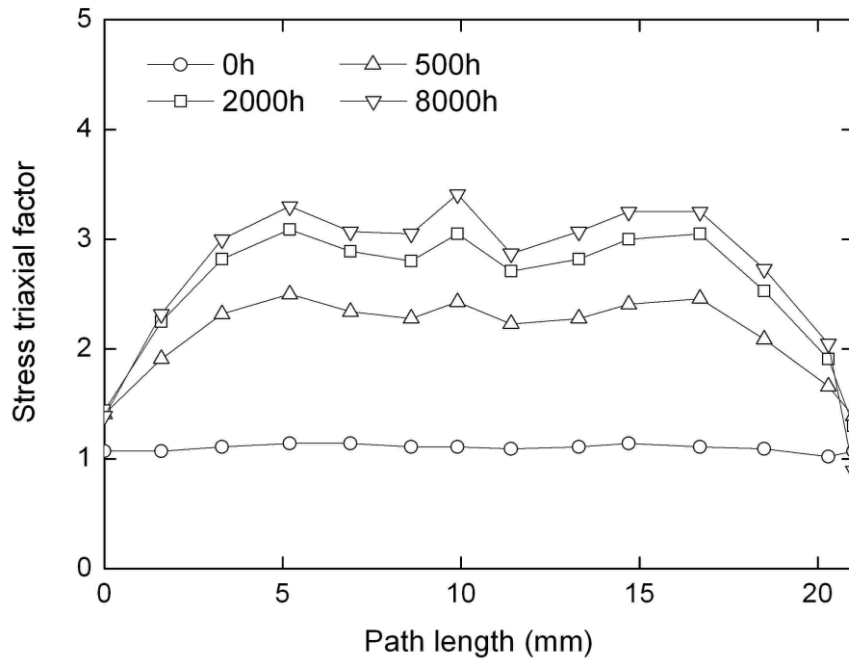


Fig. 3-18. Distribution of stress triaxial factor in Path B in weak HAZ of the thick welded joint during creep at 600°C for 90MPa.

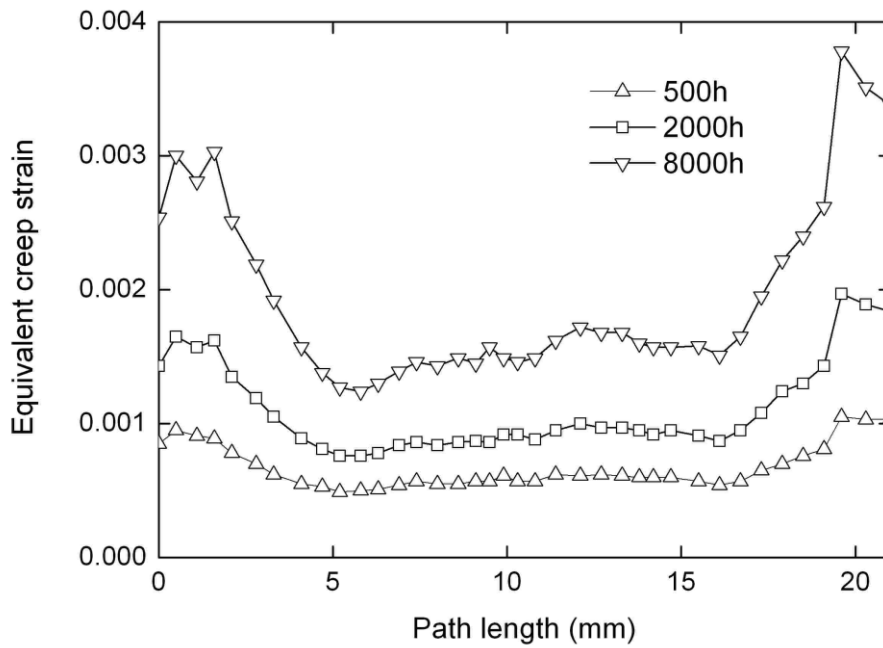


Fig. 3-19. Distribution of equivalent creep strain in Path B in weak HAZ of the thick welded joint during creep at 600°C for 90MPa.

Fig 3-19 shows that the equivalent creep strain is in high level in the surface parts (both front and back sides) comparing with the other parts in the weak HAZ at any time steps, which agrees well with the large surface deflection observed on the HAZ during creep. The strain is increasing with time and the strain gradient also becomes larger with time near to the surface parts. The deep and steep slopes of the strain curve are located in the range of 2-5mm from the surfaces. It is the location where the number and area fraction of creep voids are the highest and increase with time.

We also pasted the simulation map for equivalent creep strain, stress triaxial factor, Von Mises stress and maximum principal stress at the simulation time of 8860h. From these, the global profile of the primary mechanical parameters can be grasped easily.

3.4 Roles of Mechanical Parameters during Creep

3.4.1 Equivalent Creep Strain and Stress Triaxial Factor

From Fig 3-13, comparing the results of numerical analysis with the creep voids measurement, the stress triaxial factor is reasonable to explain why the weak HAZ is the most damaged zones in the whole welded joint, because it accelerates the creep void formation and growth. However, the distributions of maximum principal stress and stress triaxial factor in the weak HAZ shown Figs 3-17 and 3-18 are not thoroughly consistent with the experimental void distributions of Figs 3-8 and 3-9. Creep voids are mostly like to form in a quarter depths of plate thickness, but are scarcely formed in the center of thickness. In the center of plate thickness, whereas the maximum principal stress and stress triaxiality is high, a small number of creep voids are observed. The peaks in the central location of the weak HAZ of the thick welded joint, as shown in Figs 3-17 and 3-18, should be due to the weld grooves of double U that make the mechanical parameters change abruptly.

Watanabe *et al* reported that the initiation site of Type IV damages coincides well with the stress triaxiality distribution using the welded joint with single U groove for Mod.9Cr-1Mo

steel [3-2]. Ogata *et al.* used a round bar specimen of welded joint with single U groove to obtain that the stress triaxiality affects on the number of creep void initiation and the maximum principal stress contributes to void growth by diffusion [3-9]. It seems that creep damage mechanisms of the present thick plate welded joint with double U grooves, which has more complicated structural geometry, cannot sufficiently be explained only by the effect of stress triaxiality or maximum principal stress. Based on the detailed microstructure observation on Mod.9Cr-1Mo steel weldment Lee *et al* proposed that the cavity formation at grain boundaries was caused by the strain heterogeneity among grains, and the growth of voids was assisted by the creep strain concentrated in HAZ [3-10]. In present study, creep strain is low from a quarter depths to the center of thickness (Fig 3-18), and the few voids are observed in the center of thickness. Therefore, it can be considered that both the concentration of creep strain and the high triaxial stress state in weak HAZ influence the distributions of Type IV creep voids. The large gradient of equivalent creep strain was observed in a quarter depths of plate thickness where the creep voids are mostly formed.

On the other hand, according to the vacancy diffusion theory under stress gradient of creep condition [3-11], the vacancy diffusion is controlled by hydrostatic stress gradient. In the present welded joints, vacancies are considered to accumulate near the areas of a quarter depths of thickness by diffusion under triaxial stress field, because the stress triaxiality gradient exists from the surface to a quarter depths of thickness as shown in Fig 3-18. The condensation of vacancies will accelerate the initiation and growth of creep voids in these areas for the present thick welded joint.

The creep voids begin to form at the early stage (at about 0.2 of rupture life) and the number of voids increases all the way until at about 0.7 of the rupture life. After that it can be considered that the rate of void coalescence is higher than that of void formation. With the coalescence of creep voids, they grow into the crack which is known as Type IV cracking. The area fraction of creep voids can be a good variable to predict the creep life since it always

tends to increase during creep. In case it is difficult to measure the area fraction of creep voids formed inside the weldment nondestructively, the local necking of the specimen surface in HAZ can be a life predicting variable [3-12], because the creep strain concentrates near the surface regions of HAZ as shown in Fig 3-19. In order to denote the mostly damage location along the weak HAZ inside of the plate, we plot the product of the stress triaxial factor and equivalent creep strain versus the path length shown in Fig 3-20. It can be expressed by the term $(100TF \cdot \varepsilon)$, and was named as the P-factor for discussing conveniently. The P-factor in both the two subsurface locations in the weak HAZ is large comparing with the surface and central part. It is the lowest in the surface part. It testify our assumption well by observation of void in HAZ.

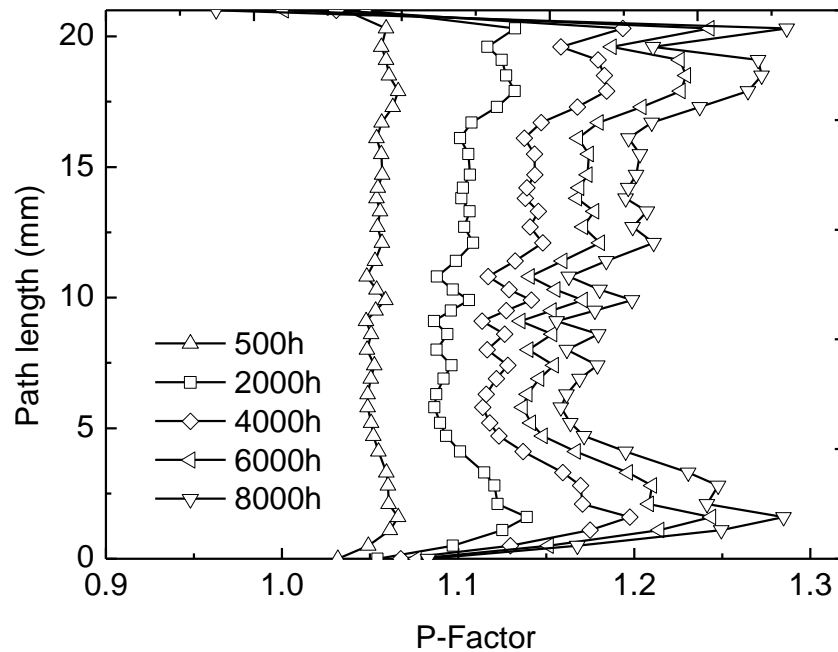


Fig. 3-20. P-factor versus the path length along the weak HAZ for the thick welded joint by FEM simulation.

3.4.2 Effects of Von Mises Stress on the Creep-Rupture Time

For comparing the two FEM models, the constraints in the weak HAZ are higher in thick model while the Von Mises stresses are smaller. The related creep tests indicated that the creep life of thin welded joint (7200h) was shorter than that of the thick welded joint (8853h) at the temperature of 600°C and under the stress of 90MPa. The constraints on the weaker zone in the welded joint might be responsible for the creep rupture time. Namely the corresponding high constraint would prolong the rupture life of the weldment. We can also contribute it to the constraints decreasing the Von Mises stress. For prediction the rupture life of the weldment, Hayhurst *et al* used a mixed rupture criterion to define the effective stress to rupture [3-13]. It is given by

$$\sigma = \alpha\sigma_1 + (1 - \alpha)\sigma_{eq} . \quad (3.4)$$

where α ranges from 0 to 1, and is stated in details in Chapter 1, σ_1 present the maximum principal stress. With inducing the effective stress to rupture considering the mixed rupture criterion, the predicting equation for the rupture life (t_f) of weldment is given by

$$t_f = \frac{1}{C(1 + \phi)\sigma^\chi} \quad (3.5)$$

where the coefficients and exponent of C , χ and ϕ are material constants in a certain temperature. Thus smaller Von Mises stress on the weaker zone of the weldment prolongs the rupture time, i.e. the constraints on the weaker zone of a welded joint is a progressive factor for servicing time. However, this is valid in short term of the specimens under the high stress levels at lower temperatures.

The differences of the simulated HAZ and the welded joint are the constraints produced in the HAZ due to the different components and the shapes of the grooves. According to this arguments mentioned above, the constraints are good to servicing time of the materials. Under

the stress levels from 80MPa to 140MPa at 600°C, the differences of the rupture lives of the simulated HAZ and the welded joint decrease with the applied stress decreasing. In the range of the testing stress levels, the creep strength of the welded joint is still stronger than that of the simulated HAZ at 600°C. These phenomena might be contributed by the short period role of the constraints on the weaker zone due to the relief. Grain boundary sliding is a kind of explain on the relief of the constraints [3-14, 3-15]. On the other hand, the voids producing in the early stage of the creep life grow up in the weak HAZ, which allow the growth of the strain in macroscopic. Therefore, the growing voids also acts on a role for relieving the constraints on the weaker zone in the weldment. Whatever the boundary sliding among the grains and the growing voids in the weak HAZ of the welded joint, they need some time to relieve the constraints. The material bearing high stress will rupture soon, which could not provide enough time. Therefore, the progressive role of the stress triaxial factor to prolong the rupture lives is prominently under high stress levels and lower temperatures. On the other hand under lower stress level, the rupture life of material could sufficiently provide the time for relieving constraints on the weaker zone of the welded joint.

The creep strain is increasing with time under a certain stress level as shown in Fig 3-12 and Fig 3-16 for the thick and thin FEM models respectively. The constraints due to the triaxial factor are stronger in the thick welded joint than in the thin welded joint. The equivalent creep strain calculated by FEM was higher in the weak HAZ of the thin FEM model than in the thick FEM model at any time step. Moreover, as shown in the Fig 3-18 and Fig 3-19 the equivalent creep strain and the triaxial factor are increasing with simulating time. In the same time steps the stress triaxial factor is larger in the location where the equivalent creep strain is small. We could believe that the creep deformation has an increasing trend during creep under a certain stress level, while it is restrained by the triaxial factor. Large triaxial factor always decreases the increasing velocity of the creep strain during creep.

It is shown that the role of the stress triaxial factor is clarified. In early stages, the stress

triaxial factor comparing with the equivalent creep strain causes the nucleation of voids in the weak HAZ of the Mod.9Cr-1Mo steel welded joint at high temperatures. In the reverse aspect, it acts on the progressive role for prolonging the rupture lives of materials due to the lower effective stress to rupture.

3.5 Conclusions

In this chapter, the damage processes in the fine-grained HAZ and intercritical HAZ of thick welded joint of Mod.9Cr-1Mo steel during creep were investigated. Stress-strain distributions in the welded joint were computed by FEM analysis with three-dimensional, three-material models (base metal, simulated HAZ and weld metal). The results can be summarized as follows;

- (1) It is found that the creep voids of Mod. 9Cr-1Mo steel weld form at the early stage of creep rupture life (0.2 of life), the number of them increases with time till 0.7 of life, and then they coalesce into the Type IV crack at the last stage (after 0.8 of life).
- (2) The creep voids are apt to form at the area of a quarter depths from the surfaces, inside the plate, in weak HAZ for the present thick plate welded joint of Mod.9Cr-1Mo steel.
- (3) It is considered that the high level stress triaxial factor combined with the large equivalent creep strain in the weak HAZ accelerate the void forming in the Mod.9Cr-1Mo steel welded joint during creep at elevated temperatures. While on the other hand, the stress triaxial factor in the weak HAZ prolongs the creep-rupture time of the welded joint due to the lower effective stress to rupture.
- (4) The constraints are always produced in a weldment due to the different properties of the sub-parts, and they are larger in the thick welded joint than in the thin welded joint with same-width weak zone.

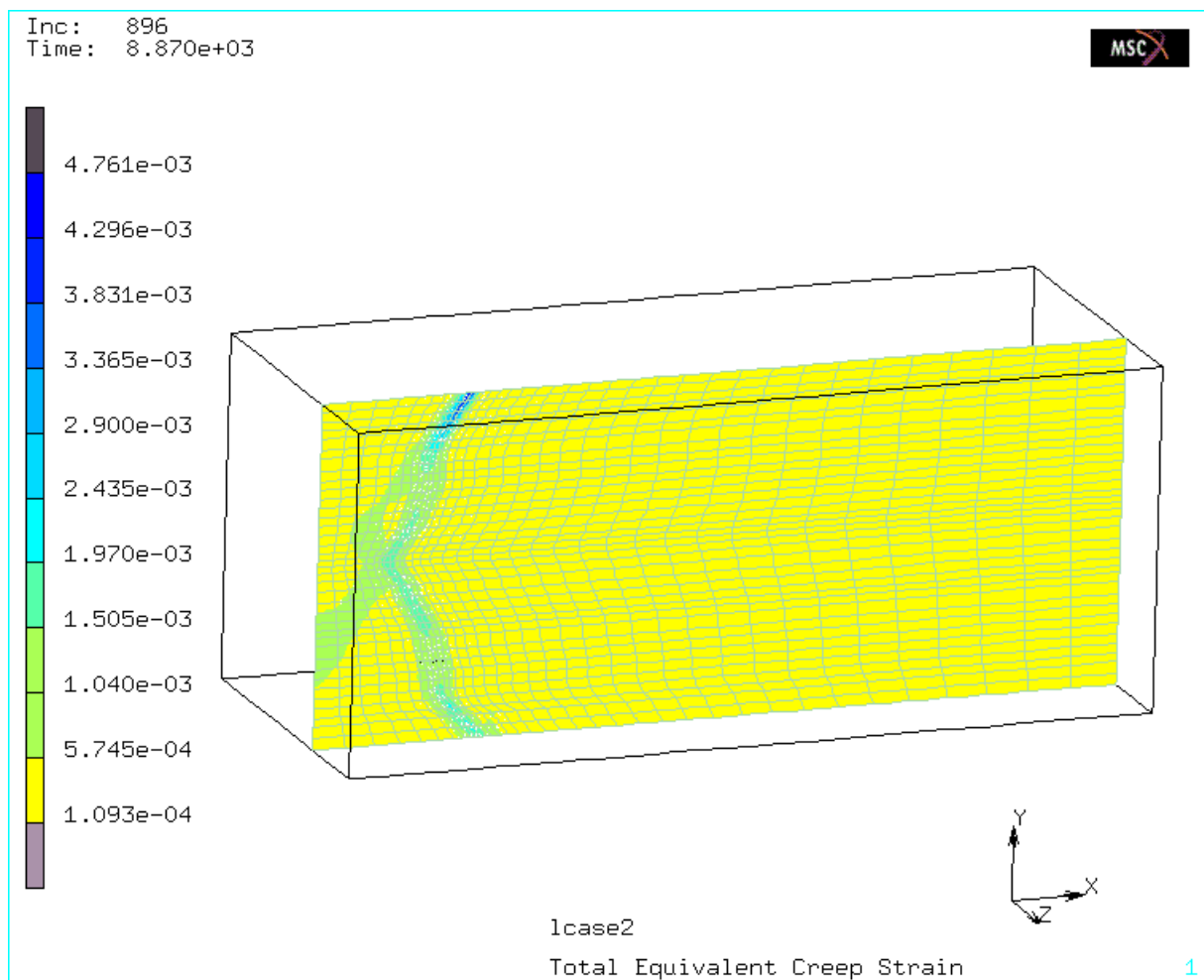
References of Chapter 3

- [3-1] J. A. Francis, W. Mazur and H. K. D. H. Bhadeshia: Material Science and Technology. **22** (2006) 1387-1395.
- [3-2] T. Watanabe, M. Tabuchi, M. Yamazaki, H Hongo and T. Tanabe: International Journal of Pressure Vessels and Piping. **83** (2006) 63-71.
- [3-3] Y. Hasegawa, T. Muraki and M. Ohgami: Tetsu-to-Hagane. **92** (2006) 618-626.
- [3-4] G. Eggeler, A. Ramteke, M. Coleman, B. Chew, G. Peter, A. Burblies, J. Hald, C. Jefferey, J. Rantala, M. DeWitte and R. Mohrmann: International Journal of Pressure Vessels and Piping. **60** (1994) 237-257.
- [3-5] T. H. Hyde, W. Sun and A. A. Becker: International Journal of Pressure Vessels and Piping. **78** (2001) 765-771.
- [3-6] L. M. Kachanov: Izvestiya Akademii Nauk SSR Otdelenie Technicheskikh Nauk. **8** (1958) 26-31.
- [3-7] D. R. Hayhurst, J. Makin, M. T. Wong and Q. Xu: Philosophical Magazine. **85** (2005) 1701-1728.
- [3-8] M. Bauer, A. Klenk, K. Maile and E. Roos: Proceedings of 3rd International Conference on Integrity of High Temperature Welds. (London: IOM Communications, 2007) pp. 257-266.
- [3-9] T. Ogata, T. Sakai and M. Yaguchi: Proceedings of 3rd International Conference on Integrity of High Temperature Welds. (London: IOM Communication, 2007) pp. 285-294.
- [3-10] J. S. Lee, K. Maruyama, I. Nonaka and T. Ito, Creep Deformation and Fracture, Design, and Life Extension (Materials Science & Technology 2005), Edited by R. S. Mishra, J. C. Earthman, S. V. Raj, and R. Viswanathan, (TMS, Warrendale, 2005) pp.139-148.
- [3-11] H. P. Leeuwen: Engineering Fracture Mechanics. **9** (1977) 951-974.
- [3-12] T. Ito, I. Nonaka, H. Umaki, K. Suzuki and K. Higuchi: Proceedings of the 38th

- Symposium on Strength of Materials at High Temperatures. (Yokohama: The Society of Materials Science, 2000) pp. 96-100.
- [3-13] D. R. Hayhurst, P. R. Dimmer and C. J. Morrison: Philosophical Transactions of the Royal Society of London. Series A, Mathematical and Physical Sciences. 311 (1984) 103-129.
- [3-14] D. J. Smith, N. S. Walker and S. T. Kimmins: International Journal of Pressure Vessels and Piping. **80** (2003) 617-627.
- [3-15] S. T. Kimmins and D. J. Smith: The Journal of Strain Analysis for Engineering Design. **33** (1998) 195-206.

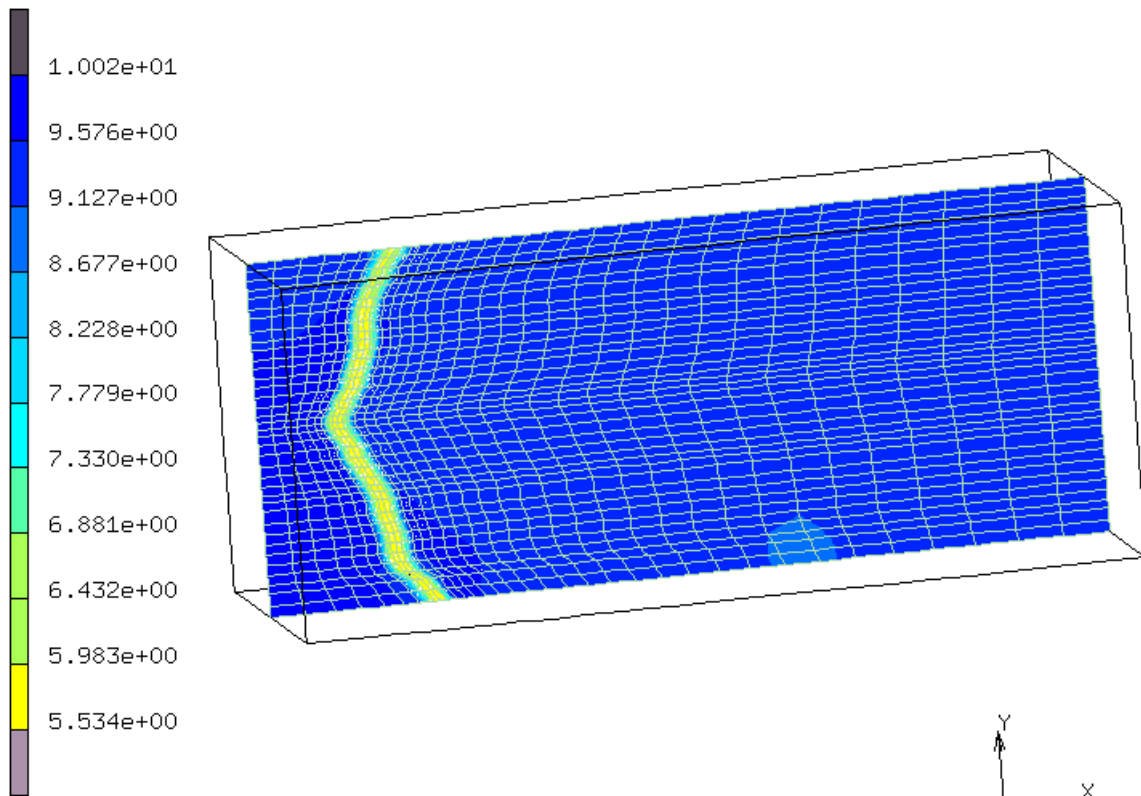
Appendix B

Some examples of the FEM calculation



I . Total equivalent creep strain map at the simulated time step of 8,960 h.

Inc: 896
Time: 8.870e+03



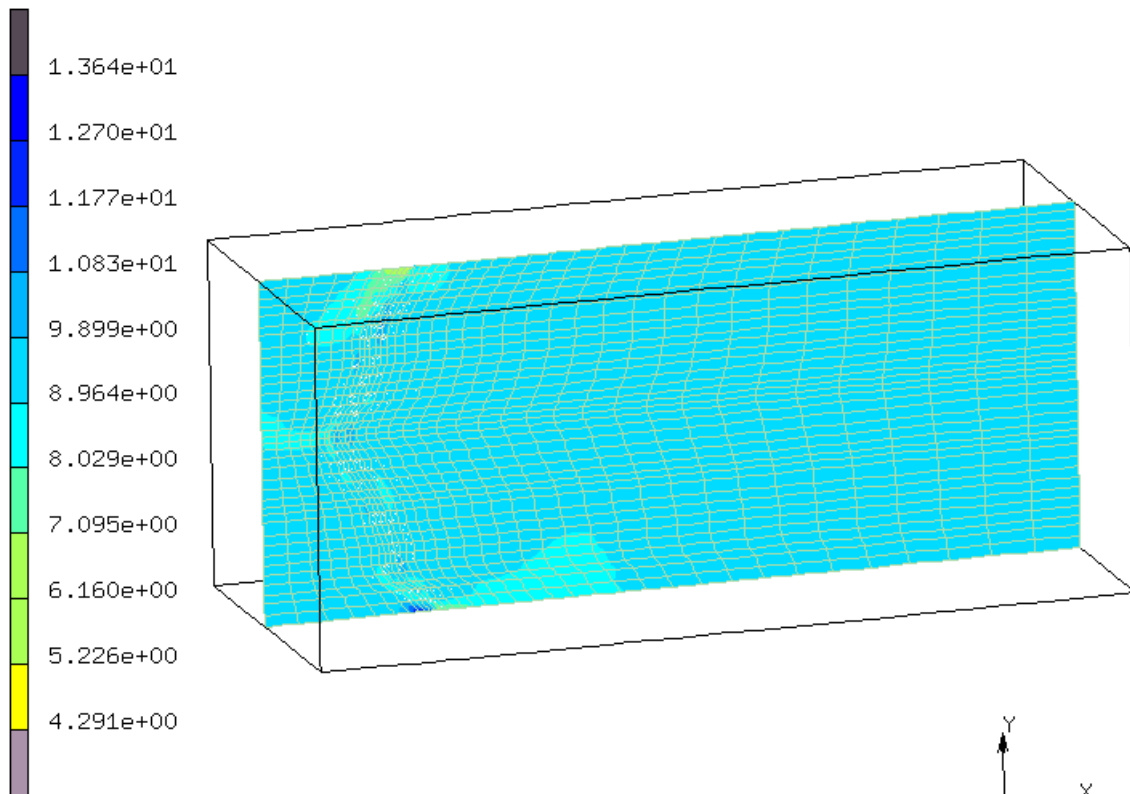
lcase2

Equivalent Von Mises Stress

1

II . Equivalent Von Mises stress map at the simulated time step of 8,960 h.

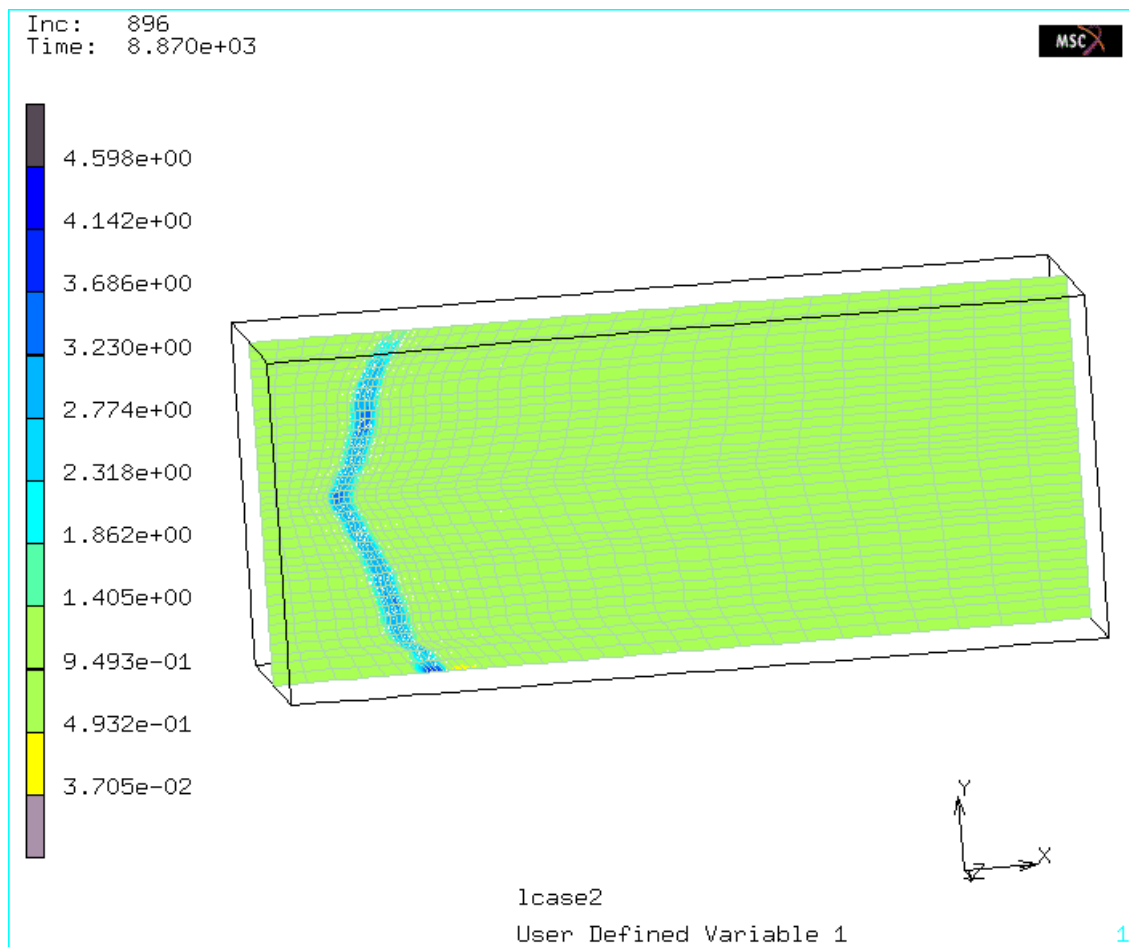
Inc: 896
Time: 8.870e+03



1case2
Comp 11 of Stress

1

III. Maximum principal stress map at the simulated time step of 8,960 h.



IV. Stress triaxial factor map at the simulated time step of 8960 hours.

Chapter 4

Evaluation of Creep Behavior with Continuum Damage Mechanics

4.1 Introduction

The 9Cr heat resistant steel normally services in header plate under low stress in thermal power plants with the consideration of mechanical properties and the cost. However, it is well known that long term exposure at elevated temperature leads the cracking due to void coalescence in the Type IV zone in weldment [4-1 and 4-2]. There have been some studies for the damage processes in the passing time. Among these works, the evaluation equations with the continuum damage mechanism (CDM) are most popular, which was first proposed by Kachanov [4-3] and subsequently modified by other researchers [4-4, 4-5, 4-6 and 4-7]. Development of the CDM is normally divided into two categories that are in macroscopic and microscopic aspects, respectively [4-8]. The macroscopic evaluation was used to predict the global deformation and damage on the materials including of the homogeneous and inhomogeneous materials. However the microscopic evaluation was conducted on the basic of the observation on micro damage such as vacancies, voids and micro cracking in the weak zone of materials. What I would express belongs to the macroscopic aspect. So far most of the evaluation works have been conducted on the homogeneous materials. But the assessment on the weldment seems to be difficult because of the complexity in addition to much cost and time. We need to consider the multiaxial stress state always exists in the complicated structures of the weldment. In additional equations to the CDM we can assume a constant level of the multiaxial stress state for material [4-9 and 4-10]. But this assumption is not valid in our case of FEM. The multiaxial stress state is much sensitive with the groove shape for a weldment

and it varies with the location in the FEM calculation. In this chapter, we propose modified CDM equations to evaluate the damage distribution and evolution in a weldment taking the conjunct role of equivalent creep strain and stress triaxial factor along the weak HAZ into account, without the consideration of the multiaxial stress rupture criteria. Since the voids nucleating and growing in the weak HAZ of the welded joint is the prior damage form, which would lead to Type IV cracking at last creep stage. Therefore, the evaluation results can be testified with consideration of the voids observation that mentioned in Chapter 2 and Chapter 3.

4.2 Constitutive Damage Equations

We had gave a detailed review on the constitutive equations with consideration of the continuum damage mechanics in its derivation procedures and historical development in Chapter 1. In this chapter, we would evaluate the creep behavior on the basis of the CDM equations. From the experienced equations under the multiaxial conditions, the relationship of creep damage and creep strain with time at a temperature can be given by follows [4-10 and 4-11]:

$$\frac{d\omega}{dt} = \frac{M[\alpha\sigma_1 + (1-\alpha)\sigma_{eq}]^\chi}{(1+\phi)(1-\omega)^\phi} \cdot t^m \quad (4.1)$$

$$\frac{d\varepsilon}{dt} = \frac{3}{2} A \frac{\sigma_{eq}^{n-1}}{(1-\omega)^n} S_{ij} t^m \quad (4.2)$$

where t is the time, and S_{ij} is the deviator respectively. σ_{eq} is the equivalent creep stress (Von Mises stress), and its solving method was mentioned in Chapter 3. Other coefficients and exponents such as n , χ , A , M , m and ϕ are the materials constants and independent of stress in conventional evaluation equations [4-12].

In Chapter 3, we discussed the mechanical parameters such as the maximum principal

stress and equivalent creep stress. They are mostly affected by the shape of grooves of a welded joint, and changing with the location variation during creep. For the complex situation, they are also variable with the creep time, so that the conventional CDM equations could not solved by only conducting several sets of simple tension creep-rupture tests. Calculating the average value of the mechanical parameters by the FEM simulation might be a good method. However, we used another method without consideration of the changing of the maximum principal stress and the equivalent creep stress in the welded joint. For utilizing the present experimental results, some modification on the conventional CDM equations was done. We used the applied stress σ_0 to substitute for the term $\alpha\sigma_1 + (1-\alpha)\sigma_{eq}$ and the equivalent creep stress in the conventional constitutive Equations (4.1) and (4.2). In second step of the modification, we induced a function of f^* with consideration of the conjunct effects of the stress triaxial factor and equivalent creep strain, for evaluating the damage distribution along the weak HAZ inside of the weldment. The function f^* was set around 1 and only reflect the damage distribution along the weak HAZ in the thick welded joint during long term creep without any effect on the creep-rupture time of components. Such we could get the modified CDM constitutive equations (4.3), (4.4) and (4.5) given by

$$\frac{d\omega}{dt} = \frac{M\sigma_0^\lambda}{(1+\phi)(1-\omega)^\phi} \cdot t^m \cdot f^* \quad (4.3)$$

$$\frac{d\varepsilon}{dt} = \frac{3}{2} A \frac{\sigma_0^{n-1}}{(1-\omega)^n} t^m \quad (4.4)$$

$$f^* = TF^{C\varepsilon} \quad (4.5)$$

where TF is the stress triaxial factor, C is equal to 100 for the modified 9Cr-1Mo steel at 600°C, and the factor ε denotes the equivalent creep strain. The inducing function of f^* is dependent of the conjunct effects of the stress triaxial factor and equivalent creep strain along the weaker zone in the welded joint from the FEM simulation. In Chapter 3, we had

summarized the conclusion that the large equivalent creep strain combining with the high level stress triaxial factor caused the nucleation of vacancy in weak HAZ of a thick welded joint at elevated temperatures. The production of the equivalent creep strain and the stress triaxial factor was used to mark the damage locations. In this Chapter the exponential function f^* containing the equivalent creep strain and the stress triaxial factor was also used to evaluate the distribution of the degree of damage in cross sectional of the welded joint during creep. Because both the two mechanical parameters are plus, one of them increasing would lead to the much serious damage. Therefore the large value of f^* refers the much critical damage. The exponents of ϕ and m are now defined as the stress dependent variables, and their solution methods will be expatiated in Section 4.2.1 and Section 4.2.2 in uniaxial and multiaxial conditions, respectively.

Integrating the equations (4.3) and (4.4), we obtain the evaluation equations as follows:

$$t_R = \left(\frac{m_1}{Mf^* \sigma_0^\chi} \right)^{\frac{1}{m_1}} \quad (4.6)$$

$$\varepsilon_R = \frac{3}{2} \cdot \frac{A}{Mf^*} \sigma_0^{(n-1-\chi)} \lambda \quad (4.7)$$

$$\omega = 1 - [1 - (t/t_R)^{m_1}]^{\frac{1}{\phi+1}} \quad (4.8)$$

$$\varepsilon = \varepsilon_R \{1 - [1 - (t/t_R)^{m_1}]^{\frac{1}{\lambda}}\} \quad (4.9)$$

where $m_1 = m + 1$ and $\lambda = \frac{\phi+1}{\phi+1-n}$. The factor of λ was ever referred as an invariable by Kim et al [4-13]. Here the factor of λ is dependent of the applied stress. The factor m and ϕ could be obtained from the relation with the applied stresses in Equations (4.8) and (4.9). The constants of M in uniaxial stress state and Mf^* under multiaxial stress state were defined as the constants and could be calculated from two sets of creep rupture tests at the same temperature. The other constants such as n , χ and A were obtained from the rupture times and rupture creep strain.

4.2.1 Uniaxial Stress State

Under the uniaxial stress state, we assume the material is homogenous, and the equivalent creep strain is same at any location and the stress triaxial factor is also same at any location with the value of 1, so that we can set the inducing factor f^* to be equal to a unit. The other six coefficients and exponents in the CDM evaluation equations (4.6-4.9) could be obtained by creep tests under different stress levels at the same temperature.

When fitting the material constants, we found that for the same material the creep-nominal time curves could be used to indicate the creep behavior under different stress levels. The damage and strain exponents m_I and λ are changing with the stresses applying on the specimen. With consideration of the data calculation among different materials, such as base metal, simulated HAZ and welded joint, the linear relations between the terms of $\log m_I$, $\log \frac{1}{\lambda}$, and the ratio of the applied stress to the yield stress were assumed as

$$\log m_I = k_1 \cdot \frac{\sigma_0}{\sigma_y} + b_1 \quad (4.10)$$

$$\log \frac{1}{\lambda} = k_2 \cdot \frac{\sigma_0}{\sigma_y} + b_2. \quad (4.11)$$

where k_1 , k_2 , b_1 and b_2 are the material constants, independent of the applied stress. σ_y is the yield stress of material and is obtained by the tensile test at the temperature corresponding to the evaluation.

4.2.2 Multi-Material Conditions

For the weldment composed of the different materials under uniaxial tensile stress, a complicated situation is caused by the differences of the material properties of the components of the welded joint. This makes the solution of the constants and the variables

difficult. We only obtained the strain recorders of the thickness welded joint under 90MPa at 600°C. The trends of the two exponents of m and λ are believed to be increase from the engineering practice. However, the present experimental results can not testify it. The two values of m and λ were just gotten under the stress of 90MPa under the temperature of 600°C.

4.3 Experiments and Discussions

4.3.1 Reviews of the Experiments

The round bar specimens with 4mm in diameter and 15mm in gauge length for simulated HAZ, those with 6mm in diameter and 30mm in gauge length for base metal, and smooth thin plate specimens for the welded joint were machined and crept in long term at 600°C with several stress levels from 80MPa to 160MPa. Several thick plate specimens were also machined from the welded joint with the specimen geometry shown in Fig 2-3d. These thick plate specimens were crept at 600°C under the applied stress of 90MPa. Their experimental recorders were listed in the Table 2-3, 2-4 and 2-5.

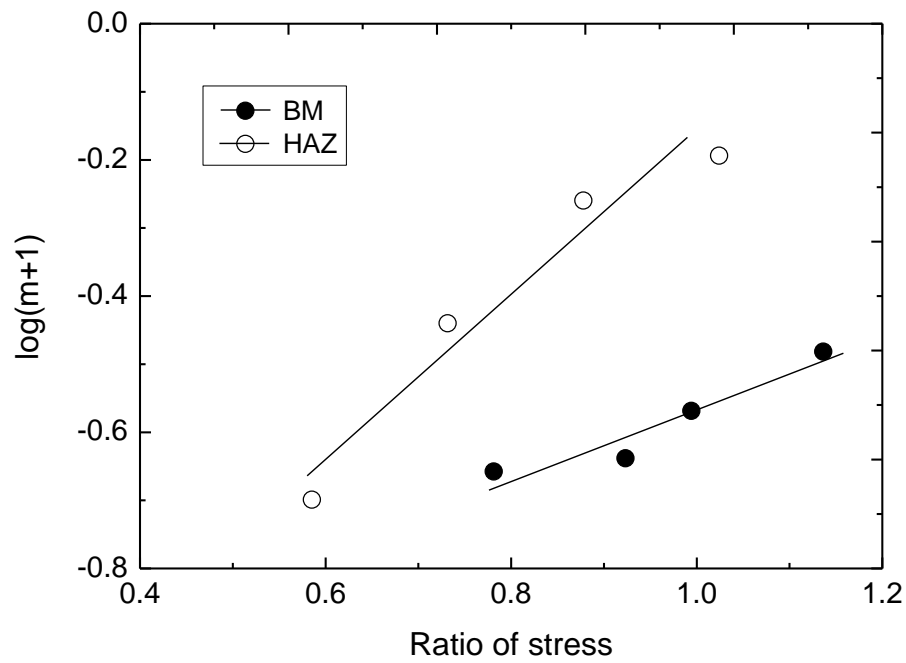
The creep tests on the thick welded joint were interrupted at about 1010, 2000, 4425, 6000, 7040 and 7970h, and its creep-rupture time is 8860h. The evolution and distribution of the voids in the HAZ of the thick welded joint were observed at the interruptions of 2000, 6000, 7040 and 7970h during creep. The observation of voids in the weak HAZ of the thick welded joint was used to testify the evaluation of damage with the modified CDM constitutive equations.

4.3.2 Logarithms of m and $1/\lambda$ Dependent on the Applied Stresses

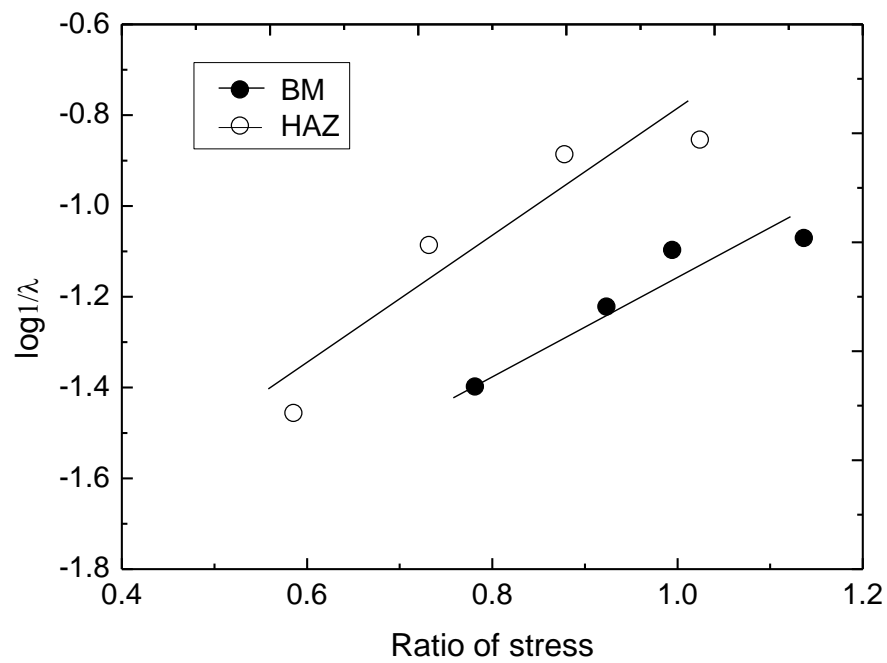
The two logarithms of m and $1/\lambda$ were fitted to the creep behavior experimental data normalized creep strain vs. normalized creep time for BM and FG-HAZ. The values of m and $1/\lambda$ were in the range from 0 to 1, but never reached these two end points. As shown in

Fig. 2, the logarithms of m and $1/\lambda$ increased in the applied stresses. Moreover, the values of m and $1/\lambda$ for the simulated HAZ were larger than that of BM at the same stress levels. Because n is a material constant independent of the applied stress, the numerator is smaller than the denominator in $1/\lambda$ $((\phi + 1 - n)/(\phi + 1))$, and the factor ϕ is monotone with the applied stress.

$1/\lambda$ tended to increase significantly with increase in the normalized secondary creep strain when the applied stress was lower than the yield stress, as shown in Fig. 3. The yield stress of BM and simulated HAZ was 140.8 and 136.7MPa, respectively. When the applied stress exceeded the yield stress, the normalized second creep strain decreased sharply with increase in $1/\lambda$, because there was not enough time for the secondary creep strain to progress and it thus was smaller than expected. This change in the relation of creep to the two logarithms m and $1/\lambda$ in the CDM equations shows that it is feasible to evaluate the creep damage with these equations.



(a)



(b)

Fig. 4-1. Relationships between exponents m_1/λ and the applied stresses at 600°C (where $m_1=m+1$ having been mentioned above).

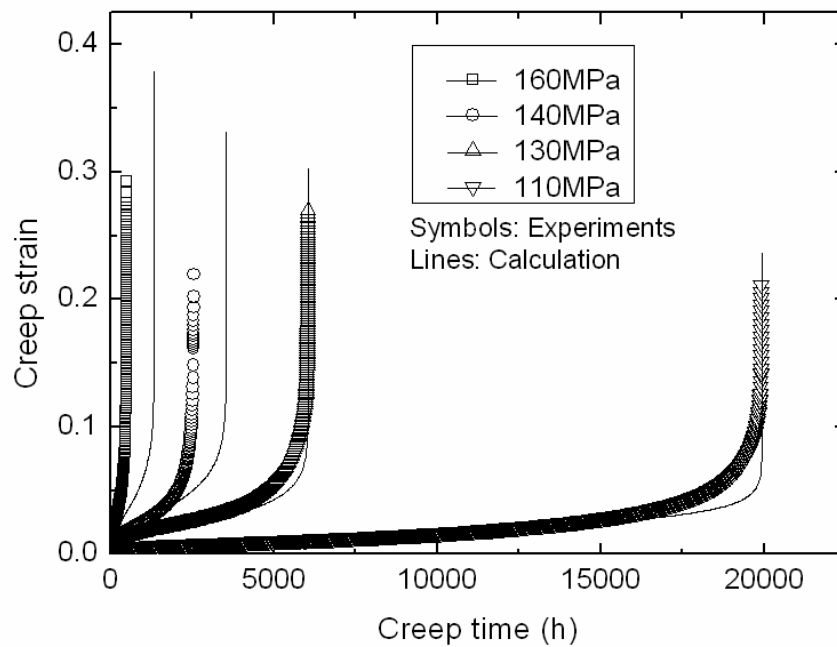
4.3.3 Global Evaluation for Strain and Damage of Base Metal, Simulated HAZ and Weldment

The constants in the modified CDM constitutive equations for the base metal, the simulated HAZ and the welded joint of the Mod.9Cr-1Mo steel at 600°C are listed in Table 4-1. These data of the welded joint were all obtained by the thin welded joints at different stress levels at 600°C. The prediction of creep strain has been conducted for the base metal and the simulated HAZ under several stress levels at 600°C, as shown in Fig 4-2. The strain evaluation on the base metal is greatly different from the experimental results conducted under the stress of 130MPa, same situation for the simulated HAZ under the stress of 100MPa. These are because the predictions of the creep-rupture time of materials are conservative. Generally speaking the predictions are good agreement with the experimental creep strain except for the tertiary stages. The calculation results of the base metal are much close to the experimental comparing with that of the simulated HAZ.

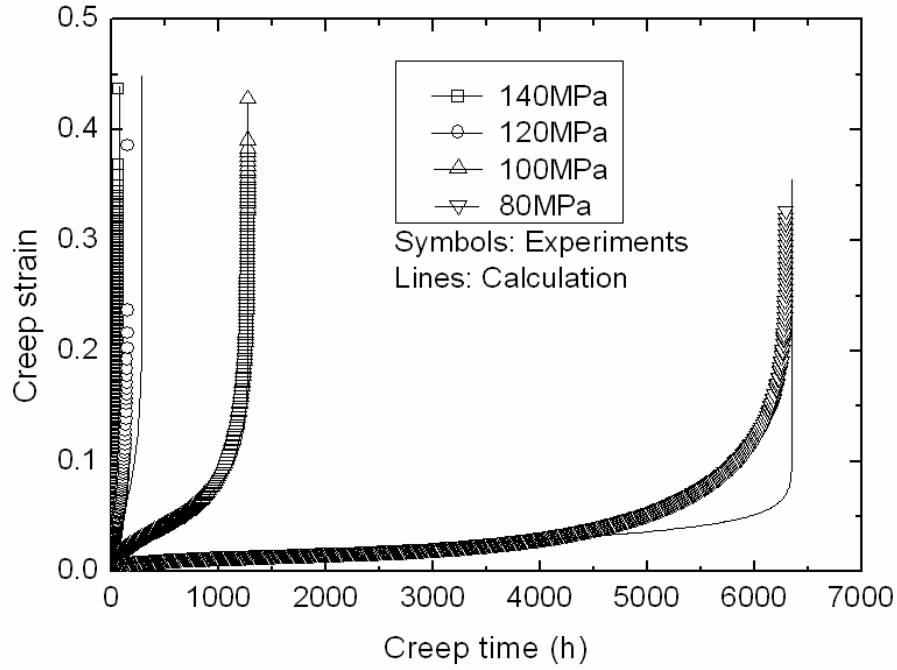
Table 4-1. Material constants for base metal, simulated HAZ and weldment at 600°C.

Constants	BM	Simulated HAZ	WJ
$s_y(\text{MPa})$	140.8	136.7	-
A	3.76E-12	1.44E-09	2.85E-07
n	4.7493	3.81	2.45
k_1	0.5415	1.159	-
k_2	0.954	1.3713	-
χ	0.4089	-0.055	0.6245
b_1	-1.08	-1.331	-
b_2	-2.111	-2.173	-
$M(\text{or } Mf^*)$	3.64E-03	4.04E-02	0.00244
m	-	-	0.14
φ	-	-	3.454

(Notes: The constants M is for the homogenous materials such as base metal and the simulated HAZ, and the term Mf^* is for the welded joint.)



(a)



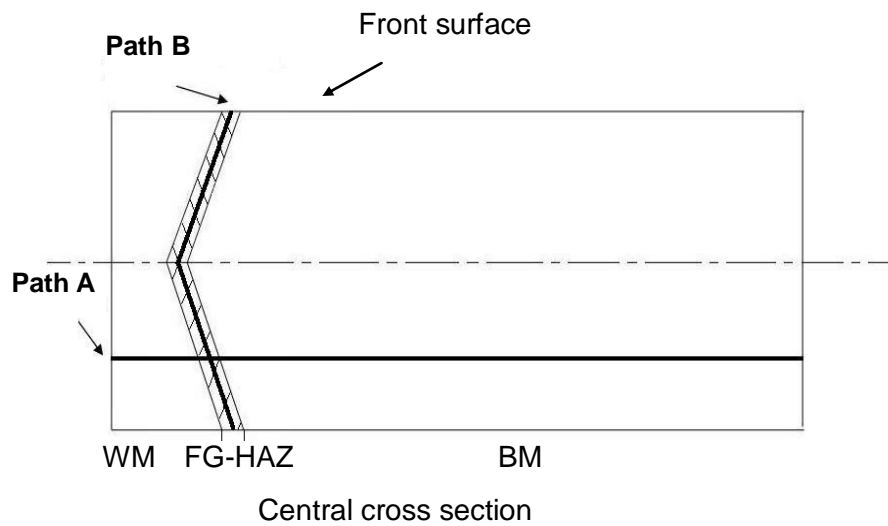
(b)

Fig. 4-2. Comparison of the calculated creep strain with experiments of a) BM and b) Simulated HAZ at 600°C.

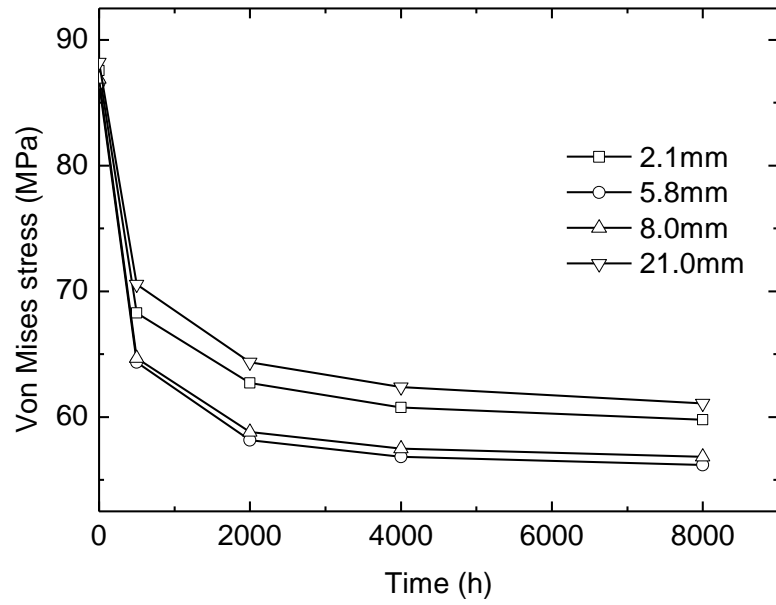
The effective stress to rupture used in the CDM equations in this study is not the term of $\alpha\sigma_1 + (1-\alpha)\sigma_{eq}$ as in the conventional evaluations [4-4, 4-6, 4-11, 4-12 and 4-14] but the engineering stress. In FEM analysis, the equivalent stress (Von Mises stress) and the maximum principal stress distributed in the weak HAZ are decreasing with time and are also changing with the location. Hence it seems difficult to search for a reasonable method to extract an average value for the above equations. The Von Misses stresses and the maximum principal stress at different positions, which are at the distance of 2.1mm, 5.8mm, 8.0mm and 21.0mm from the top surface along the ‘path B’ in FEM model as shown in Fig 4-3a, were calculated with time. It was found that the equivalent creep stress decreased with time at all of the observing positions for as shown in Fig 4-3b. The lowest Von Mises stress is in the location of 5.8mm to the top surface. Fig 4-3b indicates that the Von Mises stress decreases

deeply in early time and subsequently the reducing trends becomes slow. The maximum principal is very sensitive with the location variations: it greatly decreases with creep time in bottom surface (21mm) of the model, reduces slightly in the location close to front surface, hardly changing is found in the central part, and greatly increasing is in the early stage and suspends in the late stage in the central parts as shown in Fig 4-3c.

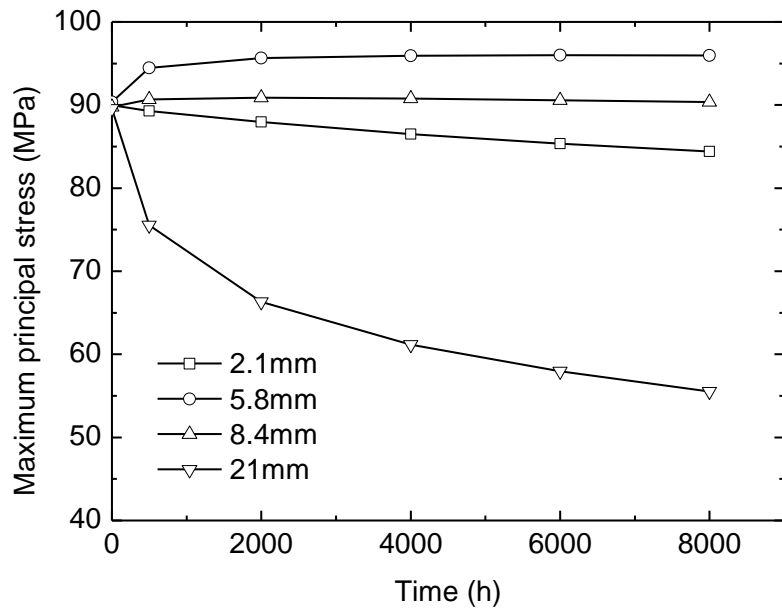
Therefore substituting the term $\alpha\sigma_1 + (1-\alpha)\sigma_{eq}$ and equivalent creep stress in the conventional constitutive equations makes the calculation easy and the evaluation procedure simply. The effects on the prediction on the creep-rupture time would be discussed in later sections.



(a)



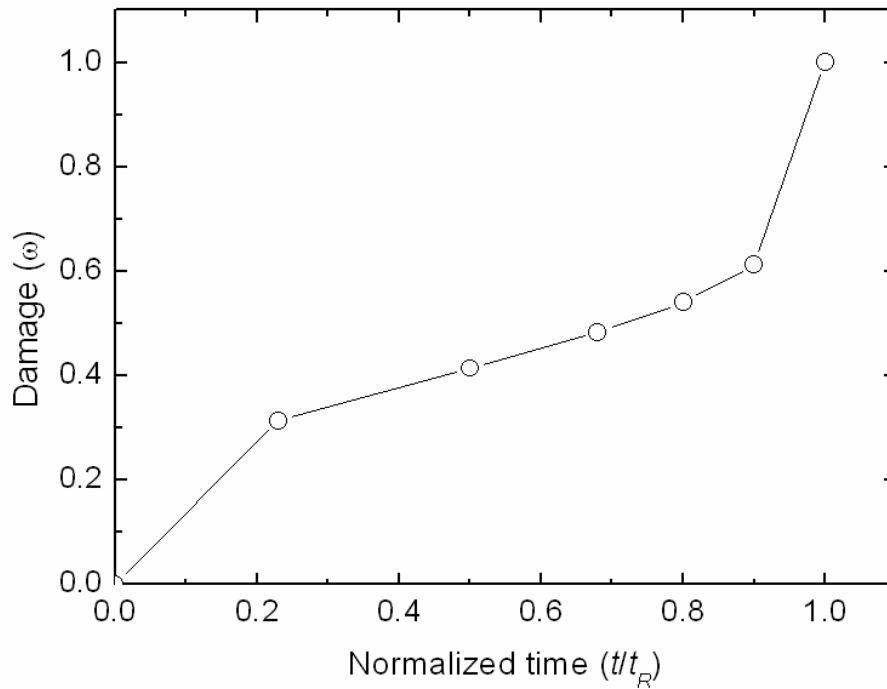
(b)



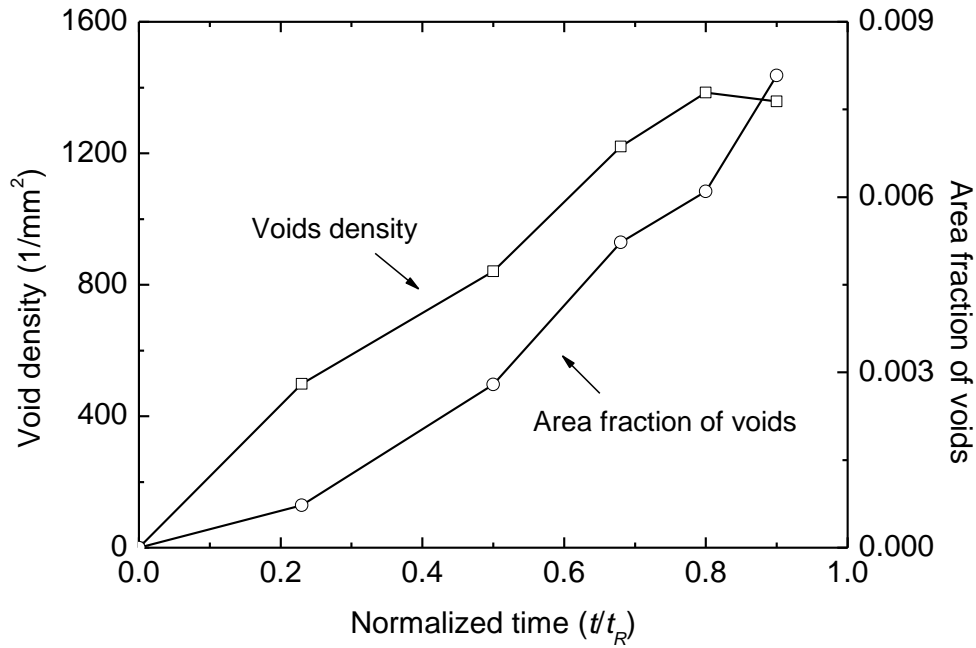
(c)

Fig. 4-3. Changes of the Von Misses stress and maximum principal stress in different locations in weak HAZ of the weldment during creep by FEM under 90MPa at 600°C.

The damage evolution prediction curve for the thick welded joint under 90MPa at 600°C is plotted in Fig 4-4a. The degree of damage reaches to 50% when the creep time is about 80% of the rupture life of the weldment. The number and area fraction of voids in the weak HAZ of a thick welded joint during creep were measured at several interruption times by using a laser microscope, and plotted in Fig 4-4b. The counting and calculating procedure was described in the previous paper [4-15]. The numbers of creep void increase before the 0.8 creep life, and decrease subsequently due to the voids connection. The area fraction of void in weak HAZ always increases with creep time, which is a good scalar quantity to mark the damage of materials.



(a)



(b)

Fig. 4-4. Damage evolution for a) prediction and b) experimental results of the thick welded joint under 90MPa at 600°C.

The predicted of the strain of the weldment were plotted against the time in Fig 4-5 with comparing the strain of the thick welded joint under 90MPa at 600°C. The rupture times are 6318h and 8853h for prediction and experiment, respectively. The calculated rupture strain is larger than the experimental results for the thick welded joint. The elongation at rupture of the evaluation is 0.016, and is larger than the thick welded joint with 0.009 in elongation. Actually, the evaluation coefficients and exponents were obtained from the thin welded joint specimens (with 17mm×5mm×100mm in dimensions) while the evaluation target was the thick welded joint specimen (with 21mm×21mm×100mm in dimensions). Large welded joint and small welded joint with the same groove of double U deserve different deformation due to the different degree of the constraints on them. Smaller constraints producing in smaller welded joint was clarified with the FEM simulation in Chapter 3. Therefore, deformation of the thin

welded joint during creep should be more closes to the prediction than that of the thick welded joint. Namely, the prediction on the deformation of weldment by the modified constitutive equations is reasonable.

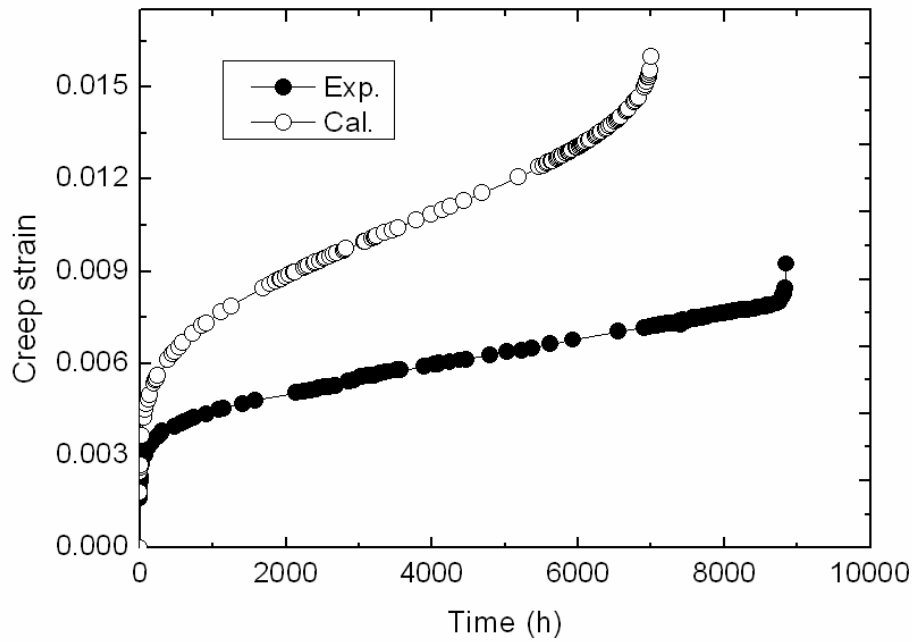


Fig. 4-5. Comparison of calculated and experimental creep strain curves for a thick weld joint under 90MPa at 600°C.

4.3.4 Evaluation of Damage Distribution in the Weak HAZ

In macroscopic aspects, the exponential factor for evaluating the damage with consideration of the conjunct effects of the equivalent creep strain and the stress triaxial factor in the weak HAZ calculated by FEM was used to evaluate the damage distributions in the thick welded joint. The evaluation is conducted in the transverse direction of the weak HAZ of the welded joint under 90MPa at 600°C. As we have mentioned in section 4.2, the introduced exponential function f^* is a scalar quantity and variable with locations in the weak HAZ. It is based on that the conjunct role of the triaxial factor and the equivalent creep

strain promotes the failure of the thick welded joint at elevated temperatures without any effect on the prediction of creep-rupture time in present study. The purpose of this evaluation primarily shows the distribution in the weak HAZ and the critical damage locations.

The final failure occurs due to the damage accumulation in all locations, and is related with the term of $\frac{\hat{\sigma} - \sigma_0}{\hat{\sigma}}$ in the weldment, where $\hat{\sigma}$ represents the break stress of the simulated HAZ. When the entire damage fraction exceeds this ratio, as a result, the failure of structure will occur. The predicted damage distributions and evolutions in the weak HAZ of thick welded joint at 90MPa and 600°C are shown in Fig 4-6. Damage factor is lower in both top and bottom surfaces while they are large in the parts close to surfaces, which can be supported with the subsurface cracks always being found in weak HAZ during long term creep. The damage factors are a little lower than the subsurface parts. On a whole, this diagram indicates that most critical damage in subsurface parts, and Type IV cracks will be produced in this zones.

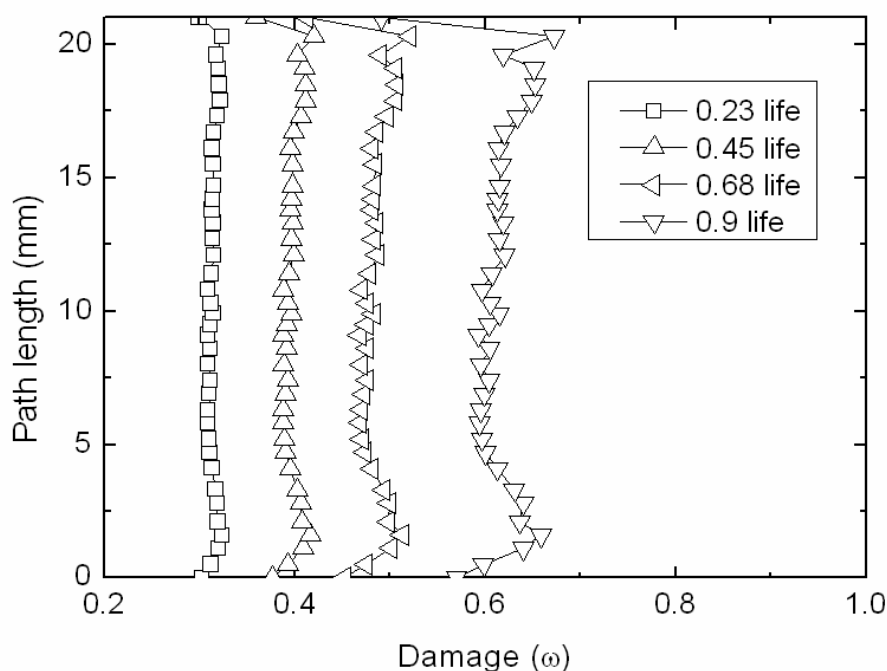
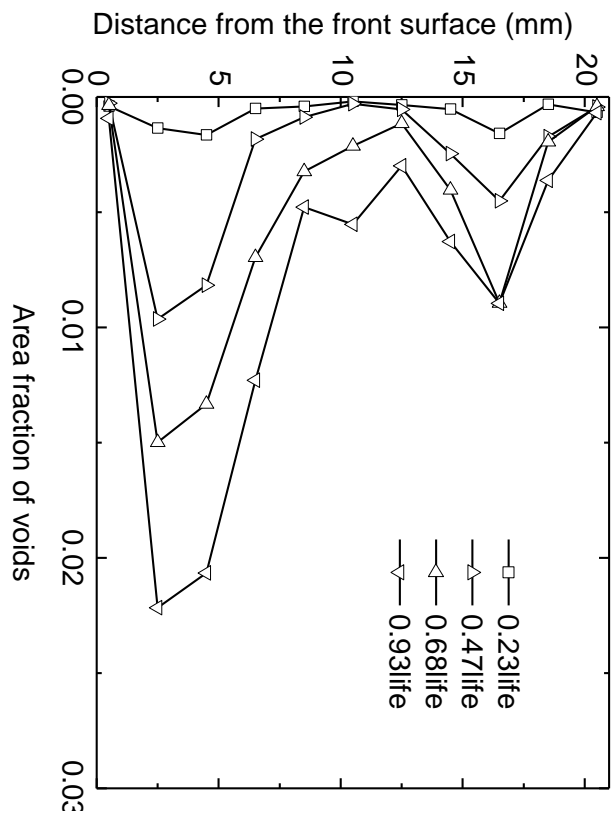


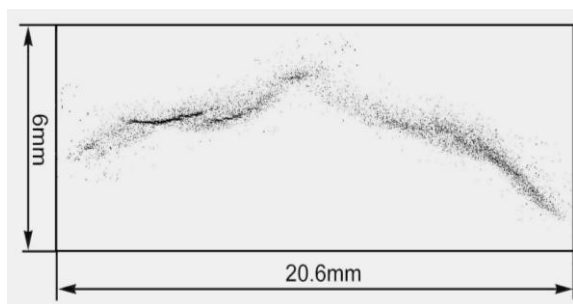
Fig. 4-6. Distribution and evolution of damage along transverse direction in the weak HAZ of the thick welded joint under 90MPa at 600°C.

Figure 4-7a shows the distributions of the area fraction of creep voids in HAZ along the thickness direction of the creep interrupted specimens, and Fig 4-7b, taken by a laser microscope, illustrates the actual profile of creep damages in weldment at 7970h. Large area fraction of void were found to focus in the 1/4 location in the transverse direction in the weak HAZ while the values of the area fraction of void in the surface parts (top and bottom) are lowest. The predicted damage distributions in Fig 4-6 are well in agreement with the experimental results shown in Fig 4-7a and profile of weak HAZ in Fig 4-7b observed by a LASER scope.

We used the function f^* with consideration of the conjunct role of the stress triaxial factor and the equivalent creep strain to predicting the damage locations, and it was testified successful.



(a)



(b)

Fig. 4-7. Distribution of the area fraction of creep voids in HAZ of the thick plate welded joint during creep at 600°C for 90MPa.

4.3.5 Creep Life Predictions

The modified CDM equations can be used to predict the creep-rupture time. Figure 4-8 compares our CDM calculations with the experimental results. The predicted results are close to the experimental results under high stress levels but not under low stress levels. As we discussed earlier, the two stress dependent constants (m and ϕ) and the other four material constants are invariable with time. However, the long term service at high temperature would deteriorate the material, which is the reason the predictions for the BM, simulated HAZ and particularly the welded joint are higher than the experimental creep life under low stress levels. The creep tests conducted under the high stress levels would lead to the short period creep life of material. However, at lower stress levels the creep-rupture time is corresponding longer than that under high stress levels. In long term creep the material deteriorates due to the changing of microstructures and the high temperatures enhances the behavior. Thus the material has changed in creep strength. The material constants particular M and χ are scalar quantities, and obtained from the short term creep testing. They are incredible to predict the creep-rupture time of materials under lower stress levels and at elevated temperatures. We used the material factors M and χ as the invariables to predict the creep-rupture life. The predicting results testified no agreement with the experimental results under the stress lower than 70MPa at 600°C.

Sawada supported that the degradation of the materials is due to the formation of large Cr_{23}C_6 , Laves phase and Z phase [4-16 and 4-17]. The degradation and damage mechanism would be discussed in Chapter 5 in details. Therefore, we proposed that the material factors M and χ is the function the applied stresses in these phenomenological evaluation equations, which should be better for predicting the creep-rupture life of materials under lower stress levels.

Figure 4-9 shows the comparison of the creep-rupture life of experiments and calculation with the Manson-Haferd method at the three temperatures. This calculation method gives a

much conservative prediction comparing with the CDM constitutive equations.

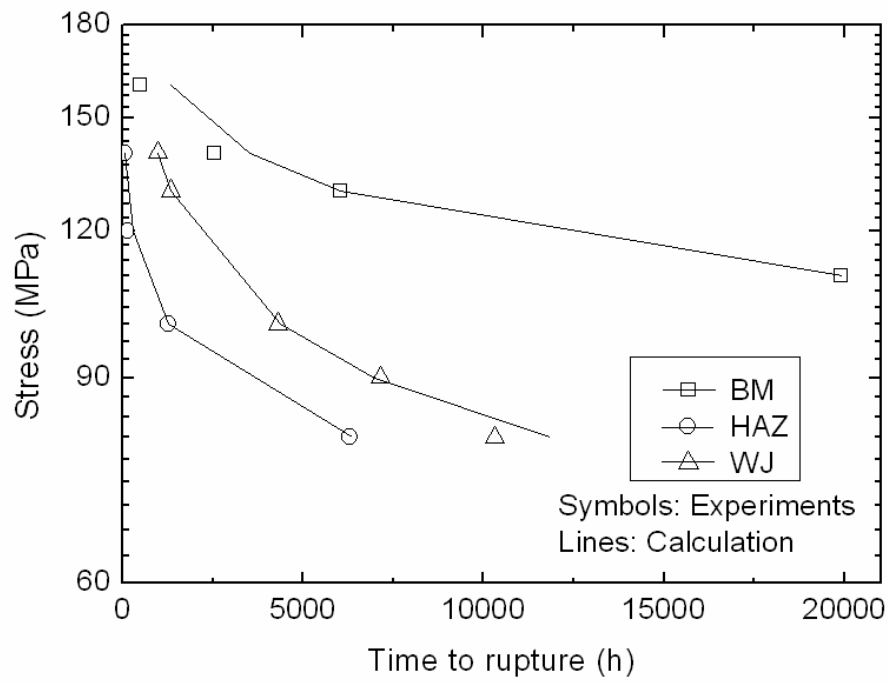


Fig. 4-8. Prediction of creep-rupture time of the BM, WJ and simulated HAZ with the modified constitutive equations comparing with the experimental results at 600°C.

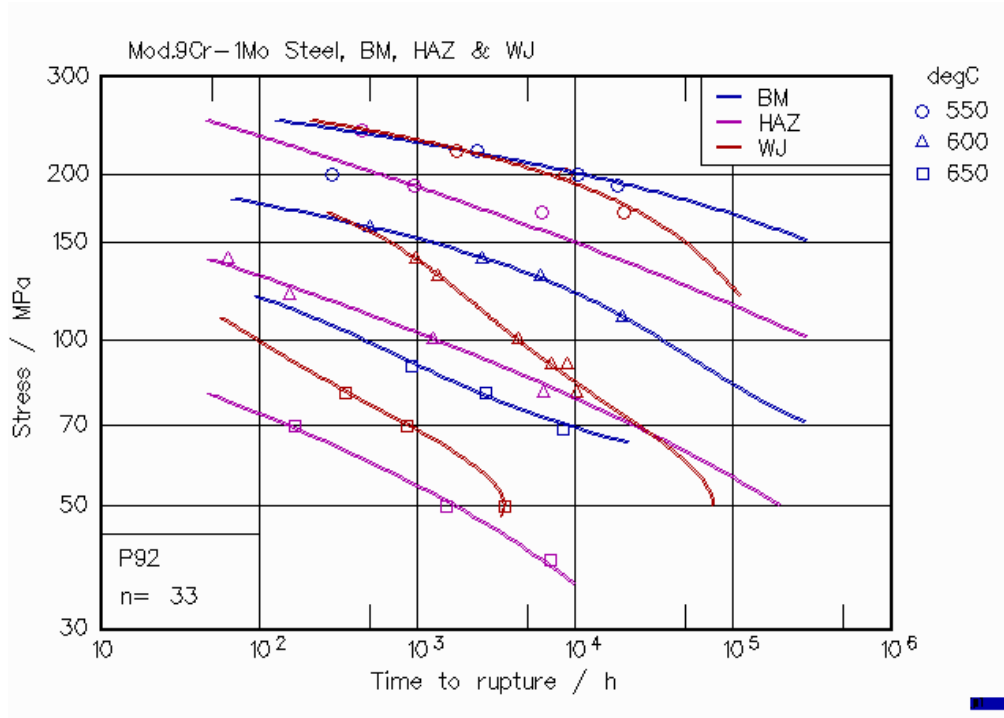


Fig. 4-9. Prediction of the creep-rupture time by the Manson-Haferd TTP equations comparing with the experimental results at 600°C.

4.4 Effects of the Substitutions by the stresses on the Creep-Rupture Life

Just as we have mentioned above the inducing of the exponential function f^* do not have any effects on the prediction of creep-rupture time of the weldment in the present study. We have done some modification on the CDM constitutive equations with substituting for the term $\sigma_1 + (1 - \alpha)\sigma_{eq}$ with the applied stress. The factor α was multiaxial stress rupture criteria and ranged from 0 to 1. σ_{eq} was the equivalent creep stress and could be obtained by FEM calculation. Its formula could be expressed by

$$\sigma_{eq} = \frac{\sqrt{2}}{2} [(\sigma_1 - \sigma_2)^2 + (\sigma_2 - \sigma_3)^2 + (\sigma_3 - \sigma_1)^2]^{1/2} \quad (4.12)$$

σ_1 , σ_2 and σ_3 are the principal stress. Normally both the equivalent creep stress and the maximum principal stress are all changing with time and with location variation. The equivalent creep stress is lower than the maximum principal stress and 60-70% of it, which

has been stated in the Chapter 3. Thus the rupture stress in CDM equations was lower than the applied stress σ_0 due to the role of multiaxial stress rupture criteria α . The readers might suspect whether the changing of effective stress to rupture affects the prediction or not. The answer is “NEVER”. Actually, the substitution of the applied stress for the stress in the mixed criteria could not affect the rupture time prediction for the weldment comparing with the conventional methods. Since σ_0 was adopted, the related constants M and m in the equation (4.12) would also change comparing with the conventional constitutive equations.

We had discussed the triaxial factor prolonged the creep rupture life of material with decreasing the Von Mises stress under high stress levels in Chapter 3 while it accelerated the nucleation of voids with combining with the equivalent creep strain under lower stress levels. The stress triaxial factor has a two-sided role on the creep life of material servicing at high temperatures. In this chapter, we induced the function with consideration of the triaxial factor and equivalent creep strain to evaluate the damage distribution along the weak HAZ of the thick welded joint. However, its effects on the creep life of the material were almost neglected in the present study. The differences of the creep lives of the homogenous material and the heterogeneous material (between the simulated HAZ and the welded joint) could be embodied by the other material constants, such as M and χ . The relation between the triaxial factor and the constraints for the material had been clarified that the constraints focusing on the weaker zone would increase with the value of the stress triaxial factor. Also we knew that the multiaxial stress rupture criteria in the range from 0 when rupture time wholly depended on the maximum tension stress to 1 when the rupture time was dependent upon the maximum effective stress. Namely the constraints on the components are the unearthly largest when the multiaxial stress rupture criteria is equal to 0. The factor α has an inverse trend with the gradient of constraints in the material, hence increases with the decreasing of the stress triaxial factor. If the multiaxial stress rupture criteria will be used to predicting the rupture life,

the increasing trends of it should be considered since the constraints are relieved in long term servicing.

4.5 Summary of Chapter 4

A CDM approach was used to evaluate the creep damage of the thick welded joint of the Mod.9Cr-1Mo steel at 600°C, with the aid of FEM simulation. On the basis of the interrupted creep tests we determined the materials constants for the CDM and discussed the void evolution processes. The conventional evaluation equations for creep damages have been modified by substituting the engineering stresses for equivalent creep stress and the terms containing stress without considering of the multiaxial stress state. The linear relation of the logarithm of m_1 (and $1/\lambda$) with the applied stress in homogeneous material was used to fit the material constants. By introducing a function of f^* , we can successfully predict the damage distribution and evolution in the weak HAZ of a weldment with considering the effects of the conjunct role of the stress triaxial factor and the equivalent creep strain in the weldment. The effects of the triaxial factor and the equivalent creep strain on the creep rupture life were almost neglected.

References of Chapter 4

- [4-1] S. J. Brett, D. J. Allen, J Pacey: **CHIFI International Conference**, (Milan, 1999) pp. 873-884.
- [4-2] S. J. Brett, D. L. Oates, C. Johnston: **ECCC Creep Conference**, (London, 2005) pp. 563-572.
- [4-3] L. M. Kachanov: Izvestiya Akademii Nauk SSR Otdelenie Technicheskikh Nauk. **8** (1958) 26-31.
- [4-4] D. R. Hayhurst, P. R. Dimmer and M. W. Chernuka: J. Mech. Phys. Solids. **21** (1973) 431-446.
- [4-5] A. C. F. Cocks and M. F. Ashby: Metal Science. (1980) 395-402.
- [4-6] A. A. Becker, T. H. Hyde, W. Sun and P. Andersson: Computational Material Science. **25** (2002) 34-41.
- [4-7] S. T. Tu, R. Wu and R. Sandström: International Journal of Pressing Vessel and Piping. **58** (1994) 345-354.
- [4-8] T. Yu, M. Yatomi and H. J. Shi: **6th Japan-China Bilateral Symposium on High Temperature Strength of Materials**, (The Society of Materials Science Japan, 2007) pp. 137-142.
- [4-9] D. R. Hayhurst: J. Mech. Phys. **20** (1972) 381-390.
- [4-10] T. H. Hyde, W. Sun and A. A. Becker: International Journal of Pressing Vessel and Piping. **78** (2001) 765-771.
- [4-11] D. R. Hayhurst, P. R. Dimmer and C. J. Morrison: Philosophical Transactions of the Royal Society of London. Series A, Mathematical and Physical Sciences. **311** (1984) 103-129.
- [4-12] F. R. Hall and D. R. Hayhurst: The Royal Society. **433** (1995) 383-403.
- [4-13] W. G. Kim, S. H. Kim and W S Ryu: Japan Society of Mechanical Engineers: **Proccedings of CREEP7**. (Japan Society of Mechanical Engineers, 2001) pp. 167-172.

- [4-14] D. R. Hayhurst, M. T. Wong and F. Vakili-Tahami: JSME International Journal, Series A. **45** (2002) 90-97.
- [4-15] Y. K. Li, H. Hongo, M. Tabuchi and Y. Monma: International Journal of Pressure Vessel and Piping. (*to be published*)
- [4-16] K. Sawada, K. Miyahara, H. Kushima, K. Kimura and S. Matsuoka: JSME International Journal. **45** (2005) 1934-1939.
- [4-17] K. Sawada, H. Kushima and K. Kimura: JSME International Journal. **46** (2006) 769-775.

Chapter 5

Creep Mechanism of a Welded Joint of Mod.9Cr-1Mo Steel

5.1 Introduction

A typical application of the 9Cr heat resistant steel is the header plate in thermal power plants with the consideration of mechanical properties and the cost. However, it is well known that long term creep exposure at elevated temperature leads the cracking due to void coalescence in the Type IV zone in weldment [5-1 ~ 5-2]. The reasons for the damage can be discussed in two aspects: they are macroscopic mechanism and microscope mechanism. In macroscopic aspect discussed in the previous chapters, we have got the conclusion that the conjunct role of the stress triaxial factor and the equivalent creep strain accelerate the nucleation of the voids in the weak HAZ of the Mod.9Cr-1Mo steel at high temperatures. The coalescence of voids finally lead to the Type IV cracking in the weak zone. The weak zone is composed of the fine-grained HAZ and intercritical HAZ in the welded joint. In this Chapter, we focus on the damage mechanism in the microscopic aspect on the basis of the conclusion in the previous chapters. In the microscope aspect, the most popular is the strain heterogeneity among grains causing the nucleation and large strain contributing its growth that was proposed by Lee [5-3]. Other models also were proposed, such as the diffusion, sliding models. However they have not been clarified yet. Therefore, we would also use the modified models to explain the microscope mechanism of the nucleation and growth of voids in the weak HAZ in the thick welded joint.

5.2 Creep Damage Locations in the Welded Joint

That which part is the weakest location, or where the Type IV cracks are produced for the

welded joint of the Mod.9Cr-1Mo steel are still the controversial topics currently. In this section, we try to clarify it from the creep testes, microhardness measurement and micro observations.

5.2.1 HAZ in the Welded Joint

The rapid heating and cooling during the joining process inevitably leads to the formation of the HAZ which contains ferritic multi-phase. According to the traditional metallurgy the HAZ is composed of three different parts. They are of the fully quenched, partially quenched, and tempered zone due to peak temperatures during weld. The three parts are produced by the effect of the peak temperatures above A_{c3} , between A_{c3} and A_{c1} , and lower than A_{c1} respectively. The fully quenched zone in the HAZ can also be divided into two parts: the coarse-grained HAZ and the fine-grained HAZ because of the microstructural changes in welding as shown in Fig 5-1 [5-4]. This figure is suitable to the Mod.9Cr-1Mo ferritic heat resistant steel. During weld, the locations that are heated above the temperature of A_{c3} , where the solid metal melts and then recrystallization occurs with the fast cooling, is known as the fully quenched zone. The zone affected by the temperatures from A_{c3} to 1100°C is named as the fine-grained HAZ in the welded joint of the Mod.9Cr-1Mo steel. This zone is composed of the fine martensite and fine ferrite for high chromium steels. When the temperatures are much higher than the A_{c3} , such as high than 1100°C , the microstructures there are overheated, which provide enough time for the grains growing up, hence the zone with the special heat-treatment was named as the coarse-grained HAZ. Also the so-called intercritical HAZ is produced around the peak temperature $A_{c1}\sim A_{c3}$ because some of the prior phases do not transmit fully into austenite due to the lower temperatures and the rapidly heating. The intercritical HAZ is corresponding to the partially quenched zone in the HAZ of the Mod.9Cr-1Mo steel. In this zone when the temperatures are higher than A_{c1} , the austenite transmitting occurs with the fast heat input and then the fine martensite is produced inside the

austenite grain with the fast cooling due to the weld. Thus the intercritical HAZ is composed of the fine-martensite phase and ferritic grains in large size, etc. Therefore, the residual phase in large sizes mixing with the fine grains in this zone is defined as the intercritical HAZ. When the peak temperatures are lower than the temperature of A_{c1} , which leads no phase transmitting, the region affected with the temperatures is defined as tempered zone. The microstructures in this part are not changed but deserving the tempering. Next part of the intercritical HAZ is the base metal without affected by the thermal recycle during weld. Base metal is the weaker zone under high stress levels while it has good creep resistance due to the good toughness. In another side of the HAZ, near to the coarse-grained HAZ is the weld metal that shows high resistance in creep for the Mod.9Cr-1Mo steel.

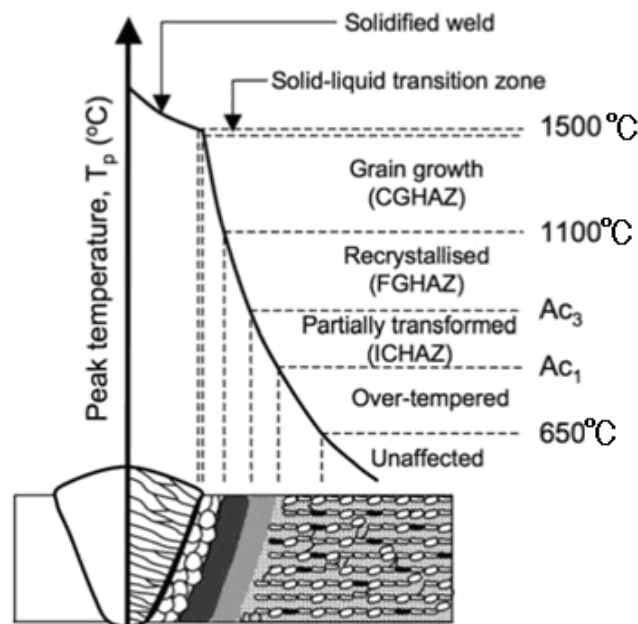


Fig. 5-1. Corresponding peak temperatures for the HAZs in a welded joint of the high chromium ferritic heat resistant steel [5-4].





5.2.2 Weak Zone in the Welded Joint

For the high chromium steel, the typical damage form is the Type IV cracking in

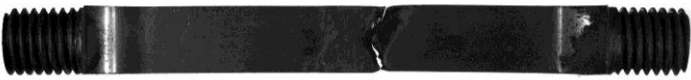



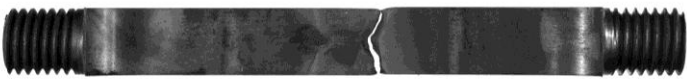
engineering application in practice. Normally, the conditions are high temperatures and low levels of the applied force. However, there are other types of damage form when the external conditions alter.

5.2.2.1 Rupture Results

The welded joint fractures at the base metal at high stress and low temperatures as we mentioned according to the experimental observation in Chapter 2. The welded joint with $17\times5\times100\text{mm}$ in dimensions called Thin welded joint in present study were crept at 550, 600 and 650°C , and the specimens fractured after crept are as shown in Fig 5-2 a, b and c. Under the temperature of 550°C , the welded joints were ruptured in base metal at the stress higher than the stress of 220MPa while they were failure in the HAZ lower than the stress of 200MPa. The creep tests indicate that the creep strength of the weak HAZ is higher than the base metal under high stress levels at low temperatures. This reasons have been discussed in Chapter 3, the constraints on the weak HAZ due to the stress triaxial factor decrease the Von Mises stress (components of the effective rupture stress to creep-rupture time) in short period when the boundary sliding and diffusion of atoms are not prominent. Therefore under high stress levels, the weaker zone in the welded joint of Mod.9Cr-1Mo steel is base metal but the weak HAZ. However, at testing temperatures such as 600 and 650°C , the welded joint were all fractured in the HAZ under the stresses lower than 140MPa. In this case, the constraints lose its controlling on the creep behavior at high temperatures, and the micro mechanism succeeds to it.

	550°C, 240MPa $t_r = 451.6\text{h}$	BM
	550°C, 220MPa $t_r = 1783.9\text{h}$	BM
	550°C, 200MPa $t_r = 8662.6\text{h}$	HAZ
	550°C, 170MPa $t_r = 20460.6\text{h}$	HAZ

a)

	600°C, 140MPa $t_r = 983.9\text{h}$	HAZ
	600°C, 130MPa $t_r = 1341.7\text{h}$	HAZ
	600°C, 100MPa $t_r = 4324.8\text{h}$	HAZ
	600°C, 90MPa $t_r = 7147.1\text{h}$	HAZ
	600°C, 80MPa $t_r = 10330.5\text{h}$	HAZ

b)

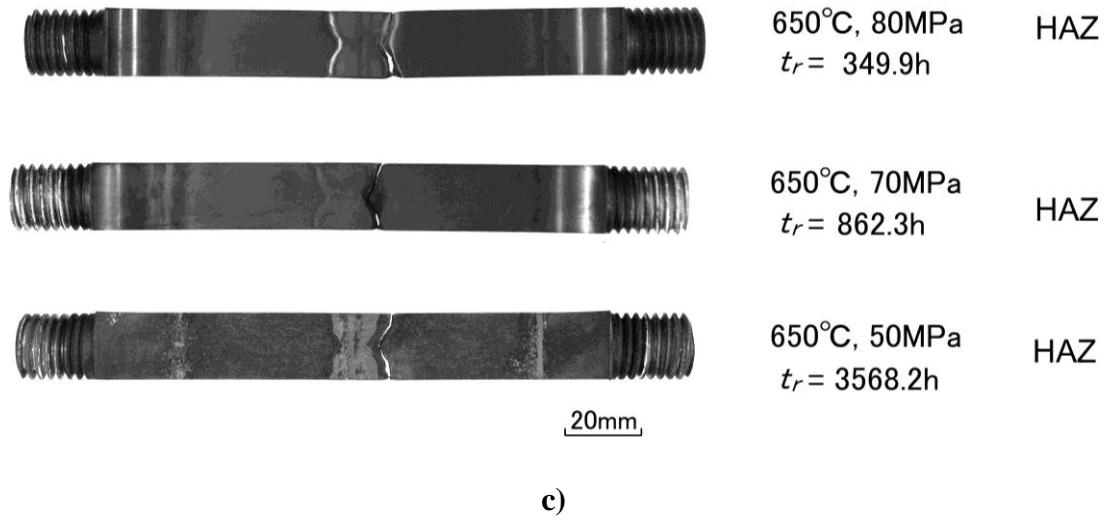


Fig. 5-2. Fractured locations in the thin welded joints crept at different temperatures in the stresses ranging from 50MPa to 240MPa.

Actually the weaker zone is still a confusing topic under the stress in low levels at high temperatures. The intercritical HAZ was thought of the weakest zone during long term creep in prior references [5-3, 5-5 ~ 5-8]. They support the assumption that might be due to the creep strain heterogeneity among the grains because the sizes of grain in the intercritical are different greatly [5-3]. Some researchers supported that the fine-grained HAZ was the location for crack producing [5-9 ~ 5-17]. The basic of it is small grains that have the weak resistance to the creep damage comparing with the large grains with fine sub-grains in the theoretic [5-18]. Hasegawa clarified the lives relation of the fine-grained HAZ and base metal on the base of the differences of the grain sizes respectively [5-19]. The predicting lives of the fine-grained HAZ and the base metal can be indicated by the squared ratio of grain diameters inside the different parts. The relation can be expressed by Equation (5.1).

$$\frac{t_{rHAZ}}{t_{rBM}} = \left(\frac{d_{HAZ}}{d_{BM}} \right)^{rp} \quad (5.1)$$

where t_r is the creep life of materials and the factor d indicates the grain diameter in average.

p is a material constant and usually is equal to 1.3 for the high chrome heat resistant steel, and r is the Monkman-Grant constant in the function of $\log t_r + m \log \left(\frac{d\varepsilon}{dt} \right)_m = C$ [5-20]. In order to solve this constant, we can firstly plot a diagram of the minimum creep strain rate versus the rupture life of material, and the slope of the lines is the value of r . The slopes of the base metal and HAZ are same since they all belong to the high Cr steel and have no large differences in chemical compositions. The BM and HAZ in the equation represent the base metal and fine-grained HAZ, respectively. Generally, according to the grain size of the base metal the much smaller grain size in the fine-grained HAZ, the much shorter servicing time of the welded joint. However, this method is valid only in the condition that the fine-grained HAZ is the weakest zone to be resistant creep at high temperatures. Therefore, it is need to do experiments in details to clarify.

Actually, differentiating the fine-grained HAZ from the intercritical HAZ is a difficult procedure since the intercritical HAZ is a narrow zone in the HAZ, due to the fast cooling when the peak temperatures range from Ac_3 to Ac_1 and other complicated reasons. Therefore, the intercritical HAZ was classified into the fine-grained HAZ as the weaker zone when we conducted the FEM simulation in Chapter 3. The location near to the fine-grained HAZ could be same to the fine-grained HAZ while the location near to the tempering zone was classified into the tempering zone. For the mechanical calculation we think it is a valid assumption.

5.2.2.2 Weak Zone in HAZ Selecting

We conducted the creep tests for the simulated HAZ reproduced at different peak temperatures at 550°C and 600°C as shown in Fig 5-3. The results were discussed in Chapter 2 in details. The Ac_3 line for the Mod.9Cr-1Mo steel in the figure apparently shows that it is closed to 925°C and Ac_1 is lower than 825°C. The peak temperatures ranging from 900°C to 925°C lead to the minimum rupture time for the specimens at different stress levels. The figure shows that the minimum creep strength transmits from the intercritical HAZ to the

fine-grained HAZ with the increasing of the applied forces at temperature of 600°C. The peak temperature was selected as 900°C to reproduce the weak zone of the HAZ (later we call it weak HAZ for convenience), also indicated that the intercritical HAZ is the weakest zone to creep resistance in the uniaxial stress state in present testing extents. The simulated HAZs in 925~950°C show a little higher than the simulated intercritical HAZ in creep strength while they are much lower than the base metal. It is apparently we select the intercritical HAZ as the weak HAZ in Chapter 3 according to Fig 5-1. However, we do not indicate that the whole intercritical HAZ are the weakest zone in a welded joint because we could not know the situations of the simulated HAZ affected by the peak temperatures between 900~925°C. Even this selecting zone might not be the weakest HAZ, but it would be valid since the corresponding relation to weld metal can be reflected.

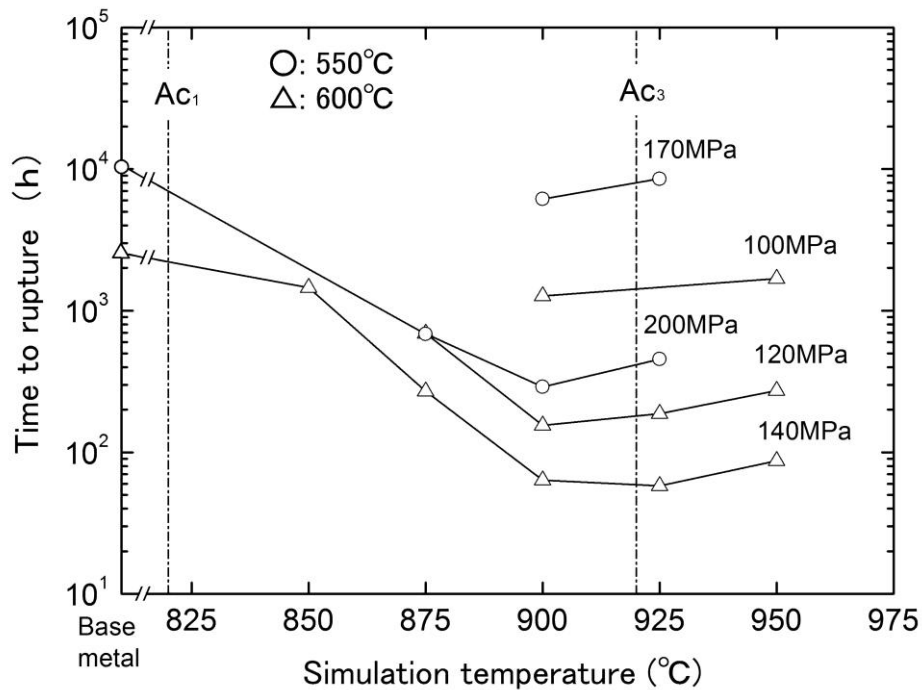


Fig. 5-3. Comparison of the creep-rupture time among the simulated specimens at different peak temperatures (Creep testing conditions: at temperature of 550°C and 600°C, and under the stress ranging from 100MPa to 200MPa).

5.2.2.3 Micro-hardness and Voids Distribution

In order to clarify the actual location of the weak zone in the HAZ in thick welded joint, we also conducted the microhardness measurements in the longitudinal direction of welded joint. It was carried out on the rupture specimens crept at 550°C and 650°C. Comparing with the welded joint in the condition as weld, we plotted the Fig 5-4. In the horizontal coordinate the '0' location denotes the bond line in the welded joint, and separates the weld metal and the HAZ in left and right side respectively. On the right side of the bond line, the coarse-grained HAZ, fine-grained HAZ, intercritical HAZ, tempered zone and base metal had been denoted in location order in the figure. With the hardness observation on a whole, the hardest location is the bond line among the three listed specimens while the hardness in weld metal is comparative lower. The coarse-grained HAZ is the transmitting zone from the high level of hardness (weld metal) to the lowest hardness (in other parts of the HAZ). The lowest location in the as weld specimen is in the tempering zone while after creep tests the weakest hardness transmits into the mixing zone of the fine-grained HAZ and intercritical HAZ. When the specimen was crept at the temperature of 550°C, the weakest location in hardness is close to the tempering zone and is most probable the intercritical HAZ. After checking the rupture specimen of welded joint crept at the temperature of 650°C, the weaker location in hardness is close to the coarse-grained HAZ and is most probable the fine-grained HAZ. These indicate that the effects of the temperature on the material degradation are larger than the time. Large precipitates could be easily produced at high temperatures in the grain boundaries so that the hardening effect of the smaller precipitates is lost. According to the locations (a), (b), (c) and (d) in the Fig 5-4, the related optical microstructures had been investigated by OM as shown in Fig 5-5. Locations such as (a) and (c) can be known to show the coarse-grained HAZ and the exactly location of the boundary of intercritical HAZ / tempering zone. The smallest grain size in the Fig 5-5b could be differentiated from all the four photographs clearly so that around the 'b' location denoted in Fig 5-4 could be made sure of the fine-grained HAZ. The

location of 'd' in Fig 5-4 denotes the tempering zone, and has no apparent differences with that of the base metal shown in the Fig 5-5e. Figure 5-5f is the microstructure of simulated HAZ at the peak temperature of 900°C. The Ac3 point of the Mod.9Cr-1Mo heat resistant ferritic steel is about 920°C denoted in Fig 5-3. Therefore the simulated HAZ is actually the intercritical HAZ. Comparing with the Fig 5-5b, the sizes of the microstructures in the intercritical HAZ (simulated HAZ at 900°C) are not homogeneous. Smaller and large grains are there in simultaneity. The microhardness at 650°C decreases greatly in 'b' location, and the actual value is almost same to that in the part close to the tempered zone.

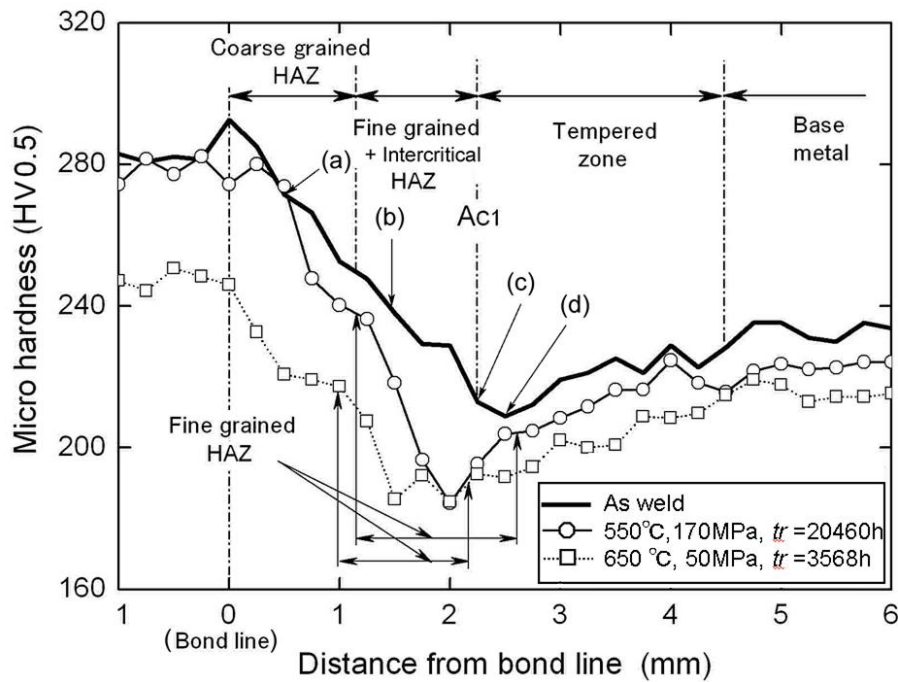


Fig 5-4. Comparison of microhardness-distribution in the welded joints at the different conditions (as weld, crept under 170MPa at 550°C and under 50MPa at 650°C, respectively).

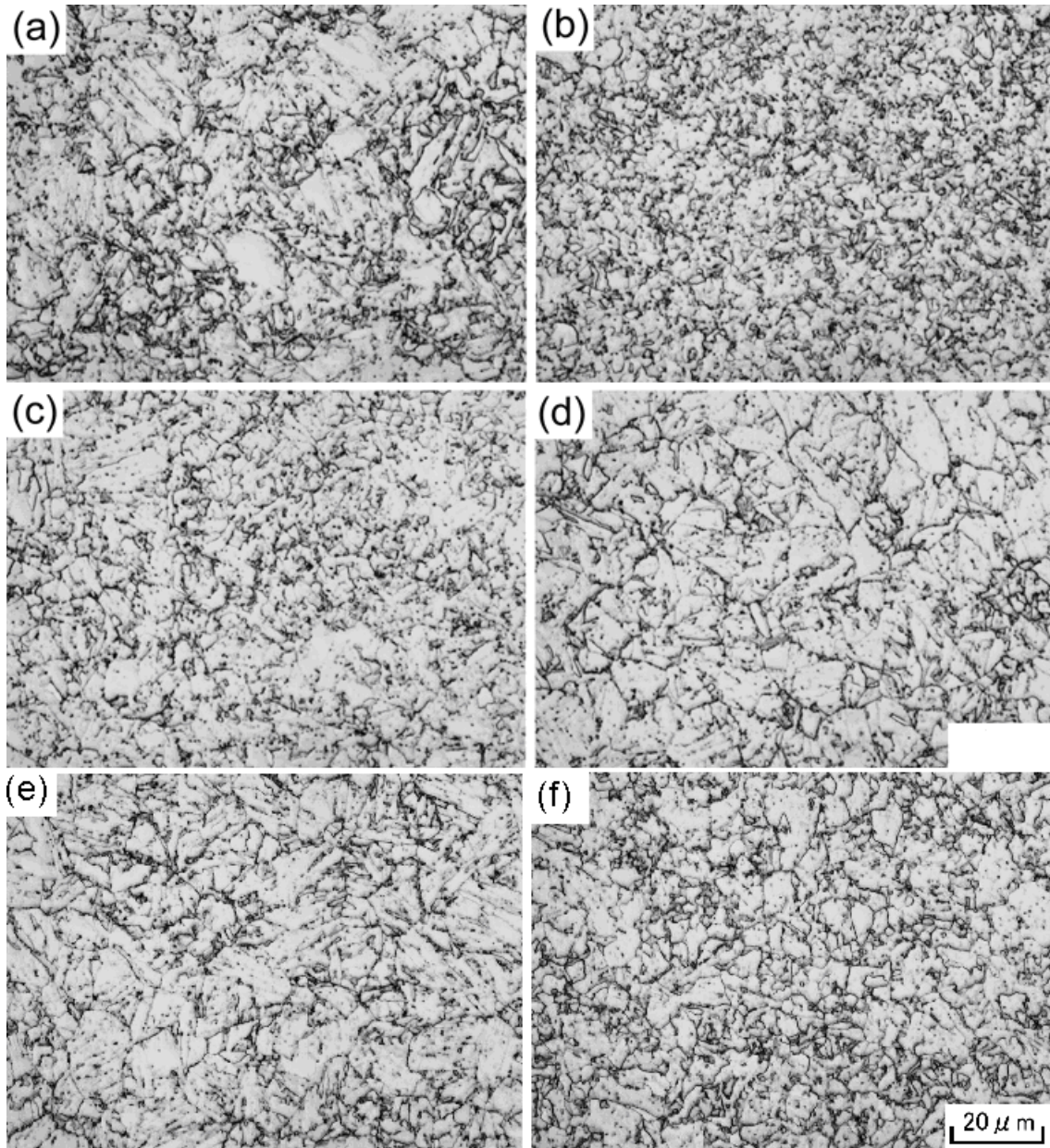


Fig. 5-5. Comparison of the microstructures of the thick welded joint indicated in the respective locations (a), (b), (c) and (d) shown in Fig 5-4, (e) for the base metal, and (f) for the simulated HAZ by OM.

In terms of the Chapter 1, the voids grow up in the fine-grained HAZ (or intercritical HAZ) and finally lead to Type IV cracking at about 80% of the rupture life. The voids as the damage form almost occupied the whole creep life of the weldment at elevated temperatures. Therefore the voids nucleated in the HAZ should be discussed in detailed for evaluating the

final cracks.

Suppressing the nucleation and growth of void in HAZ can be a good countermeasure to prevent Type IV damage at elevated temperatures. The Fig 5-6 was obtained from the thick welded joint crept under 90MPa at 600°C. The observation was conducted at the interruption of 7970h and 80% of the rupture life with the aid of laser microscope. The voids could hardly be found in the weld metal and in the base metal as shown in Fig 5-6 a and c. As shown in the Fig 5-6 b, the voids can be observed both in the fine-grained HAZ and in the intercritical HAZ though we did not give a clear boundary of the fine-grained HAZ and intercritical HAZ. The intercritical HAZ is defined as the boundary of the fine-grained HAZ and the tempering zone in the welded joint, where the grain sizes increase from the fine-grained HAZ to the tempered zone. The voids could also be observed in the tempering zone of the welded joint in the below figure but it is small in number. Moreover, there are less voids were observed in the coarse-grained HAZ. The small number of voids in the coarse-grained HAZ and tempering zone would not reflect the rupture life of the welded joint during high temperature exposure. Namely these two in the HAZ of the Mod.9Cr-1Mo steel welded joint are not listed in the weaker zones and not the emphasized topic in the terms of the damage mechanism. Experimental evidence of the discussion above is indicated in the Fig 5-7. The voids could be only observed in a large number in the fine-grained HAZ as well as the intercritical HAZ of the welded joint. The diagram indicated that the microhardness had a well reverse relation with the void number in the mixing zone of the welded joint. The part with the lowest microhardness has the weakest resistance to the creep at high temperatures. The photograph and experimental data in Fig 5-7 are obtained from the interruption about 90% of creep life in the experiment conducted under 90MPa at 600°C. The voids are produced in the zone 1.0~2.3mm in distance to the bond line, which is composed of the fine-grained HAZ and the intercritical HAZ, which circles the joint of the two sub-HAZs.

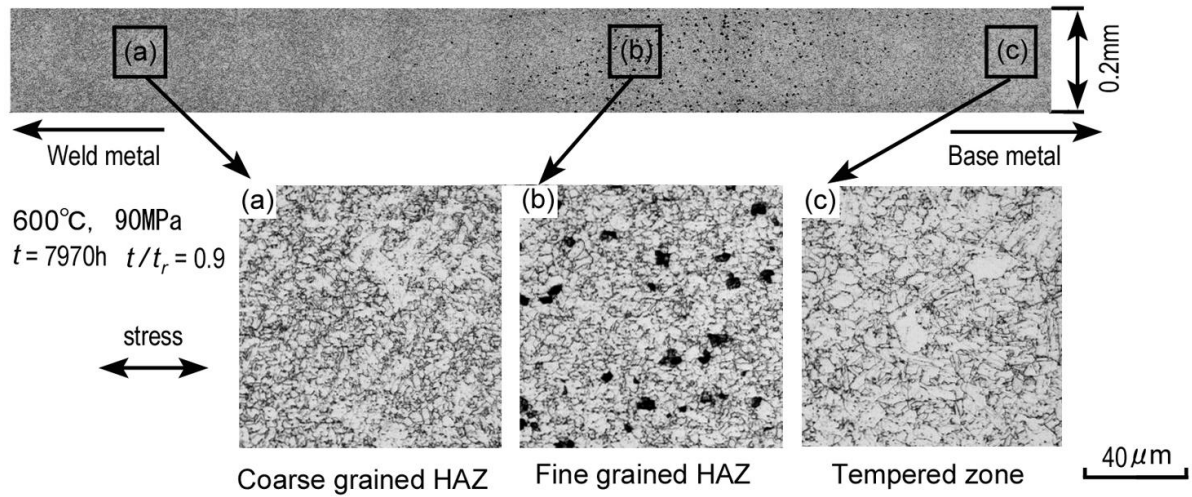


Fig 5-6. Voids distribution in the HAZs of thick welded joint of the Mod.9Cr-1Mo steel at the creep time of 7970h crept under 90MPa at 600°C observed by LASER microscope.

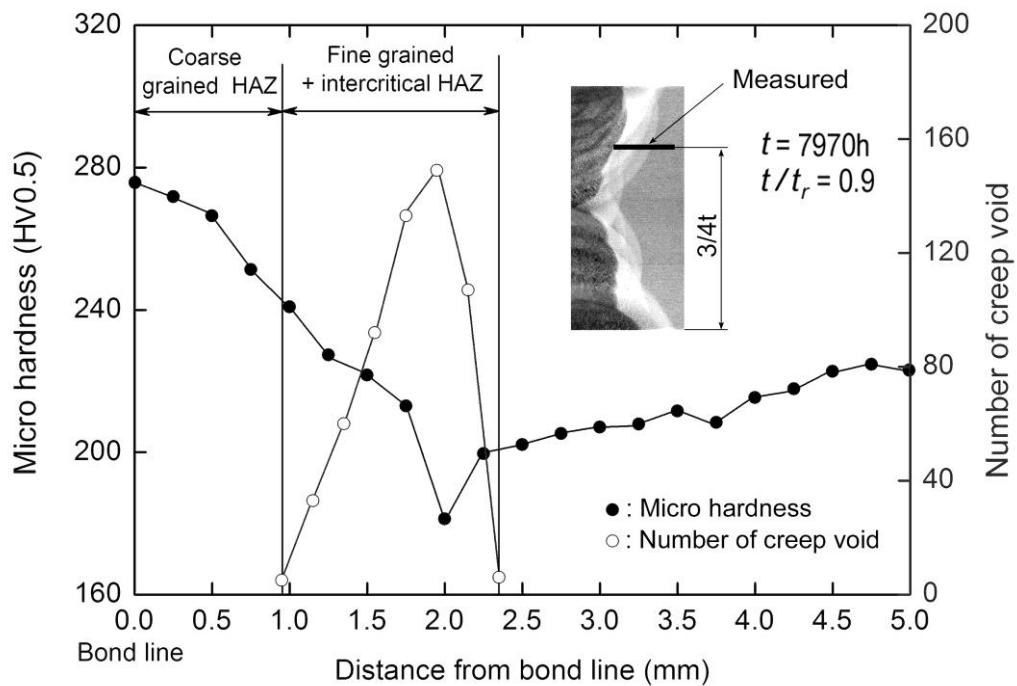


Fig. 5-7. Microhardness and the voids distribution in longitudinal direction of the thick welded joint at 7970h at creep temperature of 600°C under 90MPa.

Thus corresponding locations of the sub-HAZ had been clarified. The fine-grained HAZ

and the intercritical HAZ are both the potential failure zones in a welded joint. The voids tend to be produced in the boundary of fine-grained HAZ and intercritical HAZ, where the grain sizes are smaller. An important observation on creep voids and hardness had been found that the weaker zone in welded joint transmitted from the intercritical HAZ to the fine-grained HAZ with the servicing time increasing at related high temperatures. The creep temperature greatly accelerates the transformation speed since the transformation at 550°C reaches to intercritical HAZ but the transformation at 600°C arrives at the fine-grained HAZ. Moreover, the microhardness values can be a valid scalar to localize the weak location in the welded joint.

5.3 Void (Vacancy) Nucleation

That the crack finally occurs in the base metal under high testing stresses is due to the constraints focusing on the original weak zone (mixing zone of intercritical and fine-grained HAZ) make it crept under a corresponding lower effective stress to rupture. This part had been discussed in Chapter 3 in details. We are now discussing the damage mechanism in microscopic scale in the mixing zone under lower stress levels. The conjunct role of stress triaxial factor and equivalent creep strain accelerates the speed of the nucleation of voids during creep, which was obtained by FEM simulation comparing with the voids observations. In terms of the mechanism of creep damage, we were usually beginning on the diffusion and boundary sliding [5-21, 5-22] though creep diffusion was believed not predominant at the testing temperatures among 600°C~650°C by most researchers [5-23, 5-24]. Just as we had clarified that the potential damage locations are the intercritical HAZ and fine-grained HAZ. The Type IV zone is finally decided the boundary of the fine-grained HAZ and the intercritical HAZ in the welded joint according to the observation the voids in the thick welded joint at the interruptions during creep. We would like to investigate the damage mechanism in terms of the voids nucleation and growth during creep in long term.

5.3.1 Grain Boundary Sliding

As we had discussed the role of the stress triaxial factor on the mixing zone in thick welded joint in Chapter 3, stress triaxial factor is a complicated mechanical parameter. It enhances the creep strength of materials in short period, which is prevalent under the high stress levels and low testing temperatures. Therefore the base metal becomes relatively weak zone in the welded joint during creep. Fig 5-2a shows that the thin welded joint breaks in the base metal under the applied stresses of 240MPa and 200MPa at the temperature of 550°C, the corresponding specimens are in upside and in underside in this figure respectively. The two welded joints were ruptured at 451.6h and 1783.9h at 550°C.

However, the stress triaxial factor loses its beneficial effects to creep life due to the grain boundary sliding when the welded joint is serviced under low stress levels at high temperatures. We can say the large constraints on the weak zone accelerate the boundary sliding at high temperatures. During the process of the sliding for relieving the constraints on the weaker zone of the welded joint, the voids nucleate, which is good agreement with the FEM simulation. Thus we should begin the discussion from the micro mechanism. As we know the potential damage zones are composed of the fine-grained HAZ and the intercritical HAZ. Moreover, the boundary of the two sub-HAZs owns the largest number of voids in the later stage of the creep-rupture life. The mixing zone is named as Type IV zone for conveniently discussing later. There must be a large number of the grain boundary in Type IV zone due to the smaller grains. Comparing with the matrix of grain the grain boundary is the weak zone. Therefore, the large strain inevitably occurs in the boundary comparing with the grain matrix. The creep strain accumulation on the boundary contributes the total strain. This can be reflected in the large concave observed in the HAZ of the thick welded joint during creep as shown in Fig 5-8. The deflections were measured at the interruptions of the thick welded joint crept under 900MPa at 600°C. The weaker zone is focused with large constraints due to

the stress triaxial factor there.

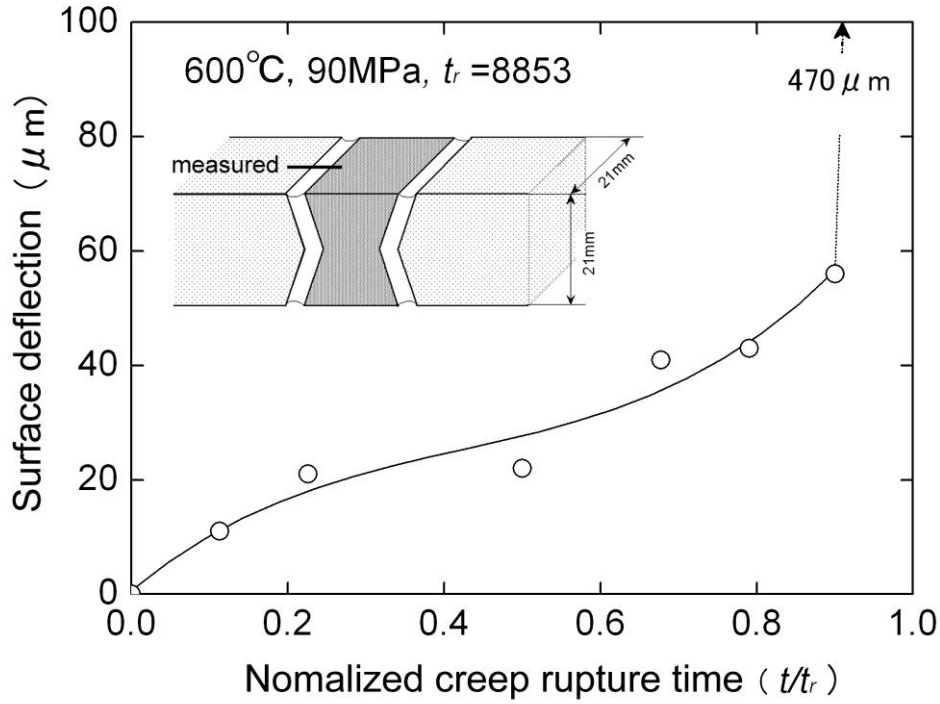


Fig. 5-8. Changes of surface deflection in the HAZ of the thick welded joint with the creep time at 600°C under 90MPa.

In applying the diffusion creep model, Onaka calculated the rate of strain in two models: Coble creep and Nabarro-Herring creep respectively, and they are given by the following Eqs. (5.2) and (5.3) [5-25],

$$\dot{\varepsilon} \approx \frac{20D_B c \Omega}{a^3 k T} \sigma_0 \quad (5.2)$$

$$\dot{\varepsilon} \approx \frac{10D_L \Omega}{3a^2 \left\{ \sum_{i=1}^N \left(\frac{V_i}{V_g} \right)^{2/3} f_i \right\} k T} \quad (5.3)$$

$\dot{\varepsilon}$ is the rate of strain, D_B denotes the grain-boundary diffusion coefficient, k is the Boltzmann's constant, T is the absolute temperature, Ω is the atomic volume, $2c$ is the thickness of the grain boundary, D_L is the lattice diffusion coefficient, f_i is the grain

volume fraction, V_i presents the single grain volume, and a denotes the average size of grains. The volume V_g is some representative value of the grain volume. From the two equations, we can get the same conclusion that the rate of strain decreases with the grains sizes. Therefore larger creep deformation usually appears in the zone containing smaller grains due to the average grain size. Though the Coble creep and Nabarro-Herring creep usually dominate at more than 0.8 of the melting temperature of materials, we believe that the reverse relation of the rate of creep strain and the grain size should exist even at $0.5T_m$ of the materials more or less.

The local precipitation grows up in the grain boundary which decreased the density of the smaller second-hard phase in the matrix. Fig 5-9, taken by TEM, indicates that the $M_{23}C_6$ grows up in fine-grained HAZ of the weldment during creep, with comparing with the base metal. It also implies that the applied stress does not enhance the growth of the precipitation since we get the same results from the aging test at the same temperature of 600°C . The temperature should be the determinative factor for the precipitation growth. Large laves phase was found in the fine-grained HAZ of the rupture tested specimen, it also could be observed by TEM but small in size in the 600°C aging specimen of the weldment.

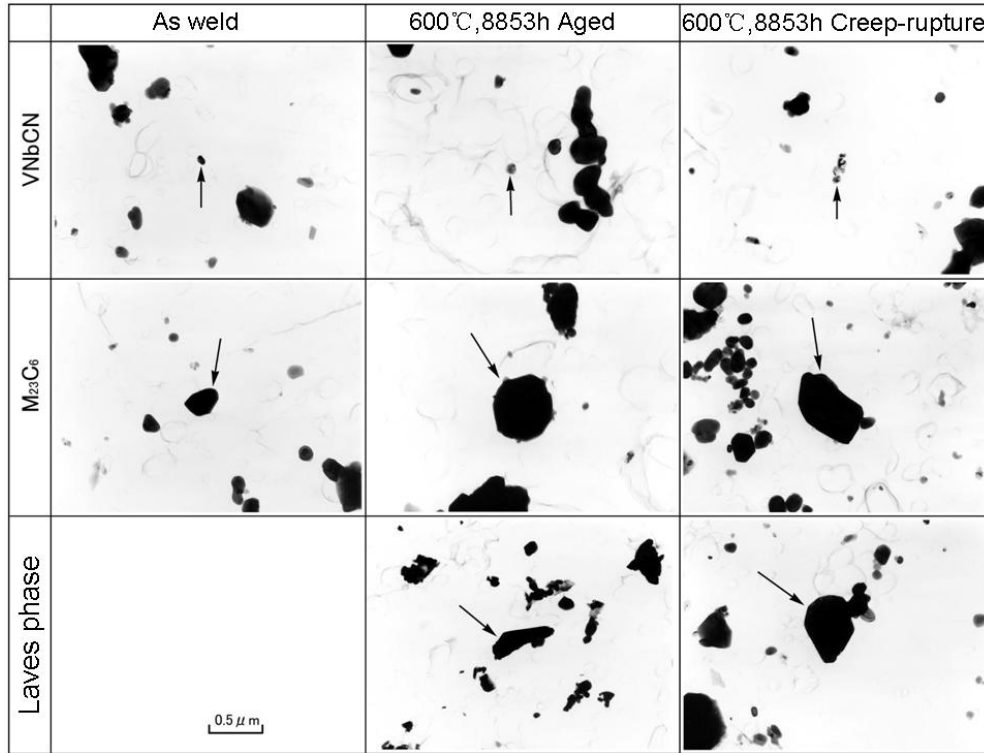


Fig. 5-9. Observations of the precipitations in HAZ of the thick welded joint at different conditions (as weld, crept at 600°C for 8853h and aged at 600°C for 8853h, resectively) by TEM.

Following to the discussion above, we propose a damage model, i.e. a void nucleation and growth model with considering the pinning role of the precipitations in the grain boundaries. The idea is illustrated schematically in Fig 5-10. We think the origin of the voids is the clustering of atomic vacancies produced by the interaction between the precipitation and the matrix. With the conjunct role of the creep deformation and the precipitates in Type IV zone, the vacancy cluster should be produced in the locations around the large precipitation near the grain boundaries. Fig 5-10 simply indicates the vacancy cluster produced around the large precipitation in the grain boundaries.

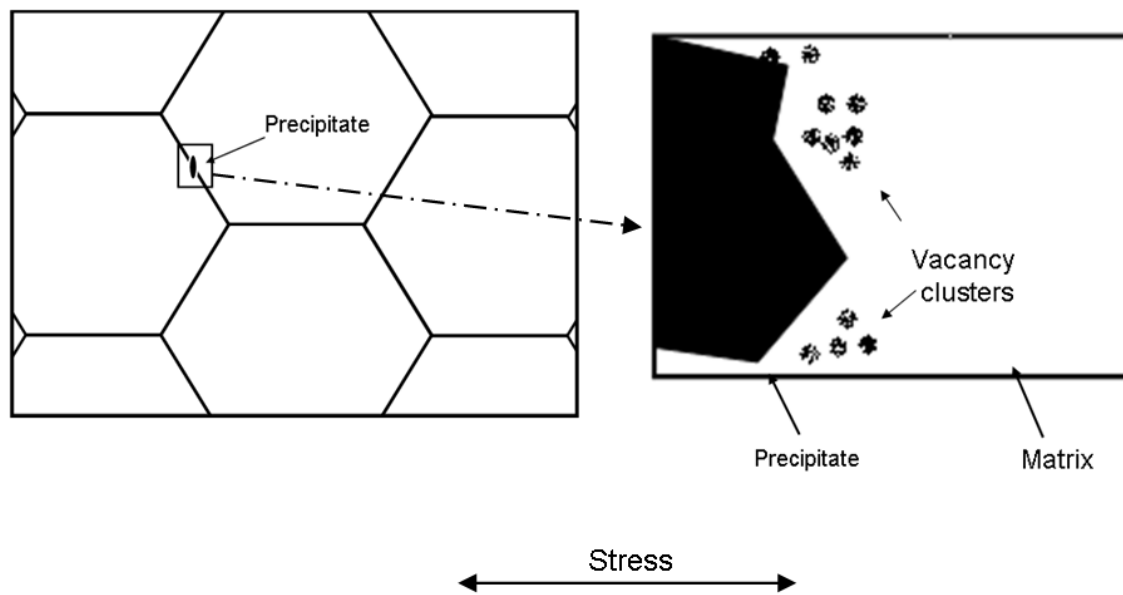


Fig. 5-10. Producing model of vacancies in grain boundaries at elevated temperatures (schematic).

Just as we have discussed above, the large creep deformation is necessary to the void nucleation during creep. The stress triaxial factor in the Type IV zone is also important for the voids producing. The large stress triaxial factor leads to the relieving in large extent via grain boundary sliding. The grain boundary sliding to relieve the constraints would also lead to large strain imbalance in the location near to the triple junction due to the external force. Strain imbalance would also be discussed in procedure of void growth later. Here we would give a definition of the strain imbalance which is strain changing with the location variations in microscope. The strain imbalance could be expressed with the term of $\frac{d\epsilon}{ds}$, where s is a certain track, along which the creep strain changes. The strain imbalance would promote the nucleation of vacancies in the Type IV zone. This tests that the FEM results are reasonable.

Lee *et al* argued that the cavity formation at grain boundaries was caused by the strain heterogeneity among grains [5-3]. In intercritical HAZ, the grain sizes are not same on a whole due to the small grains same to fine-grained HAZ and large grains similar with the base

metal. Under a certain external stress, the strain heterogeneity among the grains occurs, and it is prominent in the location near to the triple junction particularly. Therefore, we believe that it enhances the vacancy nucleation in the intercritical HAZ during high temperature exposure. However it is not the prominent coefficient in the Type IV zone in present case.

5.3.2 Diffusion during Creep

Diffusion is susceptible to temperature changes.

The absolute temperature as a function of diffusion coefficient could be given by Equation (5.4).

$$D = D_0 \cdot \exp\left(-\frac{Q}{RT}\right) \quad (5.4)$$

where, D_0 is a constants, Q is the diffusion activity energy, R is the gas constant and T is the absolute temperature. In present study the diffusion coefficient D was used to represent the frequency of the changing between the vacancy and the atoms close to it. The diffusion coefficient is higher at 650°C than at 550°C since the coefficient is increasing with the test temperature according to the equation.

After the vacancies formation in grain boundary, they usually diffuse with the time and then connected each other at elevated temperatures. Usually the many vacancies are produced in the location close to the large precipitation where the large strain imbalance occurs. Many vacancies nucleate closed to the precipitations, and among them closed vacancies are named as the vacancy cluster. The vacancies are very small in size and they could move randomly by substitution-diffusion with other atoms in matrix, which is accelerated by the hydrostatics stress. Substitution-diffusion is carried again and again, which makes the vacancies produced move freely. A new larger vacancy forms, when the two vacancies meet. With the roles of diffusion and growth, a new much larger vacancy can be produced. The impurity in matrix can accelerate the substitution-diffusion. Therefore, the voids are always found in the

boundary because the density of the impurity there is so high. We also know that the type of the crystal lattice can affect the diffusion velocity, i.e. the compact atoms would make the substitution-diffusion difficult. Therefore, the diffusion in austenite with the face center cubic is difficult to perform while it becomes easy in the ferrite and the martensite.

There is no clear critical value to differentiate the voids from the vacancies in size, there are not relative references including of it yet. When its size exceeds over $1\text{ }\mu\text{m}$, we call the vacancy as the void in present study.

The thin welded joints creep tests show that the Type IV damage are more dependent on the temperature due to the diffusions. The higher testing temperatures are used, the longer term is needed to produce Type IV cracking. The specimens of welded joint were ruptured in the base metal during creep under stress above 220MPa at 550°C, and Type IV cracks can be produced more than the time of 9000h. Failure in base metal of the welded joint did not found in the present creep tests at 600°C, and the final damage form is Type IV cracking, which can occur within 1000h. When the testing temperature is rising to 650°C, Type IV cracks can be produced about 300h during creep.

Rodriguez and Rao proposed that the vacancy formation at grain boundary precipitates and at triple junctions is a probable mechanism for material degradation at elevated temperatures [5-26]. The phenomenon of the nucleation of vacancy had been found in the positions near the precipitates and triple junction as shown in Fig 5-11a and Fig 5-11b, which is observed in fine-grained HAZ by the SEM. Diffusion is believed exiting in long term creep and contribute to the void nucleation due to atoms density in the locations where the strain imbalance is large. The strain imbalance acts an important role on the nucleation of vacancies in the grain boundary.

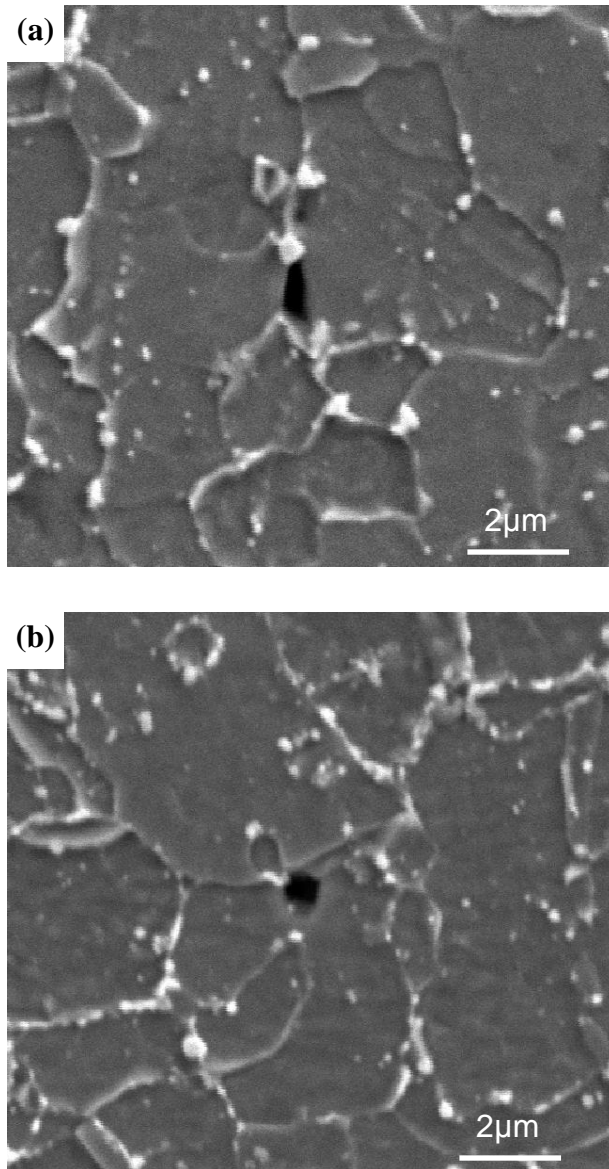


Fig. 5-11. Void formation and growth observed (a) at 6000h, and (b) at 4000h with crept at 600°C under 90MPa by SEM.

5.4 Growth of Voids and Cracks in Type IV Zone

We had discussed the nucleation of the creep void in terms of grain boundary sliding and diffusion in the mixing zone in the welded joint. After the vacancies are produced, they grow up and then form the voids, and the voids grow up and leading to the type IV cracking with the coalescing of the voids.

We just discussed the role of diffusion in the procedure of vacancy nucleation above, and diffusion also act a critical role in the growth of void. The voids grow up with the interactions of the boundary diffusions and the surface diffusions in a certain scale. Boundary diffusion charges the void growth along the grain boundaries, while surface diffusion contributes to the growth of void in volume. The studies on diffusion mechanism and diffusion velocity equations had been conducted extensively from the middle of last century, and some evaluation methods for damages of materials in high-temperature servicing were developed [5-27, 5-28].

Whatever the boundary diffusion or the surface diffusion, they should be on the base of the atom moving from one location to the other location. Therefore, we should give an emphasis on the fundamental law. Varying curvature along the profile gives rise to gradients of chemical potential which in turn produce a drift of surface atoms with an average velocity given by the Nernst-Einstein relation [5-29]

$$V_s = -\frac{D_s \gamma_s \Omega}{kT} \frac{d\kappa}{ds} \quad (5.5)$$

where V_s is the average surface velocity of atoms, κ is the curvature of a selected element of path (routine), D_s is the coefficient of surface diffusion, ds denotes an element of arc length, γ_s is the surface free energy, Ω is atomic volume and T presents the absolute temperature. For an irregular void in shape, it means the opposite deformation varies along it surface, i.e. strain imbalance appears in the surface. In the same time, the curvature of the

void surface also has a large changing tendency because it is the reciprocal of radius. Hence the strain imbalance should have a progressively proportional relation with the term of $\frac{d\kappa}{ds}$, and given by

$$\frac{d\varepsilon}{ds} \propto \frac{d\kappa}{ds} . \quad (5.6)$$

By combining Eqs. (5.5) and (5.6), the average velocity of surface atoms of void is increasing with the strain imbalance. Therefore, the voids grow up mainly in the diffusion manner and large strain imbalance could speed up the diffusion velocity of atoms in the interface of matrix/void, which can be named as self-growth. The changing of the routine length (ds) is according to the void size. For the void in different size, the factor ds is also different, and is usually no less than a void diameter. When voids connect each other, the irregular boundary of void/matrix is produced inevitably. This accelerates the self-growth of voids. Fig 5-12 indicates that the voids growth tends to a sphere like one. When the voids grow into a certain range and like sphere more and more, they would connect with the closed one and then produce a large one with large $\frac{d\kappa}{ds}$. This procedure is defined as a cycle. The newly forming void grows up with contributing of the large strain imbalance again since the new one must have an irregular shape. With the cycles, the voids grow up in the weak HAZ under a certain stress. The theory on the voids growth could be reflected in Fig 5-13 taken by SEM, in which the voids are observed in 7,170h and 7,970h interruptions. The voids grow up for decreasing the strain imbalance along the inter-surface of void/matrix, i.e. the strain imbalance is a special driving force for the growth of void.

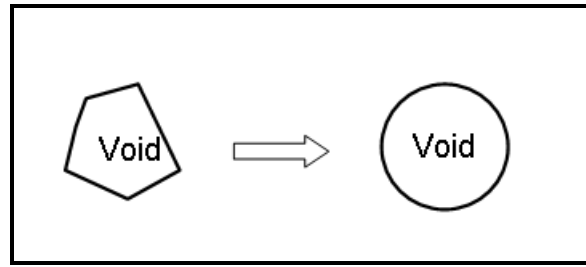


Fig. 5-12. Schematic illustration of void growth due to the strain imbalance at elevated temperatures.

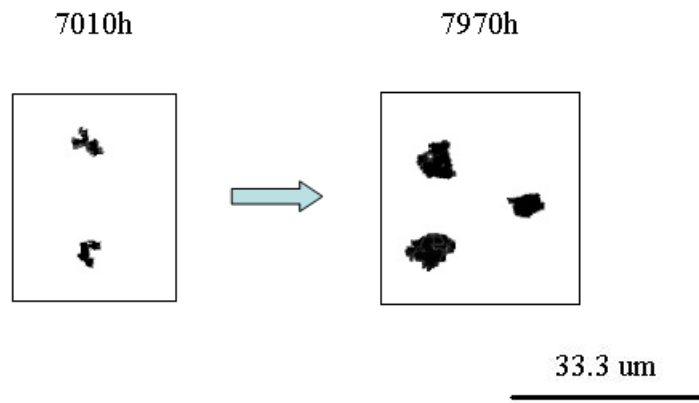


Fig. 5-13. Growth of voids observed by SEM in HAZ of the thick welded joint crept under 90 MPa at 600°C.

It is apparent that the connection of voids raises the progress of crack formation. Kitamura *et al* pointed out that the crack poses the stress singularity in the vicinity of the tip, even while the void does not. They considered the transition from the crack-like cavity to c-rack would occur when the length of crack-like cavity exceeded 15 grain boundaries as shown in Fig 5-14 [5-30]. In the present study, the grain sizes of the weak HAZ are in the range from 3 to 5 μ m in diameter, so that we can get the approximation 22.5 μ m of the length of Type IV crack in the weak HAZ, and much larger in the intercritical HAZ. The critical Type IV cracking should not be less than this value in length. Hence stress concentration should not affect the development of the void, and the diffusion tendency is homogenous in all radial

directions under a certain stress. This is well in agreement with the SEM observation of void shape since most of them appear as the shape close to a sphere.

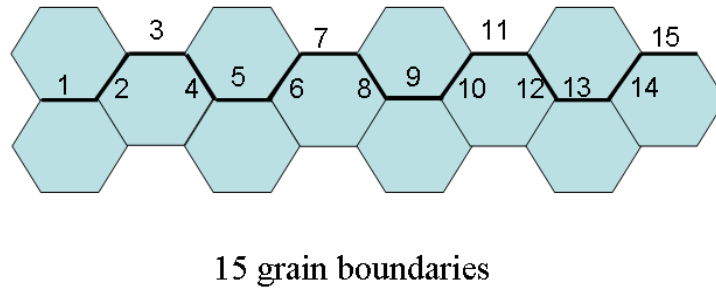


Fig. 5-14. Sketch map of crack formation and size (the bold line in the grain boundaries denoting the crack) [5-30].

By using laser microscope, the crack was not found in the specimen interrupted at 0.79 of the rupture life at 90MPa and 600°C. In this interruption step, the sizes of crack-like voids are not larger than 20 μm . However, many cracks larger than 100 μm have been observed in the Type IV zone at 0.93 of the rupture life. It means that the Type IV crack is produced in the period of 0.79-0.93 of the creep life, and after formation, the crack grows up quickly. The connection of voids takes place in the growth of crack. As soon as the crack nucleates, the concentration of stress focused on the tip zone should be responsible for its growth. The diffusion might not be prominently responsible for the growth of crack though the localized diffusion velocity in the tip zone also deeply increases.

5.5 Possible Countermeasures to Prevent Type IV Cracking

Based on the experimental observation and discussions mentioned above, the Type IV zone should be eliminated from the welded joint for reducing the probability of Type IV occurrence. According to present and previous work, we give some helpful advices for

reducing the Type IV damage tendency during creep.

Reducing the constraints on the weak HAZ in a weldment should be realized by the designers, such as simplifying the weld groove shapes and decreasing the angles of groove.

Reducing the heat input during welding can decrease the width of the Type IV zone, which is useful for delaying the creep damage due to Type IV cracking. PWHT such as partial tempering and half tempering can provide the deduction of hardness of the weak HAZ, and improvement of creep strength can be provided alternatively. These had been referred in some literatures [5-31, 5-32], which were on the basis of the experiments. However, the relation of the constraints and width of weak HAZ of a welded joint is not clear.

Reducing the impurities is another valid method to fining and strengthening the grain boundary in Type IV zone. Addition of the Boron prolong the creep life of the conventional high chrome heat resistant ferritic steel by enlarging the grain size in the Type IV zone and suspension of the growth of Cr_{23}C_6 carbide precipitation [5-33]. Actually the area fraction of the grain boundary to matrix is greatly decreasing with the large size grains forming in the Type IV zone, which reduces the potential weak zones, particular the grain boundaries.

Even we take some helpful steps to prolong the rupture life of weldment, they are still the weak zone of a whole welded joint. Though there are some arguments on the prediction of the weld-repair component at high temperature, weld repair is still recommended for the practical signification by reducing the cost of renewing a large component such as the turbines and boilers [5-34]. Weld repair even can be used in a homogeneous material when the fraction life is greatly shorter than the expected [5-35]. The CDM constitutive equations and the FEM simulation were used to evaluate the weldment after weld repair in variable repair models, the prediction of creep-rupture life shows that the process weld repair is feasible in practice. Wide and medium deep geometry of the excavation were recommended, and the original weld should be covered when weld repair was conducted [5-36].

For macroscopic creep-rupture data analysis the TTP method of Manson-Haferd parameter

is relatively conservative for predicting the creep-rupture life.

5.6 Summary of Chapter 5

Combining our microscope observation of the voids and previous research works, we discussed the damage mechanism in the thick welded joint during creep and proposed a mechanism of void growth due to localized strain imbalance in the grain boundary. The conclusions obtained in this chapter are as follows:

- 1) Type IV zone is produced at the peak temperature of Ac_3 with using the weld simulator. The damage locations can be sure in the narrow part about 1.3mm in width in the thick welded joint during high temperature servicing.
- 2) We made sure the damage locations are the mixing HAZs of fine-grained HAZ and intercritical HAZ, and encompassing their boundaries.
- 3) Micro hardness measurement shows that it can be used to denote the weaker zone in welded joint.
- 4) The thin welded joints were ruptured in the base metal during creep under stress above 220MPa at 550°C, and Type IV cracks can be produced more than the time of 9000h. Failure in base metal of the welded joint did not found in the present creep tests at 600°C, and the final damage form is Type IV cracking, which can occur within 1000h. When the testing temperature is rising to 650°C, Type IV cracks can be produced about 300h during creep.
- 5) The nucleation of void due to the conjunct role of the equivalent creep strain and stress triaxial factor can be explained in grains boundary sliding and diffusion of atoms in microscopic mechanism.
- 6) The growth of void is caused by the strain imbalance and it grows up with the atoms diffusion. The stress concentration in the tip zone should be responsible for the growth of Type IV cracking.

References of Chapter 5

- [5-1] S. J. Brett, D. J. Allen, J Pacey: CHIFI International Conference, (Milan, 1999) pp. 873-884.
- [5-2] S. J. Brett, D. L. Oates, C. Johnston: ECCC Creep Conference, (London, 2005) pp. 563-572.
- [5-3] J. S. Lee, K. Maruyama, I. Nonaka and T. Ito, Creep Deformation and Fracture, Design, and Life Extension (Materials Science & Technology 2005), Edited by R. S. Mishra, J. C. Earthman, S. V. Raj, and R. Viswanathan, (TMS, Warrendale, 2005) pp.139-148.
- [5-4] J. A. Francis, W. Mazur and H. K. D. H. Bhadeshia: Material Science and Technology. **22** (2006) 1387-1395.
- [5-5] K. Shinozaki, D. J. Li, H. Kuroki, H. Harada and K. Ohishi: ISIJ International. **42** (2002) 1578–1584.
- [5-6] H. Cerjak and E. Letofsky: **Advanced Heat Resistance Steels for Power Generation**. (1998) pp. 541.
- [5-7] E. Letofsky, H. Cerjak, I. Papst and P. Warbichler: **Proc. 3rd Conf. on Advances in Materials Technology for Fossil Power Plant**, ed. by R. Viswanathan, W. T. Bakker and J. D. Parker, (The Inst. Mater., 2001) pp. 133.
- [5-8] K. Laha, K. S. Chandravathi, K. B. S. Rao, S. L. Mannan and D. H. Sastry: Metal. Mater. Trans.. **32A**(2001) 115.
- [5-9] M. Tabuchi, T. Watanabe, K. Kubo, M. Matsui, I. Kinugawa and F. Abe: J. Soc. Mater. Sci. Jpn.. **50**(2001) 116.
- [5-10] M. Tabuchi, T. Watanabe, K. Kubo, M. Matsui, I. Kinugawa and F. Abe: Int. J. Pressure Vessels & Piping. **78**(2001) 779-784.
- [5-11] M. Matsui, M. Tabuchi, T. Watanabe, K. Kubo, J. Kinugawa and F. Abe: ISIJ Int.. **41**(2001) 126-130.
- [5-12] M. Tabuchi, M. Matsui, T. Watanabe, H. Hongo, K. Kubo and F. Abe: Mater. Sci. Res.

- Int.. **9**(2003) 23-28.
- [5-13] S. K. Albert, M. Matsui, T. Watanabe, H. Hongo, K. Kubo and M. Tabuchi: ISIJ Int.. **42**(2002) 1497.
- [5-14] S. K. Albert, M. Matsui, H. Hongo, T. Watanabe, K. Kubo and M. Tabuchi: Int. J. Pressure Vessels & Piping. **81**(2004) 221-234.
- [5-15] M. Matsui, M. Tabuchi, T. Watanabe, K. Kubo and F. Abe: J. Soc. Mater. Sci. Jpn.. **52**(2003) 119.
- [5-16] K. Shinozaki and H. Kuroki: Materials Science and Technology. **19**(2003) 1253-1260.
- [5-17] N. Komai and F. Masuyama: ISIJ International. **42**(2002) 1364-1370.
- [5-18] G. Eggeler, A. Ramteke, M. Coleman, B. Chew, G. Peter, A. Burblies, J. Hald, C. Jefferey, J. Rantala, M. DeWitte and R. Mohrmann: International Journal of Pressure Vessels and Piping. **60** (1994) 237-257.
- [5-19] Y. Hasegawa, T. Muraki and M. Ohgami: Tetsu-to-Hagane. **92** (2006) 40-48.
- [5-20] F. C. Monkman and N. J. Grant: *Proc. ASTM*, **56**(1956), 595.
- [5-21] J. Weertman: J. App. Phy, **28**(1957) 1185.
- [5-22] M. F. Ashby and R. Raj: Met. Tran., **2**(1971) 113.
- [5-23] P. J. Ennis, A. Zielinska-Lipiec, O. Wachter and A. Czyrska-Filemonowicz: Acta mater. **45**(1997) 4901-4907.
- [5-24] R. W. Swindeman, V. K. Sikka, P. J. Maziasz and D. A. Canonico: Fatigue, Environmental Factors, and New Materials, PVP-Vol. 374, ed. by H. S. Mehta, R. W. Swindeman, J. A. Todd, S. Yukawa, M. Zako, W. H. Bamford, M. Higuchi, E. Jones, H. Nickel and S. Rahman, (ASME, New York, 1998) pp. 305-312.
- [5-25] S. Onaka, A. Madgwick and T. Mori: Acta Mater. **49** (2001) 2161-2168.
- [5-26] P. Rodriguez and K. B. S. Rao: Progress in Materials Science. **37** (1993) 403-480.
- [5-27] A. C. F. Cocks and M. F. Ashby: Progress in Materials Science. **27** (1982) 189-244.
- [5-28] R. Raj and M. F. Ashby: Acta Metallurgica. **23** (1975) 653-665.

- [5-29] T. J. Chunang and J. R. Rice: *Acta Metallurgica*. **21** (1973) 1625-1628
- [5-30] T. Kitamura, R. Ohtani, T. Yamanaka and Y. Hattori: *JSME International Journal*, series A. **38** (1995) 581-587.
- [5-31] D. J. Allen: *Welding and Repair Technology for Fossil Power Plants*, (Electric Power Research Institute, Palo Alto, CA, 1994).
- [5-32] C. Coussement, M. Dewitte, A. Dhooge, R. Dobbelaere, M. Steen, E. Van Der Donckt, and L. Van Muysen: *Rev. Soud.*. **3-4**(1988), 36-52.
- [5-33] M. Kondo, M. Tabuchi, S. Tsukamoto, F. Yin and F. Abe: *Science and Technology of Welding and Joining*. **11**(2006) 216-223.
- [5-34] R. F. F. Alfonso, G. D. A. Nelson, H. R. Sergio and L. I. Alejandro: *Mat. Res.*. **9**(2006).
- [5-35] A. Klenk, S. Issler, I. A. Shibli and J. A. Williams: *Weld Repair for Creep Applications*. **2**(2003) 1-32
- [5-36] S. Jan and Å. S. Lars: *Creep Life of Pipe Girth Weld Repair*, *OMMI*. **1**(2002) 1-14.

Chapter 6

Conclusions

In the present study, a set of creep tests of the materials such as base metal, simulated HAZ and welded joint (thin and thick) of the Mod.9Cr-1Mo ferritic heat resistant steel were performed under the stress levels range from 40MPa to 160MPa at the temperatures 550, 600 and 650°C. The damage procedure in the fine-grained HAZ and the intercritical HAZ of thick welded joint at interruptions crept under 90MPa at 600°C were investigated by LASER microscope. Stress-strain distributions in the welded joint were computed by FEM analysis with three-dimensional, three-material model (containing with base metal, weak HAZ and weld metal). A group of conventional constitutive equations with continuum damage mechanics has been modified for evaluating the creep behavior of homogenous materials and the weldment. Combining with the finite element method the damage distribution along the Type IV zone was also evaluated in the thick welded joint under the stress of 90MPa at 600°C. On the basis of the interrupted creep tests we determined the materials constants for the CDM and discussed the void evolution processes. In view of the microscope observation and previous research works, we discussed the damage mechanism in the thick welded joint during creep in macroscopic and microscopic aspects, respectively. The important experimental results and conclusions obtained in present studies are summarized as the follows:

- (1) Type IV zone is produced at the peak temperature of A_{c3} with using the weld simulator.

The damage locations can be sure in the narrow part about 1.3mm in width in the thick welded joint during high temperature servicing, which is composed of the fine-grained

HAZ and the intercritical HAZ.

- (2) The thin welded joints were ruptured in the base metal during creep under stress above 220MPa at 550°C, and Type IV cracks can be produced more than the time of 9000h. Failure in base metal of the welded joint did not found in the present creep tests at 600°C, and the final damage form is Type IV cracking, which can occur within 1000h. When the testing temperature is rising to 650°C, Type IV cracks can be produced about 300h during creep.
- (3) It is found that the creep voids of Mod.9Cr-1Mo steel weld form at the early stage of creep rupture life (0.2 of life), the number of them increases with time till 0.7 of life, and then they coalesce into the Type IV crack at the last stage (after 0.8 of life).
- (4) The creep voids tend to form at the area of a quarter depths from the surfaces, inside the plate, in fine-grained HAZ and the intercritical HAZ for the present thick plate welded joint of Mod.9Cr-1Mo steel.
- (5) Micro hardness measurement shows that it can be used to denote the weaker zone in welded joint.
- (6) It is considered that the high level stress triaxial factor combined with the large equivalent creep strain in the Type IV zone in the thick welded joint accelerate the void forming in the Mod.9Cr-1Mo steel welded joint during creep at elevated temperatures.
- (7) With comparing the FEM calculation of two weldment models (for thin and thick welded joints) the relation of the constraints on the weak zone in a welded joint and the size of welded joint has been clarified. Large constraints are always produced in the weak zone in a large scale welded joint than the small scale welded joint.
- (8) The conventional evaluation equations for creep damages have been modified by substituting the engineering stresses for equivalent creep stress and the terms containing stress without considering of the multiaxial stress rupture criteria. The final evaluation of strain and creep-rupture time prediction comparing with the experimental results shows

that the modified work does not affect the calculation results.

- (9) The linear relation of the logarithm of m_1 (and $1/\lambda$) with the applied stress in homogeneous material was used to fit the material constants. According to the relation the two exponents m_1 (and $1/\lambda$) for the homogenous such as base metal and simulated HAZ could be solved under any stress level.
- (10) By introducing a term of f^* in the CDM constitutive equations, which is the function of the equivalent creep strain and stress triaxial factor along the Type IV zone, we can successfully predict the damage distribution and evolution in the Type IV zone of the thick welded joint with the aids of FEM simulation.
- (11) The nucleation of void due to the conjunct role of the equivalent creep strain and stress triaxial factor can be explained in grains boundary sliding and diffusion of atoms in microscopic mechanism.
- (12) The growth of void is accelerated by the strain imbalance. The stress concentration in the tip zone should be responsible for the growth of Type IV cracking.

List of Publications and Presentations Related to the PhD Work

Publications

- 1) M. Tabuchi, H. Hongo, Y. Li, T. Watanabe and Y. Takahashi, Evaluation of Microstructures and Creep Damages in HAZ of P91 Steel Weldment, J. of Pressure Vessel Technology, Transactions of ASME, Vol.**131**, No.2, (2009) pp.021406-1-6.
- 2) Y. Li, H. Hongo, M. Tabuchi, Y. Takahashi and Y. Monma: Evaluation of Creep Damage in Heat Affected Zone of Thick Welded Joint for Mod.9Cr-1Mo Steel, Int. J. of Pressure Vessel and Piping 86(2009) 585-592.
- 3) 本郷宏通, 田淵正明, 李永奎, 高橋由紀夫, Mod. 9Cr-1Mo 鋼溶接継手のクリープ損傷挙動, 材料, Vol.**58**, No.2 (2009) pp.101-107.
- 4) Y. Li, Y. Monma, H. Hongo and M. Tabuchi: Creep Damage Evaluation in a Thick Welded Joint of Mod.9Cr-1Mo.Steel (*To be published*).

Presentations

- 1) Y. Li, Y. Monma, H. Hongo and M. Tabuchi: Damage Mechanics Approach to Evaluate Creep Voids Leading to Type IV Cracking in Mod.9Cr-1Mo Steel Welded Joint The Sixth Asian Pacific IIW International Congress, October 10-13, 2008. Tianjin.
- 2) 李永奎, 本郷宏通, 田淵正明, 門馬義雄: Mod.9Cr-1Mo 鋼溶接継手の熱影響部細粒域におけるクリープボイドの成長, 日本鉄鋼協会 第 155 回春季講演大会, No.247, 2008 年 3 月 28 日.
- 3) Y. Li, H. Hongo, M. Tabuchi, Y. Monma and Y. Takahashi: Creep Damage Evaluation for Thick Welded Joint of Mod.9Cr-1Mo Steel, 6th Japan-China Bilateral Symposium on High Temperature Strength of Materials, August 20-24, 2007 Tohoku University, Sendai.

Acknowledgment

I feel very fortunate to have learned at Kochi University of Technology (KUT) during my Ph.D study. I would like to express my deepest gratitude to Prof. Yoshio MONMA, my supervisor, for the invaluable guidance, encouragement extended throughout the past three years. I have benefited tremendously from his unique blend of energy, technical insights and practical sensibility. I thank my associate advisors Prof. Toshimitsu YOKOBORI, Prof. Isamu NONAKA, Prof. Masafumi TANIWAKI and Prof. Kazuhiro KUSUKAWA for giving important advices.

The study was based on the collaborated project of KUT and National Institute for Material Science (NIMS). particularly I would like to say thanks to Dr. Masaaki TABUCHI and Dr. Hiromichi HONGO because they provide the guidance and supports to me in experiments and finite element simulation work at NIMS.

The staffs and teachers in International Relations Center (IRC) of KUT headed by Prof. Mikiko BAN gave me the supports in the Japanese studying and the Japanese customs, which made it convenient in the daily life. Special thanks are given to all of them.

I would like to appreciate my colleagues and friends who have directly or indirectly supported my stay in Tosayamada and my doctoral work at KUT.

During the past three years I left my wife Xudan alone in Shenyang, China. She must meet some difficulties that can not be solved by herself, for which I am indebted to her.